ANL-6261

Argonne National Laboratory

A LUNAR POWER PLANT

by

R. H. Armstrong, J. C. Carter, H. H. Hummel,
M. J. Janicke and J. F. Marchaterre

ANL-6261
Reactor Technology
(TID-4500, 16th Ed.)
AEC Research and
Development Report

ARGONNE NATIONAL LABORATORY
9700 South Cass Avenue
Argonne, Illinois

A LUNAR POWER PLANT

by

R. H. Armstrong, J. C. Carter, H. H. Hummel
M. J. Janicke and J. F. Marchaterre

Reactor Engineering Division

December 1960

Operated by The University of Chicago
under
Contract W-31-109-eng-38

TABLE OF CONTENTS

LIST OF TABLES

LIST OF FIGURES

A LUNAR POWER PLANT

by

R. H. Armstrong, J. C. Carter, H. H. Hummel,
M. J. Janicke and J. F. Marchaterre

ABSTRACT

A concept of a nuclear power plant to be assembled on earth and operated on the moon is presented. The two principal design objectives are reliability and high specific power. Wherever there is an incompatibility between these two objectives, the decision favors reliability. The design is based on the premise that the power plant must be designed on the basis of current technology and with a minimum amount of research and development.

The principal components consist of a fast reactor in a direct cycle with a mercury-vapor turbine. The high-frequency generator, hydrogen compressor for the generator cooling system, mercury-recirculating pump, and condensate pump are on an extension of the turbine shaft. The mercury vapor is condensed and the hydrogen cooled in wing radiators.

The machinery is sealed in a cylindrical shell. For transportation to the moon, the radiators are folded about this shell so that the whole assembly makes a compact cylindrical section of the transporting rocket. Upon arrival, the power plant section is disconnected and anchored in a crater of the moon. The radiators are unfolded to form four wings at 90° to each other.

There is no shielding of any component and an absolute minimum of safety devices and controls. The cost of transporting a heavy conventional power plant is traded for a light, fully automatic packaged unit which is expendable after two earth years at full-power operation.

The power plant consists of three identical units, independent, but controlled from the central control center. Normal operation requires two units. An expedition can subsist with one. Thus, the units can be standarized, their outputs synchronized, and their size and weight best suited to the carrying capacity of its transporting rocket.

The reactor is of a construction quite similar to EBR-I Mark III for which there is a large amount of operating experience.

The working fluid is mercury. This is chosen because it is known that it is suitable for use in Rankine cycles for long periods of time at the temperatures used in this design.

The rotary converters, turbine, compressor, and generator are especially designed for this duty. The generator is a 400-cycle alternating current, brushless exciter type.

The radiators are the unique component. They are considered to be the only feasible means known now of removing the low-temperature heat from the cycle. They are also the heaviest components of the plant. If in subsequent designs the temperature levels of the cycle can be lifted, the radiator weight will decrease. Compared with earth-based power plants, the specific power of this lunar power plant is very low due to these radiators, but it is felt that the design is realistic in view of the operating environment and logistics.

The radiator is a vertical tube-and-fin type built in concentric cylindrical sections of increasing diameter. The curved headers are connected by swivel joints so that, upon arrival, the radiator can be quickly unfolded from the compact cylindrical package it formed during transportation.

OBJECTIVE

A lunar expedition that intends to remain on the moon for any length of time for the purpose of making scientific observations will require electrical energy.

Some of the facilities which may require this electrical energy are:

1. military installations;
2. weather-forecasting stations;
3. television relays;
4. stellar observatories;
5. physical observatories; and
6. space craft-refueling stations.

The objective is to provide this electrical energy with a lunar plant which can meet the following specifications:

1. The power plant must be of a shape and weight that can be transported by rocket.
2. The lifetime must be two years at full-power continuous operation with automatic control.
3. It must be capable of rejecting heat to the lunar environment.
4. The machinery and controls must be able to withstand launching and landing shocks.

The subject of this report is a conceptual design of such a power plant to be preassembled and tested in as near as possible a lunar environment before launching.

RECOMMENDATIONS

The development of high-power density fast reactors for space use will ultimately result in ultracompact machines adaptable for marine, military, or other mobile use on the earth. The ground rules for this lunar reactor concept were based on the fact that mercury coolants have been used for many years in power plants and that the characteristics of the EBR-I core have been thoroughly investigated. This concept can be regarded as one which can be constructed at the present time with little or no development and, therefore, can be a starting point for more advanced concepts.

These advanced concepts will require development programs in many directions and may be directed to earth operations as well as to space applications.

For example, the use of high-temperature gas should be investigated as a working fluid for a direct-cycle, compact fast reactor as should the use of liquid metals other than mercury.

Paralleling these thermodynamic studies of other working fluids must be the development of high-temperature fuels, structural materials, turbomachinery, and instrumentation. Studies must also be made to investigate the effects of meteors and space environment on machine operation.

A program is suggested to design an ultracompact, direct-cycle fast reactor to the following specifications:

1. thermal output to be 56 Mw (minimum);
2. core volume to be 56 liters;
3. minimum efficiency of 30%;
4. power density 1 to 2 Mw/l;
5. Average heat flux (liquid metal) of 37.67 cal/(sec)(cm^2), and average heat flux (gas) 7.53 cal/(sec)(cm^2); and
6. Minimum turbine inlet temperature of 982°C.

0-0 INTRODUCTION

The moon is considered to be the most likely objective of the first manned cosmic expedition. There is an excellent reason for this choice, namely, the relatively short distance to it. The moon is an average of 238,000 miles away, while Venus, the nearest of the major planets, never comes closer than 24 million miles. Occasionally asteroids pass fairly close. Hermes in 1937 came within 400,000 miles.

The first United States Expeditionary Force will require a source of electrical energy. The current thinking is that this source will come from the conversion of nuclear to electrical power. There are many ways in which this conversion can be accomplished. The Rankine Cycle is proposed for this first design, which will be used as the basis of comparison for the more imaginative concepts. An idea of what the external appearance of this Lunar Power Plant may look like on site is shown on Fig. 0-1.

The machinery in the cycle is selected on the basis of engineering techniques and the use of materials for which there are earthly precedents. Subsequent designs will venture beyond these and endeavor to obtain functional excellence compatible with the physical phenomena existing on the moon.

The principal components of this design consist of a fast reactor in a direct cycle with a mercury-vapor turbine, a mercury pump, and a radiator-type mercury condenser (see Fig. 0-2). A high-frequency generator is on an extension of the turbine shaft.

The power plant, with four radiators folded and wrapped around it, forms a compact cylindrical section of the rocket fuselage. Upon arrival on the moon the power plant is disconnected from the rocket, anchored to the surface of the moon, and the four radiators unwrapped and stretched out at 90° to each other.

There is no shielding of any component, and an absolute minimum of safety devices and controls. The cost of transporting a heavy conventional power plant to the moon is traded for a light-weight, fully automatic packaged unit which is expendable after two earth years of full-power operation.

It is believed that power plants should consist of multiple units interconnected and controlled from a common control center. These units should be standardized and of a size and weight best suited to the carrying capacity of the transporting rocket.

The number of units in a power plant should not be less than three, and each should have a capacity capable of keeping the base operating at subsistence level until all the expeditionary personnel can take off.

The operating pressures and temperature throughout the cycle are a compromise among many factors. The principal ones are reliability and weight.

As the temperature increases, the machinery becomes less reliable, but the weight decreases.

It is believed that this first design should favor reliability, and that the degree of reliability occasioned by the use of low-pressure, low-temperature mercury as the working medium offsets the increase in size and weight of the radiator.

It would be quite easy to show a much better plant on paper if a working medium of lesser known characteristics were used in the cycle at higher pressures and temperatures.

There is enough experience with mercury at the planned pressures and temperatures to generate confidence that it can be used in this machinery for two years of uninterrupted operation at full power.

Significant numbers pertaining to the power plant are as follows:

Capacity	1 Mw
Specific Power	9.8 kg/kw
Total Weight	9800 kg
Overall Thermal Efficiency	12.2%
Dimensions of Radiator #2 Folded	
(a) overall length	485 cm
(b) diameter	214 cm.

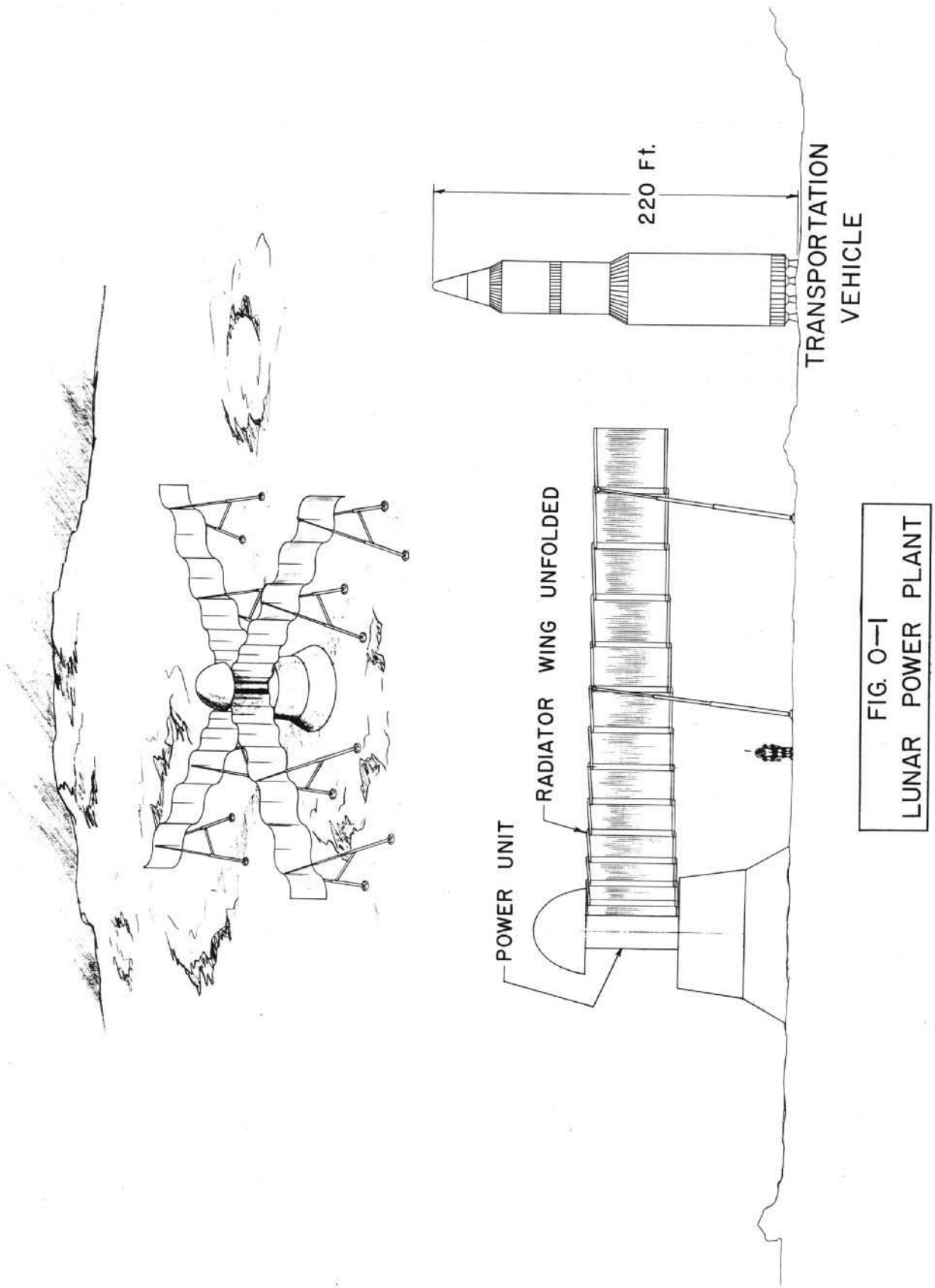

FIG. 0-1
LUNAR POWER PLANT

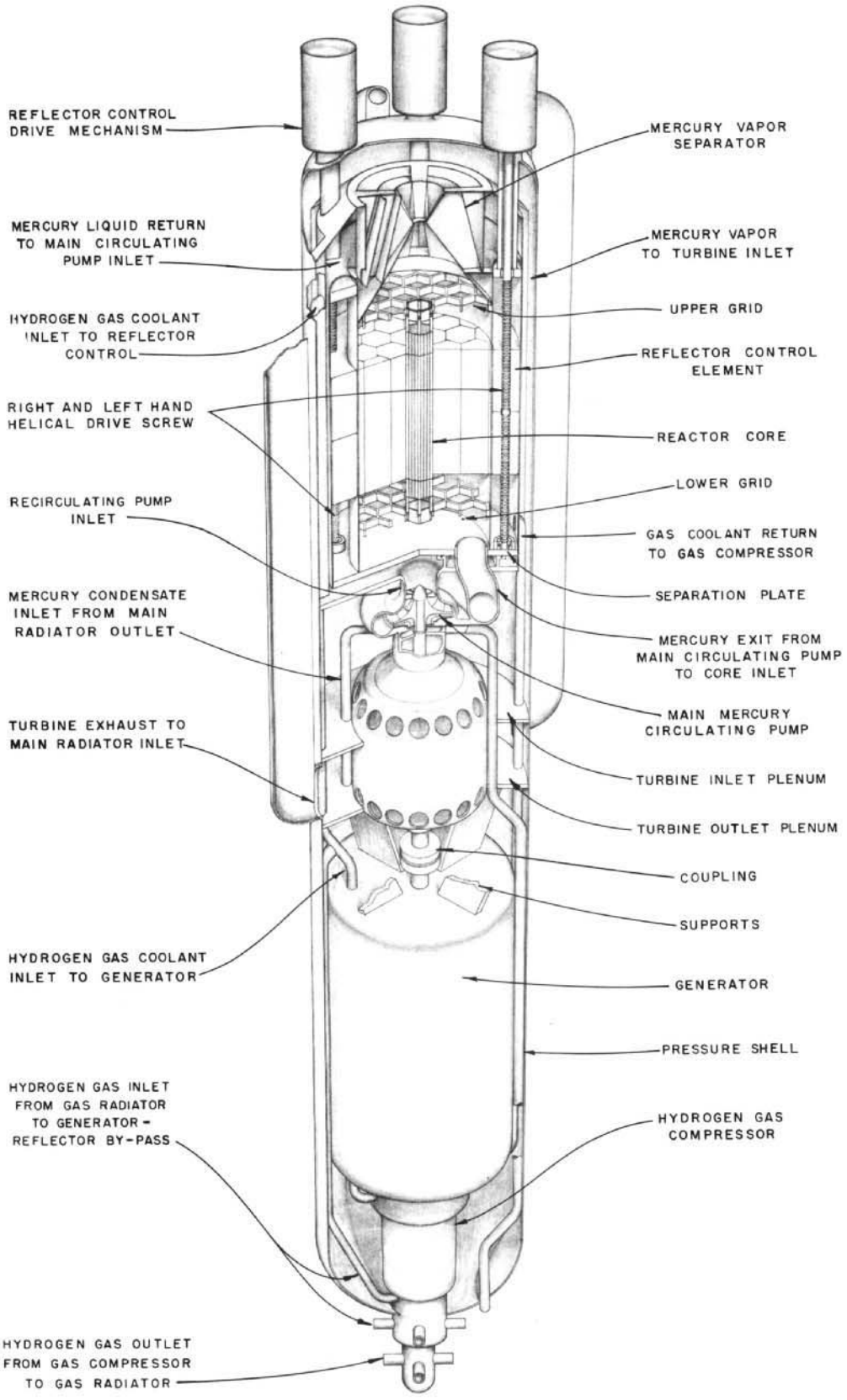

FIG. O-2
PICTORIAL OF LUNAR REACTOR

1-0 REACTOR

The significant numbers pertaining to the reactor are as follows:

Core diameter	41 cm
Core length	41 cm
Critical mass	492 kg
Enrichment	35.6%
Power density	150 kw/l (core vol)
Heat transfer surface	1.495×10^5 cm^2
% voids at full power	73%
Speed of mercury entering core	50.5 cm/sec
Reactivity worth of reflector	17%

A fast reactor with boiling mercury as the coolant appears to have the best combination of nuclear and thermal characteristics.

These characteristics are high power density, the ability to maintain an acceptable ratio of η/η_0 during two years of continuous operation, good reason to believe that it has dynamic stability, the lack of a requirement for any moderator or shielding, and the apparent ability to be controlled by the movement of a reflector encircling the shell.

Mercury was chosen as the coolant because it is the only liquid metal that has been used successfully for long periods of time in a direct, two-phase Rankine cycle. A steel containing 5% chromium and $\frac{1}{2}$% molybdenum is chosen for all surfaces in contact with mercury because there are years of experience to substantiate the fact that there will be no deteriorative effects occasioned by these two metals in contact at the temperatures which exist throughout the cycle.

The structural features of this reactor are quite similar to EBR-I Mark III, and, therefore, there is good reason to believe that it will be dynamically stable.

There is no moderator because it is a fast reactor.

Shielding shells may be transported to the moon. They would be filled with lunar soil if shielding is required for the reactor portion. Since the plant is to be fully automatic and discarded at the end of its usefulness, it is proposed to place it behind a hill or in one of the moon craters.

Calculations indicate that the cylindrical shell reflector surrounding the core will give satisfactory control characteristics.

The only maintenance contemplated is the addition of wetting agents to the mercury as needed and facilities for repairing holes in the radiator. These holes may be caused by meteoroids.

Cross sections of the power plant without the radiators are shown on Figs. 1-1 and 1-2.

The mercury coolant is pumped upwards through the core, where boiling takes place. The liquid-vapor mixture is separated in two arc separators (Fig. 1-3) above the core and the vapor is discharged to the turbine system. The liquid is returned to the recirculating pump.

The choice of materials for the plant and coolant was based on using a reactor core which can be built with existing technology without any extensive development program. Certainly other materials can be used for core construction, and advanced technology with materials capable of withstanding higher temperature could lead to substantial weight savings. The use of two arc separators is based on the work of Babcock and Wilcox[1] in separator tests. These separators appeared to have the maximum capacity of any of the separators tested.

Baffling is provided at the core inlet to distribute the flow in the inlet plenum. No orificing is provided at the core inlet since calculations indicate that no parallel flow instabilities will exist.

1-1 Mechanical Design

a. Core

The core is assembled into an annular frame which includes an upper and lower grid section, and a mercury separator at the upper end. The separator performs the function of separating the mercury vapor from the unvaporized mercury liquid and channeling the fluids into the proper flow passages, the vapor to the turbine inlet and the liquid to the circulating pump inlet.

The assembly is done as follows: The annular frame, liquid mercury passages, separator, ellipsoidal head, and upper grid are welded together, and the assembly is placed so that the grid and separator are in a down position. The hexagonal fuel assemblies are then inserted, starting at the center and working outward, then followed by the six segmental fuel subassemblies. The upper grid is then inserted and tack welded or brazed into place. The reflector control elements are then assembled with their

associate components. The entire core section is then closed by welding a separation plate above the upper grid. Projecting from the separation plate are a series of spacers which engage the ribs of the grid, thus providing additional support for the core assembly. The upper section of the outer shell is then welded in place, thus enclosing the entire reactor section. The remainder of this outer shell will be welded in place after all of the power plant package is assembled and tested. This completes the assembly of the reactor section.

b. Fuel Subassemblies

The basic fuel rod is similar to the EBR-I fuel rod except for modified end plugs and the use of 5% chromium, ½% molybdenum alloy tubing for cladding. This alloy was selected over the EBR-I zirconium tubing because of the proven corrosion characteristics of this alloy in mercury, which is backed up by 20 years of use in the General Electric Company's mercury-cooled power plants. The end plugs were redesigned to save weight and to facilitate manufacture. The basic fuel rod is a tube, 54.6 cm long with a 0.84-cm outer diameter and a 0.03-cm thickness. This tube contains a matrix of uranium carbide and 356.5 gm of 35.6% enriched uranium. This matrix is 0.76 cm in diameter by 40.6 cm long.

There are two types of subassemblies (see Figs. 1-4 and 1-5), of which 19 are hexagonal in shape and contain 61 fuel rods per assembly. The second type is segmental in shape and contains 37 fuel rods per assembly; 6 assemblies of this type are required. Thus the core contains a total of 1381 fuel rods with a total of 492 kg of 35.6% enriched uranium. The unit fuel subassemblies are not canned, but are assembled into end grids and made secure by a series of hexagonal head bolts which pass through the grid corners into tapped holes in the corner fuel rod end plugs. Thus a more uniform flow distribution is obtained and a weight saving is effected by the omission of the canning. As in the EBR-I design, each fuel rod contains three spacers to insure uniformity of flow passages and stability under dyanmic flow conditions.

c. Reflector Control

The annulus directly around the core is divided by four stringers, thus providing space for the four control-reflector elements. These elements are stainless steel or iron, each approximately 7.6 cm thick by 40.7 cm long, and each fills one-quarter of this annular area. These elements are split horizontally and are actuated by four lead screws, each of which has a right and left-hand thread. When energized by the four servo motors at the upper end of the power plant, the reflector elements move outward or inward as the need arises, thus effecting the necessary control. These reflector elements contain holes for cooling, which is provided by inlets for hydrogen gas in the upper end of the annulus.

d. Mercury Flow Passages

The mercury flows up through the core and into a separator where approximately 10% in vapor form goes to the turbine through annuli created by dividers between the outer part of the annular frame and the inside of the outer shell. The four other parts of the annulus thus formed serve as downcomers to the recirculating pump for the liquid mercury. The turbine discharges mercury vapor into a plenum from which the vapor goes to the radiator. The four radiator condensate return lines re-enter the shell at the lower end and are piped upward to the condensate pump.

e. Hydrogen Gas Flow Passages

The cool gas from the radiator enters the shell by four inlet ducts located in the upper part of the extension at the lower end of the shell, and then is ducted into the reflector control area and into the generator. The gas from the reflector area and the generator goes to the inlet side of the hydrogen gas compressor. It leaves the compressor through four outlets located in the extension of the shell and goes to the radiator.

f. External Features

The reactor plant is supported in a vertical position by a cylindrical extension below the pressure vessel. Gussets extending from the gas plenum extension to this cylinder provide additional stiffening. In the case of the foldout radiator (see Fig. 4-11) the cylindrical extension terminates in a 7.6-cm thick by 213-cm diameter base. The supporting elements are all made of structural magnesium.

In the case of the wrap around radiator (see Fig. 4-13), the cylindrical column is divided into two sections which contain bearings to permit the reactor plant to rotate as the radiator is unwrapped.

Adjacent to the mercury vapor outlet risers are a series of hinge components to which the radiator sections per Fig. 4-11 are assembled. These are not used for the radiator per Fig. 4-13, nor are the risers. A conventional tubular riser is used for the radiator per Fig. 4-13.

1-2 Heat Transfer

Significant numbers pertaining to heat transfer in the core are as follows:

Coolant	Hg + 0.02% Mg + 0.0001% Ti
Reactor Power	8.15 Mw
Inlet Velocity	50.5 cm/sec
Total Flow Rate	940,000 kg/hr
Pump Head Required at Full Flow	147 cm Hg
Average Exit Quality	11.7%
Average Exit Vapor Volume Fraction	94.5%
Average Heat Flux	54.3 watts/cm^2
Maximum Heat Flux	122 watts/cm^2
Maximum Uranium Temperature	648°C
Core Heat Transfer Area	1.495×10^5 cm^2
Core Flow Area	4.2×10^2 cm^2
Equivalent Diameter	0.361 cm

The most important consideration in the heat transfer characteristics of boiling mercury appears to be that of insuring the wetting of the heat transfer surface with the mercury. Practices at the South Meadow Generating Station of the Hartford Electrical Light Co. and the Schiller Station of Public Service of New Hampshire have indicated that this can be achieved by adding 0.35 ppm of titanium and 50-70 ppm of magnesium. The importance of this addition on the heat transfer characteristics of boiling mercury is borne out by the published literature on heat transfer to boiling mercury. Lyon et al.[2] presented data taken at atmospheric pressure for pure mercury and for mercury with 0.02% magnesium and 0.0001% titanium. The data were taken for boiling from a 1.9-cm OD horizontal stainless steel tube. The results with pure mercury suggested that the heating surface was not wetted by the mercury. The data indicated that the mercury was in film boiling over the entire range of heat fluxes tested. Data were also taken for mercury with magnesium and titanium additions at heat fluxes up to 31.5 watts/cm^2. There was no indication of an approach to a transition in the boiling mechanism.

Kutateladze et al.[3] summarizes the results of the investigations of the boiling properties of mercury and mercury amalgams in the USSR. The experiments of Korneev and Styrikovich, Semenovker, and Sorin are reported. The experiments of Styrikovich were with pure mercury, those of Korneev with mercury with magnesium added. Data for the critical heat flux as a function of magnesium concentration were presented. The maximum heat flux achieved was 43.5 watts/cm^2 with 0.05% magnesium.

Bonilla[4] presented data for a boiling mercury amalgam with 0.02% magnesium and 0.0001% titanium additions. The maximum heat flux in the experiments was 63 watts/cm^2. Again, there was no evidence of a transition in the boiling mechanism. An equation for the wall superheat as a function of heat flux and pressure was presented:

$$\Delta T = 0.22 \frac{(q'')^{0.435}}{P^{0.29}} \quad , \qquad \text{Eq. 1-1}$$

where ΔT is in °F, q" in Btu/(hr)(ft^2), and P is in psia (see Section 1-5, Nomenclature). American Standard[5] presented some preliminary experimental data for the vertical upflow of mercury, with magnesium and titanium additions. Heat fluxes up to 189 watts/cm^2 were observed at 2.24 atm. No indication of a change in boiling mechanism was observed. It was concluded that design heat fluxes of at least this high were entirely feasible at 11.6 atm. These tests were run in natural circulation with exit vapor volume fractions approaching 99%. They were apparently able to maintain steady conditions.

The results from the experimental investigations indicate that mercury boils as a normal fluid if additions are made so that the mercury wets the surface. If this is true, then the boiling theory that has been developed for other fluids can be applied to mercury. The theory of Zuber,[6] which considers the stability of a liquid-vapor interface, has been applied with success to predicting the critical heat flux for pool boiling of saturated liquids. Kutateladze[7] arrived at a similar equation from empirical considerations and suggested that it be used as a design formula, since forced flow of the liquid past the heating surface would increase the work necessary to form a continuous vapor film, and increase the value of the critical heat flux. The equation of Zuber,

$$q'' = \frac{\pi h_{fg}}{24} \rho_g \left[\frac{\sigma g (\rho_f - \rho_g)}{\rho_g^2} \right]^{1/4} \left[\frac{\rho_f}{\rho_f + \rho_g} \right]^{1/2} \quad , \qquad \text{Eq. 1-2}$$

gives, in any consistent set of units, the critical heat flux under lunar conditions to be

$$q'' = 221 \text{ watts/cm}^2 \quad .$$

While the foregoing arguments are by no means conclusive, it appears that the maximum design heat flux of 122 watts/cm^2 is a conservative value.

The limiting condition for the LP-1 core then becomes the fuel element centerline temperature. The results of fuel element irradiation experiments[8] indicate the U-2 w/o zirconium fuel pins are stable to at least 0.6 a/o fuel alloy burnup, provided the alpha-beta transition temperature (665°C) is not exceeded. Therefore, this temperature has been set as a limit on fuel element temperature. The thermal calculations were based on the following assumptions:

(1) Boiling film temperature differences were calculated by means of the equation of Bonilla.
(2) All heat is generated within the fuel alloy.
(3) There is no axial heat conduction.
(4) Uniform heat generation is maintained in the fuel pin.

The following hot channel factors were used in the thermal analysis:

	F_{θ_f}	F_{θ_c}	F_{θ_b}	F_{θ_u}
Uncertainty in Neutron Flux	1.05	1.1	1.1	1.1
Deviations from Nominal Dimensions	1.01	1.06	1.02	1.02
Inhomogeneity of Fuel Alloy	1.00	1.01	1.01	1.01
Thermal Conductivity	1.00	1.10	1.00	1.10
Film-temperature Drop	1.6	1.00	1.00	1.00
Precision of Measurement of Power Level and Transient Overloads	1.04	1.1	1.1	1.1
Overall Engineering Hot Channel Factors	1.77	1.43	1.25	1.37
Overall Nuclear Factor	1.8	1.8	1.8	1.8
Overall Total	3.2	2.58	2.25	2.47

The hot channel factors given here should be considered in the nature of specifications that the design must meet. The philosophy of using a hot channel factor assumed that all of the "hot spots" occur at the same place at the same time. This stipulation is necessary because of the nature of the plant and the need for reliability.

The procedures for a hydraulic analysis of a core of this type are well developed.[9] In the reactor system at steady-state conditions, the

condition is that $\oint dP = 0$ around the closed pump loop. This equation can be written as

$$\frac{V_c^2}{2g_c}\left[\sum N_1 + N_2 + N_3 + N_4 + N_5 + N_6 + N_7 + N_8\right]$$

$$- \frac{g}{g_c} z_{fg} (\rho_f - \bar{\rho}_{fg}) - \frac{g\ell_r}{g_c} (\rho_f - \rho_{fg}) - (\Delta P/\rho_f) = 0 \quad , \qquad \text{Eq. 1-3}$$

where

$$N_1 = f \left(\frac{\ell}{D}\right)\left(\frac{\rho_{f'}^2 A_c}{\rho_f A_d}\right)$$

N_1 - Frictional resistance in downcomer and external piping.

$$N_2 = \frac{\rho_{f'}^2}{\rho_f}\left(1 - \frac{A_c}{A_d} + K\right)$$

N_2 - Acceleration of fluid and frictional losses at the contraction from lower plenum to the heated section.

$$N_3 = \frac{\rho_{f'}^2}{\rho_f}\left(\frac{f}{D_c}\right) z_f$$

N_3 - Frictional resistance in the nonboiling segment of the heated core and reflector.

$$N_4 = 2(\Psi)\, \rho_{f'}^2$$

N_4 - Acceleration of fluid due to formation of vapor in the heated channel.

where

$$\Psi = \frac{(1 - X_3)^2}{(1 - \alpha_3)\rho_{f'}} + \frac{X_3^2}{\alpha_3}\frac{1}{\rho_g} - \frac{1}{\rho_{f'}}$$

$$N_5 = \rho_{f'} \bar{\bar{R}} \left(\frac{f}{D_c}\right) z_{fg}$$

N_5 - Frictional resistance in the boiling segment.

$$N_6 = 2\rho_{f'}\left(\frac{A_c}{A_p}\right)\left[X_3^2\frac{\rho_f}{\rho_g}\left(\frac{A_c}{A_p\,\alpha_p} - \frac{1}{\alpha_3}\right) + (1 - X_3)^2\right.$$

$$\left.\left\{\frac{A_c}{A_p\,(1-\alpha_p)} - \frac{1}{1-\alpha_3}\right\}\right]$$

N_6 - Pressure change due to expansion from the core.

$$N_7 = \frac{\rho_f^2}{(1-\alpha)\,\rho_{f'} + \alpha\,\rho_g}\left(\frac{A_c}{A_s}\right)^2$$

N_7 - Pressure loss across stream separator.

$$N_8 = \rho_{f'} R\left(\frac{\ell_r}{D_r}\right) f$$

N_8 - Frictional resistance in upper reflector.

Equation (3) can be solved for the pump head requirement. By expressing ΔP as $-K(V_{c_1}^2/2g)$, the equations can be solved for the natural-circulation velocity in the reactor during startup conditions.

The two-phase friction factor multipliers, R and $\overline{R}$, can be calculated from the following equations:

$$R = 1 + \left(1 - \frac{\rho_g}{\rho_{f'}}\right)\frac{\rho_{f'}}{\rho_g}\,X \qquad \text{Eq. 1-4}$$

$$\overline{R} = \frac{1}{z_{fg}}\int_0^{z_{fg}} 1 + \left(1 - \frac{\rho_g}{\rho_{f'}}\right)\frac{\rho_{f'}}{\rho_g}\,X \quad . \qquad \text{Eq. 1-5}$$

Kutateladze[3] states that on the basis of the work of Gremilov these equations have an accuracy of $\pm 20\%$ for the vertical upflow of mercury.

Figure 1-6 gives the vapor volume fraction from the core exit as a function of reactor power during natural circulation. Since the power required to run the pumps at full flow is only 4.6 kw, or a reactor power of 22 kw(th), the system should operate stably under startup conditions. The maximum vapor volume fraction has been set at 0.70. This fraction corresponds to a mean reactor power of 510 kw and is more than adequate to operate the auxiliary systems.

Since in a vertical upflow boiling system the velocity of the vapor is considerably higher than the velocity of the liquid, it is necessary to have a generalized correlation of vapor volume fractions, velocity ratio, velocity difference, or experimental data at the conditions of interest. One of these conditions is necessary in order to predict the mixture density in

the core. The data of Kutateladze[3] were used for this prediction. The results are shown in Fig. 1-7. This curve gives the average axial density distribution in the core of the LP-1 plant. These volume fractions of vapor are considerably higher than are normally run in a boiling reactor. The large amount of Δk in the voids raises the problem of reactor instability due to void oscillations because of variations of flow pattern. Should this be a problem, it will be necessary to increase the pumping rate to reduce the volume fraction, and also to orifice to maintain this low volume fraction across the core. The use of these high void fractions will be dependent upon experimental verification.

No orificing was used at the channel inlets because it is not necessary to maintain low temperatures of the fuel elements. Since the hydrostatic head and entrance effects can be neglected, the analysis of Ledinegg was used.[10] The condition of stability is that the curve for pressure drop for the core channels be single valued. The condition for the onset of instability is that

$$\frac{d\Delta P_c}{dW} = 0 \quad .$$

This can be reduced to the single criterion that

$$\Delta h_{c1} \leq \frac{AB}{A + \frac{1}{g_c} - \sqrt{\frac{3A}{2}\left(\frac{A}{2} + \frac{1}{g_c}\right)}} \qquad \text{Eq. 1-6}$$

where

$$A = f\ell_c/2g_c\, D_c$$

and

$$B = (v_f/v_{fg})\, h_{fg}$$

if the system is to be stable. The value for the core entrance condition is 244 (watt)(sec)/gm. The operating value for the LP-1 is 23.3 (watt)(sec)/gm; therefore, the system should not exhibit parallel channel instability. This does not preclude the occurrence of other types as mentioned previously.

1-3 Nuclear Considerations

a. Cross Sections

The eleven-group cross section set of Loewenstein and Okrent[11] was used in criticality calculations. The cross sections employed for mercury were those prepared by American Standard[12] for use with this set of cross sections.

b. Buckling

Values of the buckling B^2 as obtained by diffusion theory and by asymptotic transport theory for the LP-1 core are given in Table 1-1. Also given is the ratio of B as calculated by asymptotic solution of the Boltzmann equation to that calculated by diffusion theory. This ratio is approximately the same as that by which diffusion theory overestimates the core radius.

Table 1-1

BUCKLING VALUES FOR LP-1 CORE

Vol % (U^{235} + U^{238}) = 47.7		Vol % Fe = 20.6	
Vol % U^{235}	Vol % Hg (ρ = 13.6 gm/cm^3)	B^2 x 100, cm^{-2} (Diffusion theory)	$\frac{B(\text{Transport theory})}{B(\text{Diffusion theory})}$
15.0	0	0.775	1.032
20.0	0	1.028	1.050
25.0	0	1.262	1.062
15.0	31.7	1.013	
20.0	31.7	1.393	1.030
25.0	31.7	1.745	1.040

c. Reactivity Calculations

One-dimensional diffusion theory calculations have been used thus far in analysis of LP-1. For accurate study of the reflector control, two-dimensional calculations would be required, but this did not seem to be justified at the present stage of the study. The error in diffusion theory for this size of reactor, as indicated in Table 1-1, is sufficiently large that one would prefer a transport theory calculation, but acceptable results can probably be obtained by adjusting diffusion theory.

The exact value of fuel enrichment is not important at the present stage of the study, and no adjustment has been made in the present work.

One-dimensional calculations in cylindrical geometry have been carried out for the following problem specifications:

Problem 1 Core
47.7 vol % fuel (U^{235} + U^{238})
20.6 vol % iron
31.7 vol % void
Radius 20.4 cm

Reflector 100 vol % iron
Outer radius 31.0 cm (including extrapolation distance of 3.1 cm).

Equivalent bare height 53 cm (actual core height 40.6 cm).

Problem 2 — Same as Problem 1 except that void in core is filled with liquid mercury (ρ = 13.6 g/cm^3).

The following results were obtained from these problems:

The critical concentration in Problem 1 was calculated to be 19.4 vol % U^{235}, and the radial buckling was 0.0065 cm^{-2}.

The critical concentration in Problem 2 was calculated as 16.5 vol % U^{235}, and the radial buckling was 0.0078 cm^{-2}.

The difference in reactivity for the same U^{235} concentration in these problems was 8.0% k. For hot liquid mercury (ρ = 12.5 g/cm^3) relative to the voids, the difference would be 7.3% k.

This calculation is not very satisfactory since it does not give accurately the worth of mercury at the upper and lower core boundaries, where the worth is a maximum.

The reactivity worth of the reflector was calculated for both cases by calculating the critical buckling for a bare reactor. For the case of no mercury, a radial extrapolation distance of 3.3 cm was used. The total worth of the reflector was found to be 17% k. In the case of the mercury-filled core the extrapolation distance of the bare core was calculated to be 2.2 cm. The reflector in this case was found to be worth 12.5% k. In the normal operating condition the core will contain mostly voids (see Fig. 1-7), which indicates the effective worth of the reflector should be closer to 17% than to 12.5%. A value of 15% will be assumed for the total worth.

The radial maximum-to-average power distribution for the case of complete voids is 1.42. For no voids the value of the ratio of maximum to average is greater, but the void case is the one of interest here. The axial maximum is 1.24, which results in a combined maximum-to-average value of 1.76.

Under actual operating conditions there will be an axial distribution of voids as given in Fig. 1-7. One-dimensional calculations in slab geometry were performed in the axial direction to evaluate the worth

of voids and the power distribution. For these calculations the core height was taken to be 40.6 cm, and the top and bottom reflectors to be 10 cm thick. These reflectors were assumed to be 68.3 vol % steel and 31.7 vol % coolant space.

In Problem 3, the coolant space in core and axial reflectors was assumed filled with hot mercury (ρ = 12.8 g/cm^3). An extrapolation distance of 2.9 cm was used at the outer boundary of upper and lower reflectors.

In Problem 4 the axial mercury density distribution was assumed to be that given in Fig. 1-7. In this case the extrapolation distance at the top of the upper reflector was 5.0 cm. In both problems the radial buckling was assumed to be 0.0060 cm^{-2}, which, as seen from Problems 1 and 2, is too low. The difference in reactivity between a core filled with hot liquid mercury and a core with the void distribution shown in Fig. 1-7 was calculated to be 7.6%. This value is an overestimate because the effectiveness of the radial reflector actually varies with the void content of the core in such a way as to reduce the reactivity difference. In Problem 1 (all liquid) and Problem 2 (all vapor) in the coolant space, the radial buckling was found to be 0.0078 and 0.0065 cm^{-2}, respectively. This change in radial buckling corresponds to a 2 vol % change in U^{235} concentration, or about 5% k. Since there is still some liquid in the reactor during operation, this change is an overestimate of the correction. Assuming the correction to be 3% to 4%, the reactivity in voids is approximately 4%. This figure is evidently a crude estimate which needs to be refined by doing two-dimensional calculations before a dynamic analysis can be carried out. As already noted, the one-dimensional calculations in cylindrical geometry for complete void as compared to hot liquid mercury gave a reactivity difference of 7.3%. An estimate of 5% Δk is based on the calculated per cent of vapor by weight at operating conditions.

The reactivity held up in voids is sufficiently large that there is the possibility of exceeding prompt criticality through fluctuation. This condition would be much more serious in the proposed fast reactor than in a water-moderated thermal reactor, since the fast reactor could have a period of the order of microseconds. Under these conditions, accidents could occur, in which there would not be time for the shutdown mechanism of formation of coolant vapor to act.

From the flux distribution obtained in the axial problem with voids a rough estimate of the change in reactivity with motion of the reflector has been made. A one-group perturbation theory treatment was used with the worth of the reflector at any axial position assumed proportional to the square of the axial flux. This involves the assumption that the effect of the reflector opposite any axial position is to alter the transverse leakage at that position, this leakage constituting an effective absorption.

The results of this calculation are given in Fig. 1-8, where the fractional reflector worth removed is given as a function of the distance that the two halves of the reflector have each moved from the closed position at the center. The total worth of the reflector is estimated to be about 15% k, and 68% of this, or about 10% k, is estimated to be removed when the reflector is in the full-open position of a 24-cm separation of the halves (see Fig. 1-1). This should be sufficient to take care of reactivity in voids, temperature coefficient, burnup, and shutdown. Thus, on the basis of rather crude and preliminary calculations, the reflector control as proposed here appears feasible unless the reactivity held in the voids has been significantly underestimated.

With the metal fuel element assumed to be used, there is no difficulty in incorporating sufficient U^{235} to achieve criticality and, in fact, the fuel alloy volume could be reduced if necessary. With a ceramic or cermet fuel element the situation would be different, and trouble might be encountered in obtaining a high enough fuel concentration for this small a reactor.

1-4 Reactivity Variation

This reactor is designed to operate at full power for two years. Enough excess reactivity was initially designed into it and held in reserve in the form of reflector position so that it should remain critical over the period of operation.

The isotopic content of the fuel and the neutron flux are continually varying because of transmutation due to neutron capture in the isotopes existing at any instant and because of neutron leakage from the core. Since each isotope has a different set of cross sections, the flux and reactivity must vary with irradiation time in order to maintain a constant power in the reactor. This is an enriched uranium fuel; therefore, the reactivity will decrease with operating time. Theoretically, the reactivity would eventually increase if the life of the fuel rod were not limited by irradiation damage.

The variation of neutron flux and reactivity during the two years is considered to be represented by the following equations, the solutions of which are shown in Fig. 1-9. The nuclear constants used are shown on Table 1-2.

$$\phi(t) = \frac{K}{\sum \Sigma_f} \qquad \phi_0 = 0.5 \times 10^{16} \qquad K = 147$$

$$\eta = \frac{\nu \Sigma_f}{\Sigma_a}$$

$$d(FP)/dt = N - \phi(t)\,\sigma_a\,(F.P.) \qquad N = 4.56 \times 10^{18}$$

$$\frac{d\,U^{235}}{dt} = -\phi(t)\,\sigma_a\,U^{235}$$

$$\frac{d\,U^{236}}{dt} = \phi(t)\,(\sigma_c\,U^{235} - \sigma_a\,U^{236})$$

$$\frac{d\,U^{235}}{dt} = -\phi(t)\,(\sigma_c\,U^{236} - \sigma_a\,U^{237})$$

$$\frac{d\,Np^{237}}{dt} = \lambda U^{237} - \lambda\,Np^{237}$$

$$\frac{d\,U^{238}}{dt} = -\phi(t)\,\sigma_a\,U^{238}$$

$$\frac{d\,U^{239}}{dt} = \phi(t)\,\sigma_c\,U^{238} - \lambda U^{239}$$

$$\frac{d\,Np^{239}}{dt} = \lambda U^{239} - \lambda\,Np^{239}$$

$$\frac{d\,Pu^{239}}{dt} = \lambda Np^{239} - \phi(t)\,\sigma_a\,Pu^{239}$$

$$\frac{d\,Pu^{240}}{dt} = \phi(t)(\sigma_c\,Pu^{239} - \sigma_a\,Pu^{240})$$

$$\frac{d\,Pu^{241}}{dt} = \phi(t)\,(\sigma_c\,Pu^{240} - \sigma_a\,Pu^{241})$$

Table 1-2

NUCLEAR CONSTANTS

	$\sigma_f \times 10^{+24}$ (barns)	$\sigma_a \times 10^{+24}$ (barns)	$\sigma_c \times 10^{+24}$ (barns)	λ (sec^{-1})	ν
U^{235}	1.60	1.92	0.32		2.51
U^{236}	0.11	0.30	0.19		2.51
U^{237}		0.50		1.2×10^{-6}	2.51
U^{238}	0.05	0.20	0.15		2.51
U^{239}		0.20		4.9×10^{-4}	2.51
Np^{237}	0.32	0.15		1×10^{-8}	2.70
Np^{239}	0.90	0.15		3.42×10^{-6}	2.70
Pu^{239}	1.80	2.04	0.24		2.92
Pu^{240}	0.34	0.51	0.17		2.47
Pu^{241}	1.94	2.2	0.26		2.47
Pu^{242}	0.34	0.51	0.17		2.47
F. P.		2.00			

1-5 Nomenclature

A	Area
B	Buckling
C	Constant
cp	Specific heat
D	Equivalent diameter
F. P.	Fission products
f	Friction factor
g	Local gravity
g_c	Gravitational constant
h	Heat transfer rate, enthalpy
K	Loss coefficient
k	Reactivity

ℓ	Length
N	Fluid resistance
P	Pressure
q	Heat generation per unit volume
q"	Heat flux
T	Temperature
t	Time
W	Mass flow
V	Velocity
v	Specific volume
X	Vapor weight fraction
z	Length of fuel rod
α	Vapor volume fraction
η	Fast fission neutrons per thermal neutron capture
λ	Decay constant
ρ	Density
σ	Cross section, surface tension

Subscripts

a	Absorption
c	Core, capture
d	Downcomer
e	Exit
f	Liquid phase
f'	Saturated liquid phase
fg	Boiling phase; latent heat
g	Vapor phase
o	Inlet
p	Plenum
r	Riser
1, 2, 3, 4, 5, 6	Refers to position in the system (see Fig. 7-5)

1-6 Bibliography

1. Moyer, W. H., Final Report, Subcontract No. 534, Babcock and Wilcox Co. Report No. 5316.

2. Lyon, R. E., Froust, A. S., and Katz, D. L., Boiling Heat Transfer with Liquid Metals, Chemical Engineering Progress Symposium Series, 51, No. 17.

3. Kutateladze, S. S. et al., Liquid Metal Technology, Supplement to Atomnya Energia (1958), No.2.

4. Bonilla, C. F. et al., Pool Boiling Heat Transfer with Mercury, Reactor Heat Transfer Conference, No. 1-2, New York, N. Y. (1956).

5. An Evaluation of Mercury-cooled Breeder Reactors, American Standard Report ATL-A-102.

6. Zuber, N., Hydrodynamic Aspects of Boiling Heat Transfer, AECU-4439 (June 1959).

7. Kutateladze, S. S., Heat Transfer in Condensation and Boiling, Second Edition, AEC translation 3770.

8. Kittel, J. H. and Paine, S. H., Effects of High Burnup of Some Cast Uranium-Zirconium Alloys, Presented at the Winter Meeting of the American Nuclear Society, 1957.

9. Lottes, P. A., Petrick, M., and Marchaterre, J. F., Lecture Notes on Heat Extraction from Boiling Reactors, ANL-6063.

10. Ledinegg, M., Unstabilitat der Strömung bei Naturlichem und Zwangsomlauf, Die Warme, pp. 891-898 (1938).

11. Loewenstein, W. B. and Okrent, D., The Physics of Fast Power Reactors, A Status Report, Proceedings of the Second United Nations International Conference on the Peaceful Uses of Atomic Energy, Geneva (1958), Vol. 12, p. 16.

12. Evaluation of Mercury-cooled Breeder Reactors, American Standard Report, ATL 118 (1959).

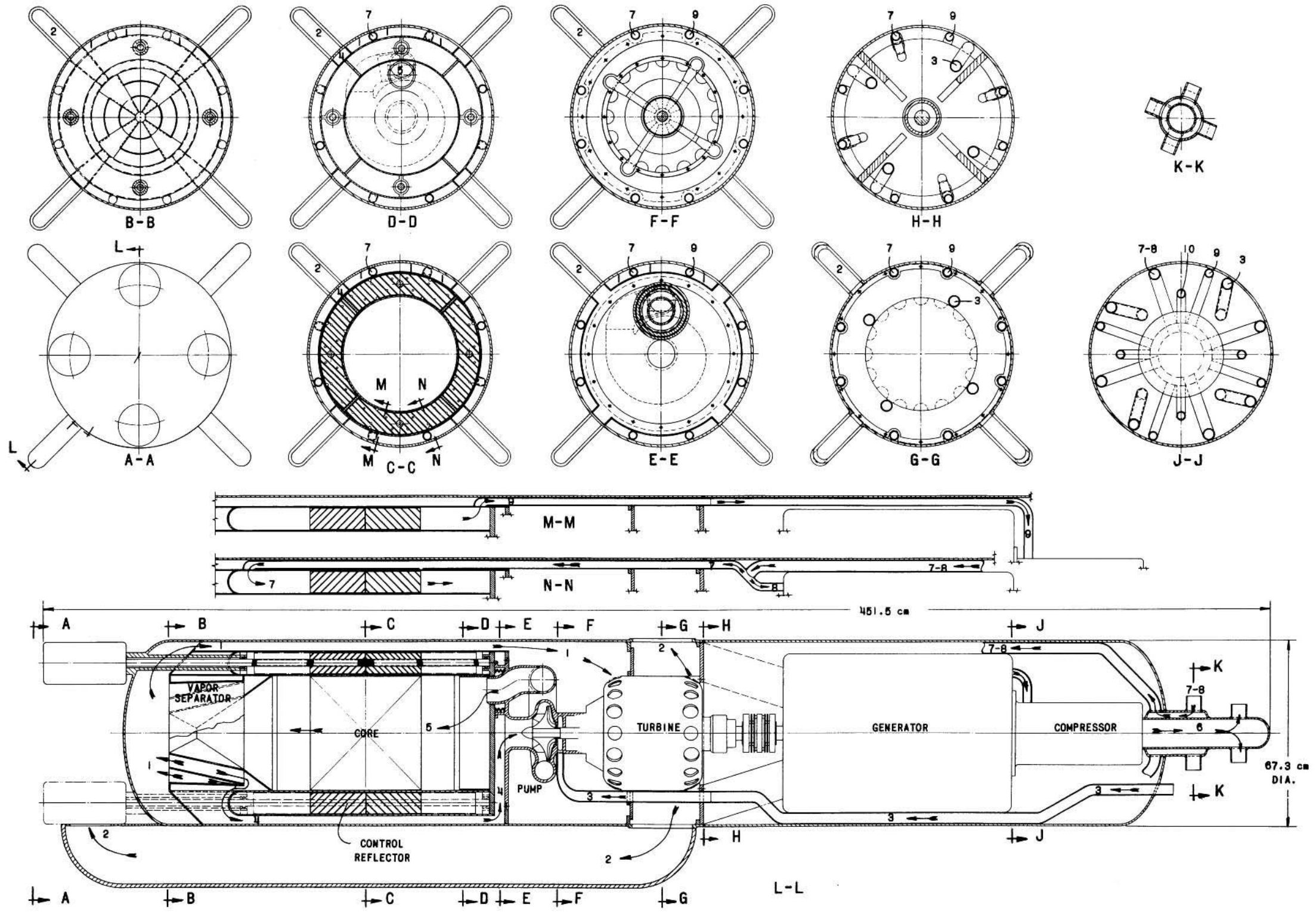

FIG. 1-1
REACTOR CROSS SECTION-VERTICAL

LEGEND

1 Hg VAPOR FROM REACTOR TO TURBINE INLET
2 Hg VAPOR FROM TURBINE OUTLET TO RADIATOR INLET
3 Hg CONDENSATE FROM RADIATOR OUTLET TO CONDENSATE PUMP INLET
4 Hg LIQUID FROM REACTOR TO CIRCULATING PUMP INLET
5 Hg LIQUID FROM CIRCULATING PUMP OUTLET TO REACTOR
6 GAS OUTLET FROM GAS COMPRESSOR TO GAS RADIATOR
7 GAS INLET FROM GAS RADIATOR TO REFLECTOR INLET
8 GAS INLET FROM GAS RADIATOR TO GENERATOR INLET
9 GAS OUTLET FROM REFLECTOR OUTLET TO GAS COMPRESSOR INLET
10 GAS OUTLET FROM GENERATOR OUTLET TO GAS COMPRESSOR INLET

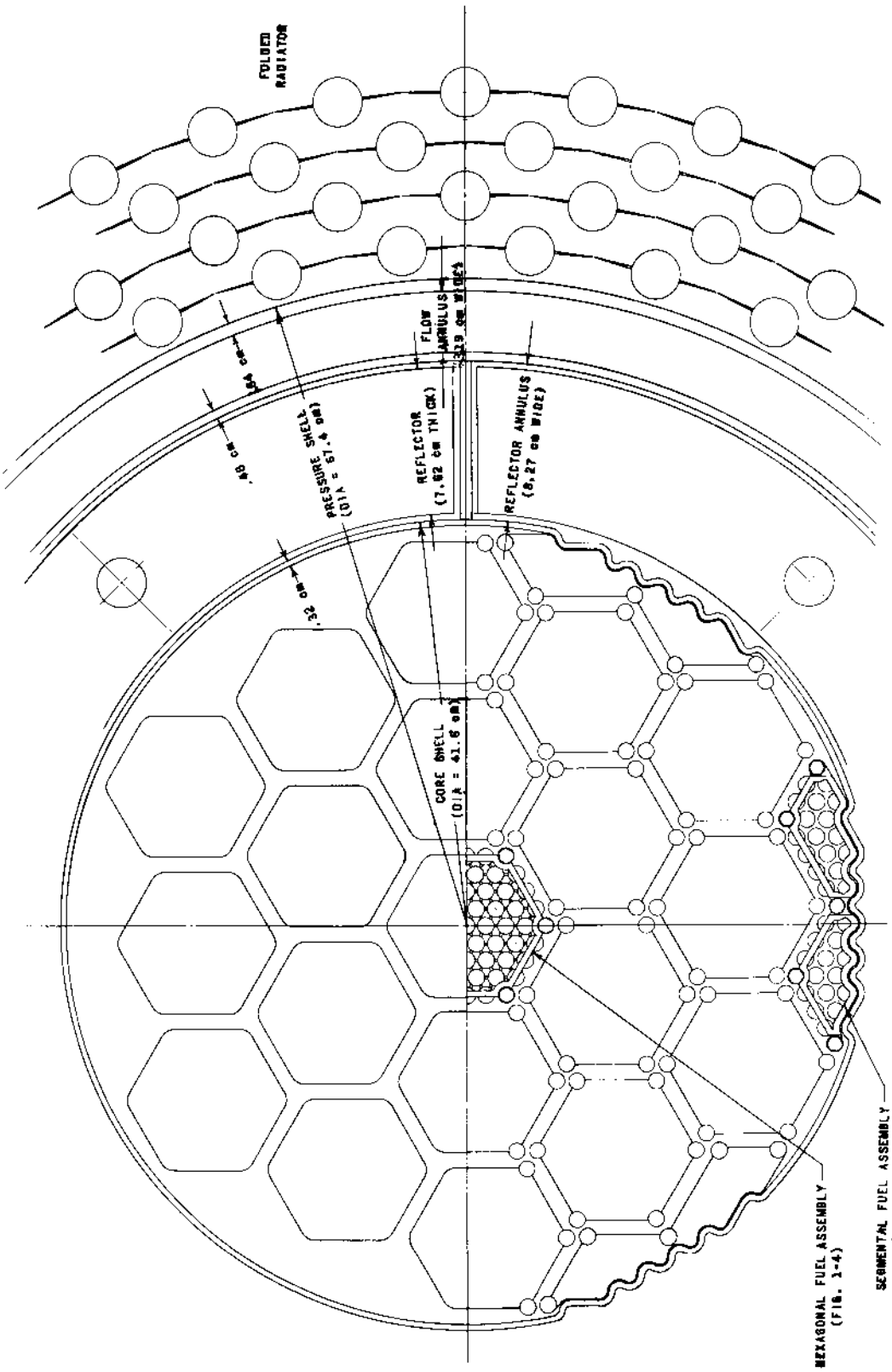

FIG 1-2
REACTOR CROSS SECTION -HORIZONTAL

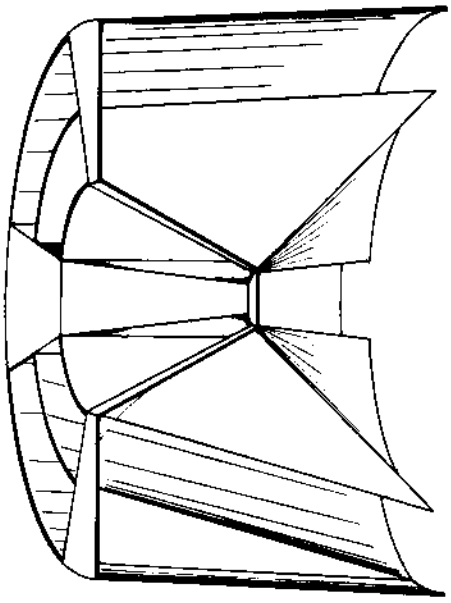

FIG. 1-3
MERCURY VAPOR SEPARATOR

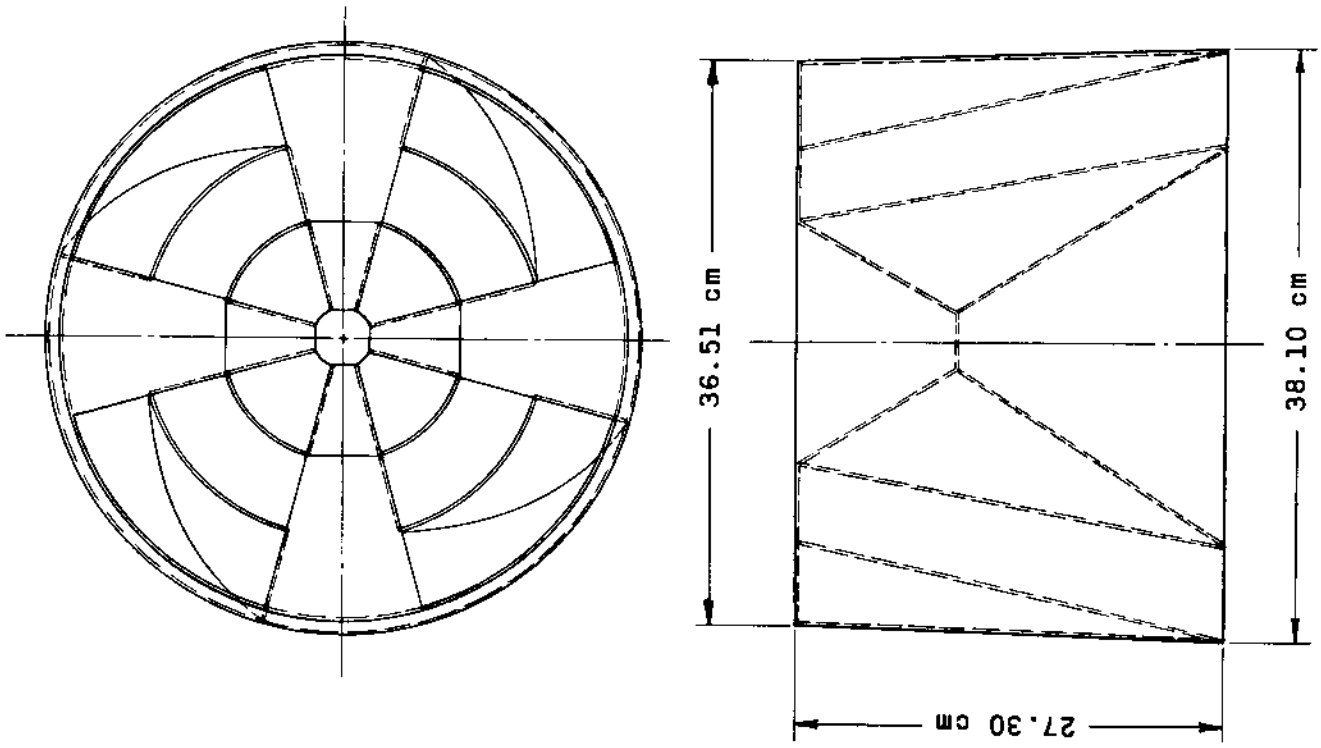

FUEL ASSEMBLY

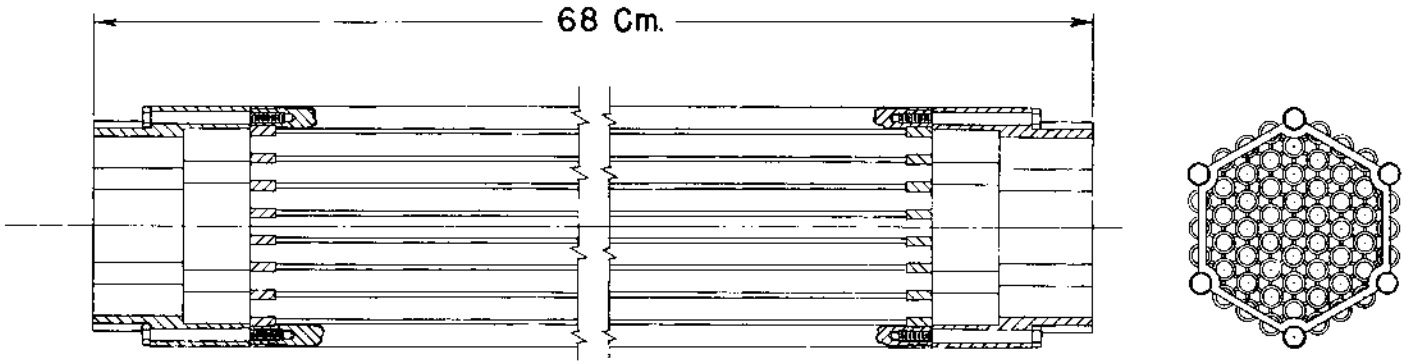

DATA

HEAT TRANSFER AREA	6604	Cm^2
EQUIVALENT DIAMETER	.361	Cm.
WEIGHT OF ASSEMBLY	30.32	Kg.
FLOW AREA	13.7	Cm^2
U235 IN ONE FUEL ROD	127.0	Gm.
U238 IN ONE FUEL ROD	229.4	Gm.

DETAILS OF SPACERS

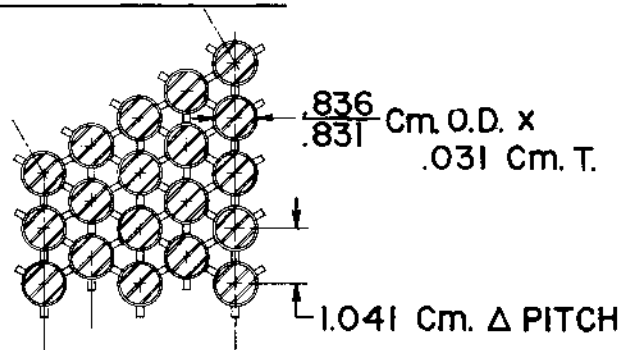

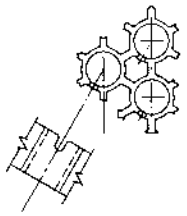

END REFLECTOR FUEL SECTION END REFLECTOR

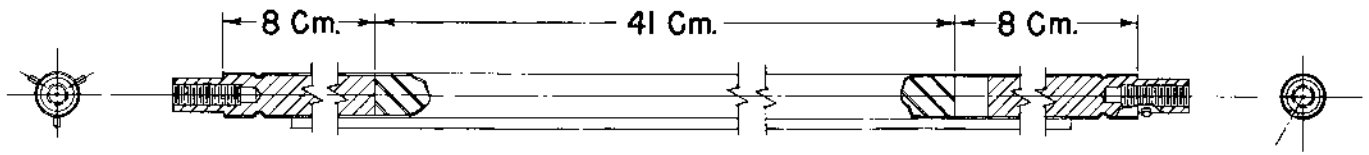

FUEL ROD DETAILS

FIG. I-4
FUEL ELEMENT SUB-ASSEMBLY
HEXAGONAL

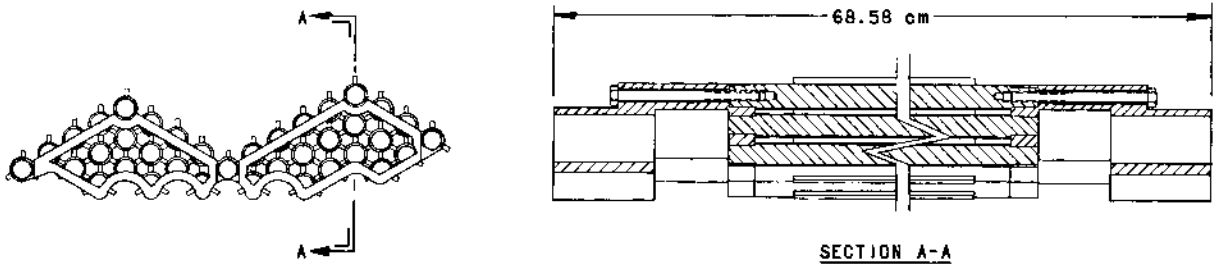

SECTION A-A
FUEL ASSEMBLY SEGMENT

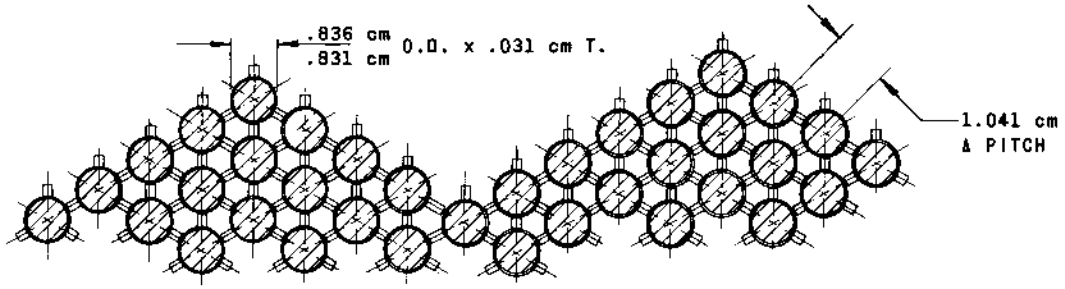

SECTION THROUGH CENTER OF ASSEMBLY

DATA

HEAT TRANSFER 4005 cm^2
EQUIVALENT DIAMETER .361 cm
WEIGHT OF ASSEMBLY 18.41 Kg.
U^{235} IN ONE FUEL ROD 127.0 Gm.
U^{238} IN ONE FUEL ROD 229.4 Gm.
MATERIAL 5% CHROME - 1/2 MOLY

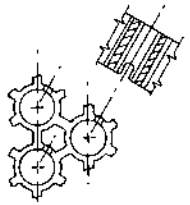

PARTIAL VIEW OF TUBE SHEET

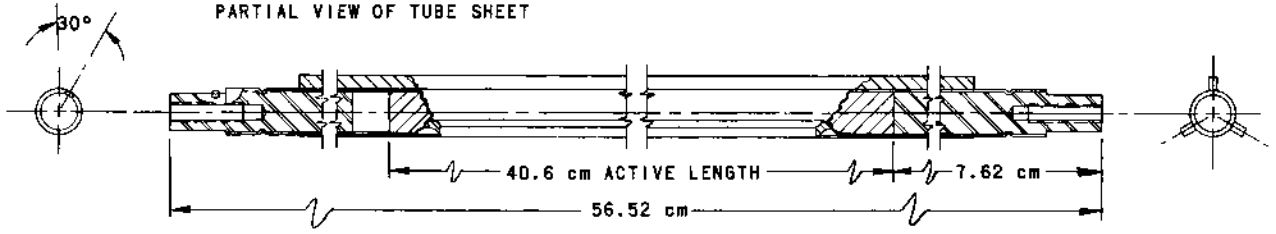

FUEL ROD

FIG 1-5
FUEL ELEMENT SUB-ASSEMBLY
(SEGMENTAL)

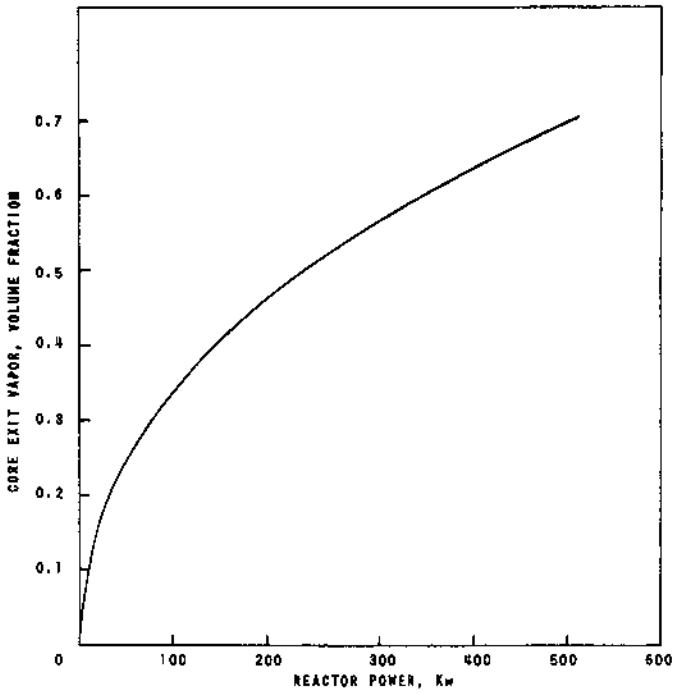

FIG. I-6
CORE EXIT VAPOR VOLUME FRACTION
AS A FUNCTION OF REACTOR POWER

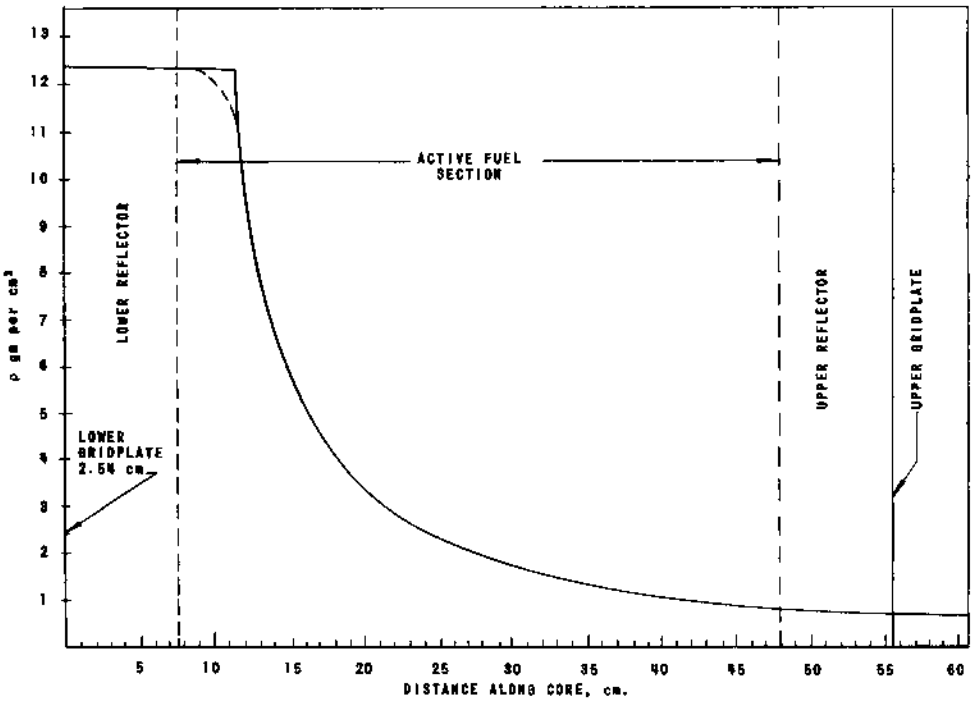

FIG. I-7
DENSITY DISTRIBUTION IN CORE

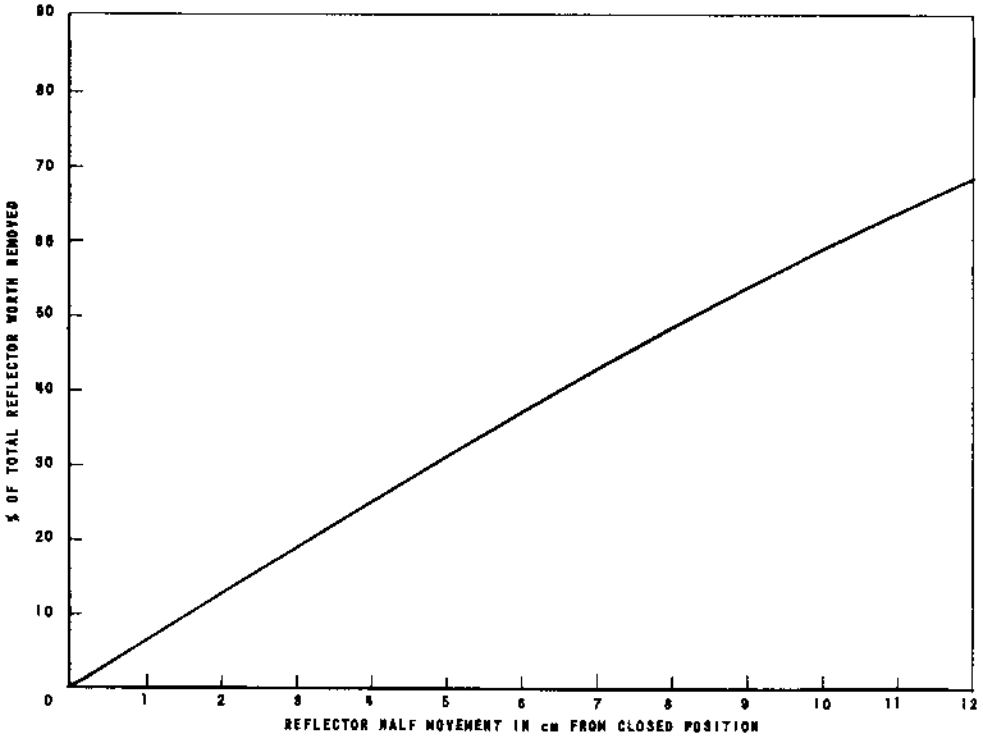

FIG. I-8
REFLECTOR WORTH VS. POSITION

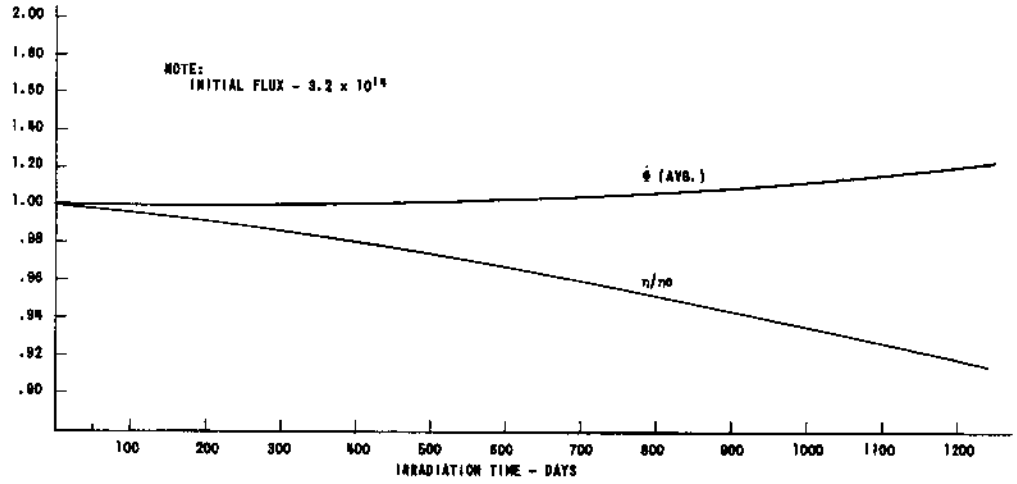

FIG. I-9
REACTIVITY & FLUX VS. IRRADIATION TIME

2-0 MERCURY VAPOR TURBINE

Turbine power	1100 kw
Speed	6000 rpm
Maximum blade speed	100 m/sec
Initial vapor pressure	11.9 atmos
Initial temperature	538°C
Exhaust pressure	1.29 atmos
Weight	250 kg

The type of turbine represented in this conceptual design is a two-pressure stage impulse turbine. There appears to be very little choice among this design, a single-stage impules, and a velocity stage machine. It is felt that there is a slight gain in using pressure staging for this application. The cross section of the turbine is shown on Fig. 2-1.

Each of a series of chambers formed by parallel disc-shaped partitions, called diaphragms, has a simple impulse turbine enclosed in it. All wheels are fastened to the same shaft. Each chamber receives the mercury vapor in turn through groups of nozzles placed on arcs.

The pressure drop is divided into as many steps as there are chambers, each being called a pressure stage. The resultant vapor velocity in each stage is relatively small, allowing reasonably lower blade velocities and preventing excessive loss by vapor friction. Figure 2-1 also shows the pressure and velocity of the mercury vapor as it flows through the nozzles and blade.

The Rankine cycle for this installation is shown on Fig. 2-2. From this cycle it is estimated that the thermal efficiency of the power plant is 12.2%. The temperature-entropy diagram is on Fig. 2-3.

The vector diagram in the blading and the details of blading are shown in Fig. 2-4.

The turbine and circulating pumps are preassembled and tested before final assembly into the power plant. The turbine and pump assembly is mounted into the annular casing and supported by the mounting plate which is integral with the pump volute. A mounting shoulder on the annular case mates with this mounting plate, and a metallic gasket between them provides the necessary seal. Socket head screws are used to tighten the assembly. The pump discharge pipe is inserted into an opening in the separation plate and sealing between them is accomplished by means of a bellows element on the pump discharge pipe and by a supplemental gas-filled "O" ring, also assembled to the extension on the pump discharge pipe. The turbine casing contains an integral ring which parallels a ring welded to the outer shell. Both rings are tapped for

assembly purposes. After the mounting plate on the pump volute is secured, a separation ring is assembled to the turbine ring. The shell ring thus provides an intake plenum for the mercury vapor. Here, also, sealing is accomplished by gaskets, and assembly by socket head screws. Similarly, the discharge plenum of the turbine is created by another separation ring which mates with a shoulder on the turbine case and a ring welded to the outer shell. Sealing and attachment is also accomplished in a like manner. This final separation plate also contains mounting brackets for the generator. The generator is then mounted to these brackets. Misalignment between the turbine output shaft and the generator input shaft is corrected by a mechanical coupling. Finally, the hydrogen compressor is assembled to the output shaft of the generator. The entire power package can then be pretested. The final step is to weld the lower section of the outer shell into place.

2-1 The Rankine Cycle

The flow of working medium and the power required by the machinery operating in the Rankine cycle (see Fig. 2-2) are:

Turbine power	1100 kw
Flow of mercury vapor through the turbine	24 kg/sec
Recirculating pump power	10 kw
Condensate pump power	3 kw
Heat required from the reactor	8.15 Mw
Heat rejected	6.06 Mw
Cycle efficiency	12.2%

2-2 Nozzles and Blading

The following assumptions were made (see Section 2-5, Nomenclature, for meaning of symbols)

1. $\eta_n = 90\%$
2. Speed ratio = 0.45
3. Nozzle Angles = 20°
4. $\gamma = \beta$
5. T/R = 0.55
6. One-half of the pressure drop is taken in each set of nozzles.

The blade efficiency was determined from the velocity diagram Fig. 2-4. The ideal velocity leaving the nozzle is 25×10^3 cm/sec.

$V_2 = 22.46 \times 10^3$ cm/sec

$V_b = 10.09 \times 10^3$ cm/sec

$V_{w3} = 0$ cm/sec

$E_{b\ell} = 4.3$ cal/gm

$\eta_{b\ell} = 70.1$

Nozzle and Blade Dimensions	1st Stage	2nd Stage
Pitch diameter of nozzles and blades, cm	32.0	32.0
Mean blade periphery, cm	95.8	95.8
Number of nozzles	18	18
Nozzle angle, degrees	20	20
Nozzle pitch, cm	6.1	6.1
Nozzle height, cm	3.8	3.8
Nozzle width, cm	4.39	4.39
Number of blades	63	63
Blade pitch, cm	1.52	1.52
Blade height (entrance, cm)	4.1	5.0
Blade height (exit, cm)	4.8	2.3
Blade width, cm	2.5	2.5
Length of nozzle, cm	6.4	6.4
Angle of divergence	10°	10°

2-3 Bearings

The main bearings are journal bearings lubricated with mercury. The mercury, which runs out of the ends of the bearing, is continuously blown down to the condenser. Since the generator and turbine are on the same shaft, one thrust bearing is shown. It is of the Kingsbury type, mercury lubricated (see Fig. 2-1).

2-4 Labyrinth Packing

Labyrinth packing is used on the generator end of the shaft only. It is not required on the thrust bearing end since this bearing is totally enclosed. The labyrinth packing (Fig. 2-1) has alternating constrictions and enlargements so that all of the kinetic energy developed by flow through a constriction is dissipated by turbulence in the enlargement. When steady flow is established through such a packing, there will be nearly complete throttling of the vapor. Since this packing is on the low-pressure end of the turbine, there will be very little leakage. The leakage is blown down to the radiator condenser.

2-5 Nomenclature

$E_{b\ell}$	Blade work
T	Vapor passage width
R	Radius of blade
V	Vapor velocity
V_b	Blade speed
V_r	Relative velocity of vapor
V_w	Exit velocity of whirl
β	Blade exit angle
γ	Blade entrance angle
η_n	Nozzle efficiency
$\eta_{b\ell}$	Blade efficiency

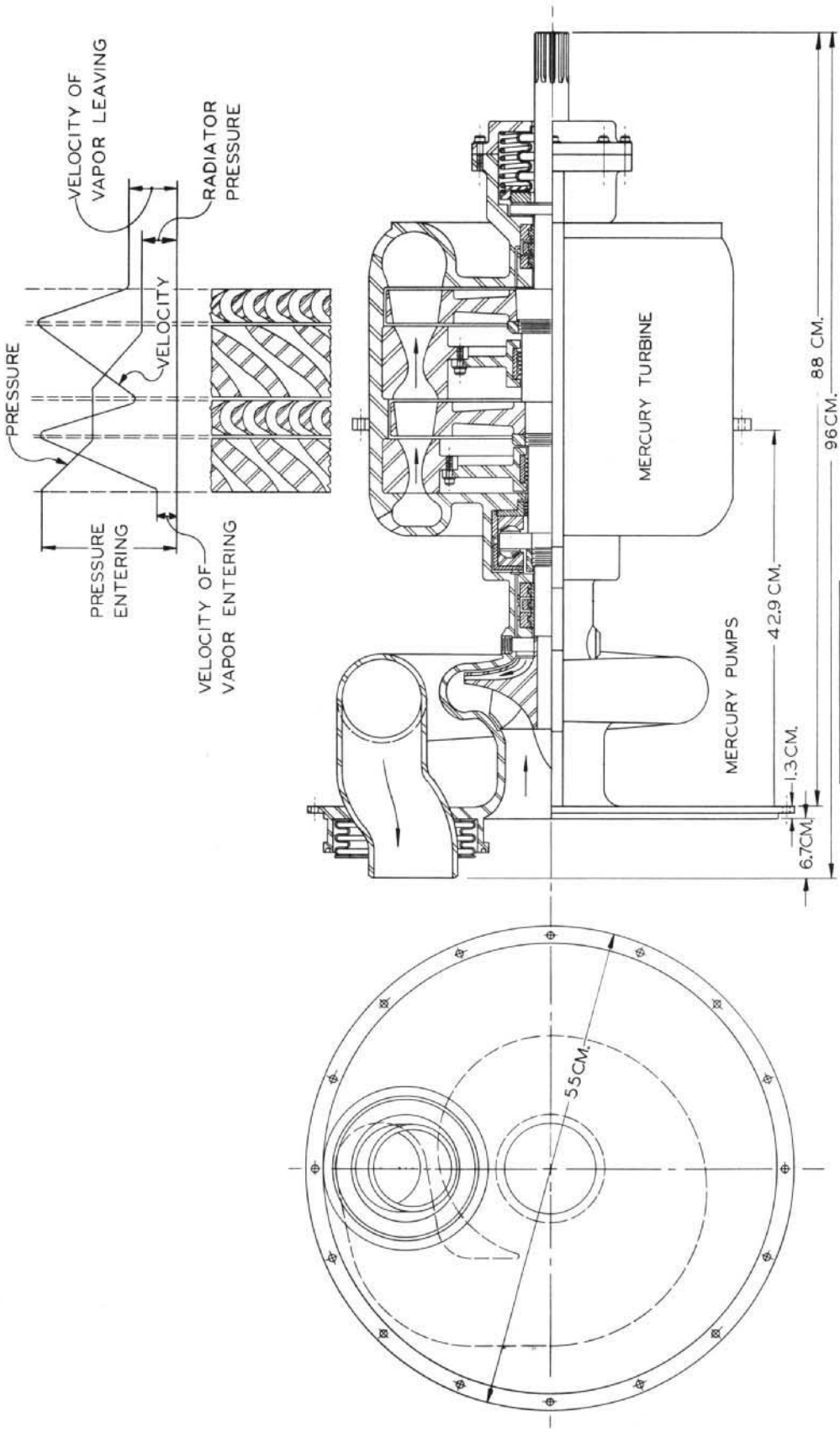

FIG. 2-1
CROSS SECTION OF
TURBINE & PUMPS

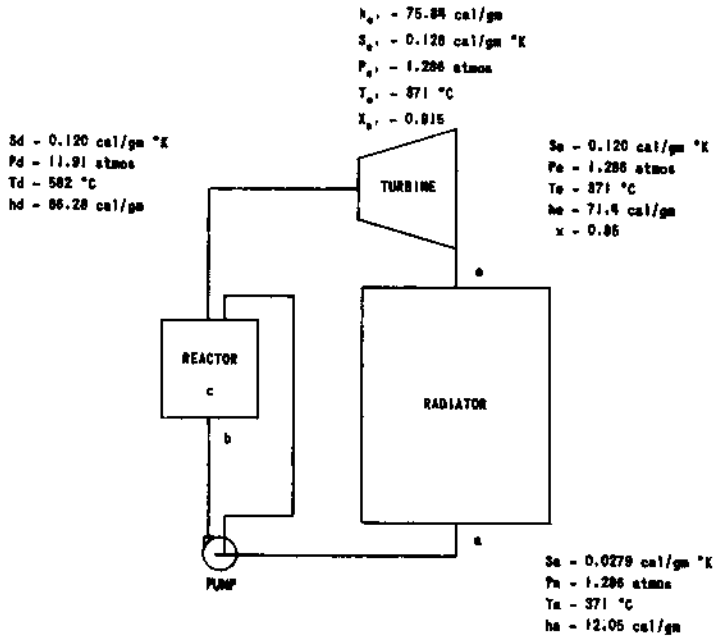

FIG. 2-2
RANKINE CYCLE

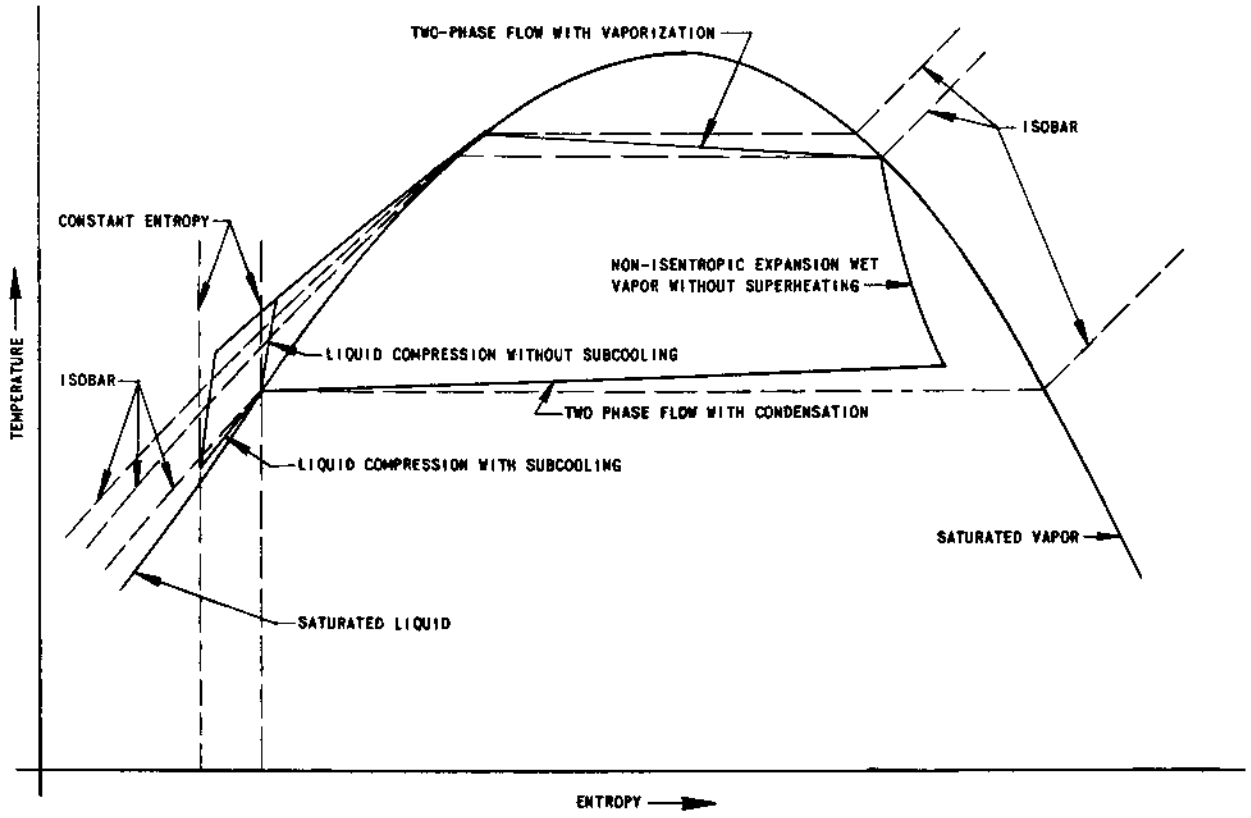

FIG. 2-3
TEMPERATURE ENTROPY DIAGRAM

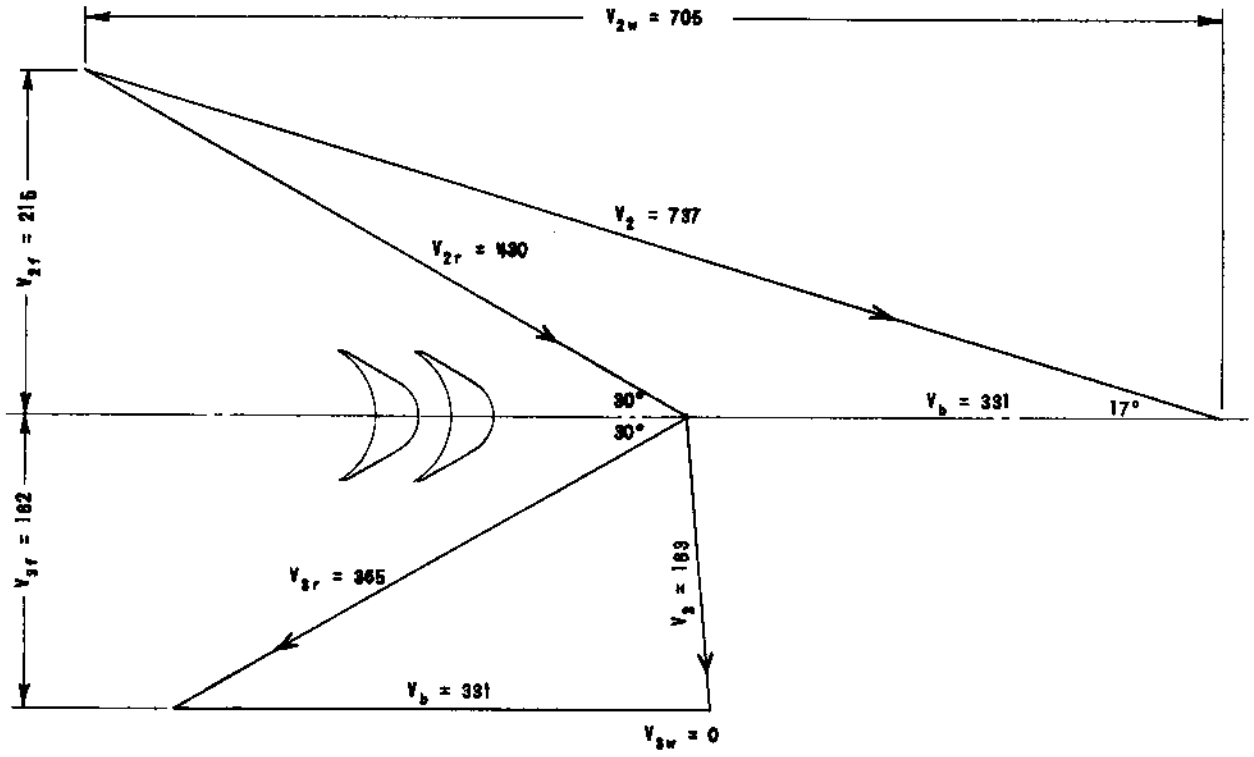

VELOCITY DIAGRAM PER STAGE

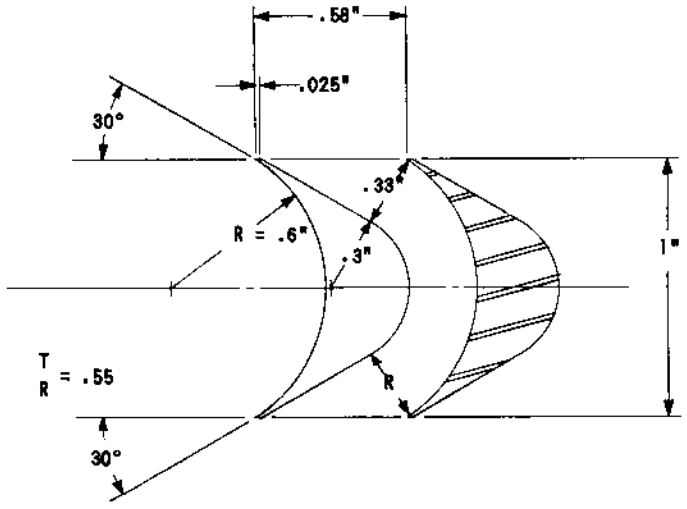

DETAIL OF BLADING

FIG. 2-4
BLADING & VELOCITY DIAGRAM

3-0 GENERATOR

Type	AC Brushless
Continuous Rating	1000 kva
Power Factor	0.75, lagging to 1.00
Overload 2 min	1500 kva
Overload 5 sec	2000 kva
Speed	5700-6300 rpm
Overspeed	7600 rpm
Weight	454 kg

It is proposed to convert the mechanical energy of the turbine to electrical energy by means of a 1000-kva generator system to be developed by the Bendix Corporation, with the same features as their current brushless AC generator systems.

This type of generating system, in capacities less than 1000 kva, is used extensively in aircraft. It is proposed for this lunar power plant because of its proven reliability, light weight, compactness and brushless exciter.

3-1 The Brushless AC Generator System

The brushless AC generator system offers many advantages, but the most obvious is the absence of exciter brushes, thus eliminating the possibility of commutator trouble and brush dust in the machinery. The replacement of the exciter brushes eliminates the need of usual maintenance, contingent upon their use. There is no corresponding maintenance required for the brushless generator rectifier, which is a static device without moving parts. This feature enhances the chances that the lunar power plant can operate for two years without breakdown.

A brushless exciter system (Fig. 3-1) is the unique feature of this generator. A 600-cycle permanent magnet generator, mounted on the main shaft, supplies part of its output to the voltage regulator and control panel, where it is rectified to energize a stationary exciter field. This sets up a flux which generates an AC voltage in the exciter field. Part of the exciter rotor is a three-phase wye-connected winding, the output of which is connected to three silicon power rectifiers mounted on the rotor. After being rectified, this exciter output is supplied as direct current through the main AC generator field winding to produce the flux that is used to generate an AC voltage in the main AC generator stator. Thus the system is capable of supplying generator excitation, and power for voltage requisition and protective functions without the assistance of an external power source.

The generator is a class C, high-temperature salient pole, 6000-rpm generator, together with a 12-pole AC exciter and rectifier, mounted so as to rotate with the exciter armature and main alternator field assembly.

3-2 Windings and Insulation

The stator core (Fig. 3-2) is constructed of a stack of 3.25% silicon-iron laminations, properly annealed and treated to obtain optimum magnetic properties, minimum hysteresis, and eddy current losses. It is firmly held together by a cage construction of nonmagnetic stainless steel end rings and support bars. The slots in the stator core are insulated with a Teflon glass slot cell. This material is employed because of its excellent mechanical abrasive resistance, high strength, and exceptional dielectric and high-temperature properties. This material is extremely expensive but provides so much greater protection against high temperatures due to short-time overloads that it is considered to be worth the high cost. The insulation on the rectangular wires consists of a specially wrapped glass covering bonded with silicon resin.

The stator end connections are made by a method which provides for a lap connection between the turns of individual coils and a long or wave connection between group ends. The connection reduces the length and weight of these end connections and at the same time reduces the resistance of the stator winding by as much as ten per cent (10%) in some cases. In addition, the new winding provides more clearance between the end turns and thus provides better cooling and more adequate spacing between the turns of individual groups and between phases.

The exciter stator core assembly consists of a short stack of laminations which contain twelve (12) individual poles at the outer diameter, which are ground to size so as to obtain the proper concentricity when installed in the stator housing. A molded Melamine Glass insulator surrounds the pole piece. The field coil is then machine wound into place. Each coil consists of approximately 275 turns of Number 21 heavy silicon-insulated wire, and is impregnated by vacuum treatment with silicon resins. This field is designated to operate with the silicon transistor regulator, described elsewhere.

3-3 Rotor Construction

The main generator rotating field (Fig. 3-3) consists of a stack of Armco ingot iron laminations assembled as a group, together with the Amortisseur winding which is welded to the copper end punchings, skewed one (1) slot pitch and then pressed onto the main shaft, which is fluted or splined to provide a positive press fit to the rotor core onto the shaft. This method of attaching laminations to the shaft has been successful in preventing armature cores from loosening, even when the rotors are

subjected to the worst possible torsional vibration. Melamine Glass end punchings are used to insulate the ends of the core and a 0.015-inch thick asbestos glass material is used to insulate the sides of the pole pieces. Rotating field coils of edgewise-wound construction are employed in this rotor. To obtain the optimum heat transfer characteristics from the field coils to the cooling air, alternate pairs of turns are staggered $\frac{1}{16}$ in. with respect to the adjoining pairs. This particular staggering feature increases the effective cooling area of the field coils more than twice that which would be obtained with a straight-sided coil. The rotating field coils are wound out of strip copper, 0.022 in. by 0.250 in. Special fixtures are used to wind the coils without tension, which results in coils which are uniform in resistance and dimension.

The coils are insulated by means of a black oxide and Heresite coat. After the coils are put in place on the rotor and properly wedged, the entire rotating field assembly is given two (2) vacuum-impregnation treatments with silicon resin. The insulation properties of this field assembly are such that the rotor can be operated at 250°C continuously for well over 1000 hours.

The coils are held firmly in place by means of aluminum wedges along the magnetic length and by means of one (1)-piece, stainless steel, nonmagnetic support bands on the end windings. Over each coil end, immediately under the band, a small aluminum support piece is employed. This support piece is provided with reverse tapered holes into which pure lead is swaged in order to effect a precise dynamic balance.

The exciter rotor is comprised of a short stack of twenty-nine (29) gauge, 3.25% silicon-iron laminations, held together by means of rivets below the magnetic section and connecting the support bands on the ends. A heavy Melamine Glass, cup-shaped end punching is provided and made an intimate part of this core assembly, together with a copper connecting disc, onto which three (3) special lock nuts are attached by small bolts and small lock nuts. The silicon diode type of rectifier is screwed tightly into the lock nut to make intimate contact with the copper connecting disc. In this design, three (3) 35-ampere Westinghouse silicon diodes are employed in a three-phase, half-wave connection to provide the field current to the main field of the AC generator.

The exciter armature winding is a conventional, three-phase, delta-connected, 12-pole, AC generator winding. Teflon glass slot cells and silicon glass wedges are employed to retain the windings in the slots. Solid stainless steel support bands are used over the end windings to retain them. Final dynamic balancing is provided by reverse taper holes in the outer support of the exciter armature, with any correction required being applied to the drive end of the main generator rotor.

Locations of the rectifiers were chosen in order to obtain optimum cooling for them and to provide means for ready replacement, should the rectifiers become defective. Careful consideration was given to the effects of centrifugal force on the performance, durability, and life of the rectifier. The Westinghouse Company has indicated in technical papers that their rectifier constructions will withstand a satisfactory force of fifteen thousand (15,000) g's, which is considerably beyond the forces which will be imposed upon them in most applications.

3-4 Permanent Magnet Generator

A permanent magnet generator is provided to feed into a three-phase bridge rectifier and to provide DC power for the silicon transistor regulator and for other control purposes.

3-5 Bearings and Lubricants

Because of the choice of the insulating materials, the overall performance of the generator has been upgraded so that the bearing problems stand out significantly in comparison to any electrical difficulties. To cope with this improved performance, a special shaft construction has been created, which permits cooling hydrogen to be taken from the anti-drive end through passages in the main shaft, back to the drive end bearing. Heat exchanger support castings are used to draw the heat from both the inner and outer races by means of this specially ducted coolant hydrogen. Both bearings are assembled onto the shaft with a slight press fit which varies from line to line by 0.0005 in. The tolerances are 0.0002 in. on both ID and OD of the bearing, and 0.0003 in. on the shaft journal. A standard width bearing is used at the anti-drive end and the double width type at the drive end. The reason for this is that the drive end runs hotter and it is desirable to use a bearing with larger mercury capacity in the hotter areas. Both bearings are precision Class 7 bearings, having an internal clearance of 0.0007 in. to 0.0011 in. They are both heat stabilized for operation at 190°C.

3-6 Generator-Cooling System

Hydrogen is forced through the generator by the hydrogen compressor mounted on the main shaft.

3-7 Transistorized Voltage Regulator

The voltage regulator is a static transistorized voltage regulator designed to supply excitation to the generator.

The voltage regulator consists of five basic circuits. These are: voltage sensing and pulse modulator, reactive load division, saturation amplifier, power supply, and buildup circuit.

3-8 Sensing and Pulse Width Modulator

The three-phase AC line voltage is fed to a half-wave rectifier circuit made up of three silicon diode pairs with a voltage rating in excess of any transient voltages which may be impressed on them. No transformers are used in this circuitry. The rectified three-phase voltage is applied to one leg of a reference bridge circuit containing the voltage reference element. The reactive load division sensing transformer output is a single-phase, full-wave rectifier circuit, made up of two silicon diodes with a voltage rating in excess of any transient voltages which may be impressed on them. The rectified output is applied to the second leg of the reference bridge circuit.

The bridge output is balanced by means of a potentiometer when the input AC voltage is within the limits defined by the governing specification. A filter network is also connected across the sensing rectifier bridge and acts to shape the voltage ripple to a 1200-cycle-per-second triangular wave with a peak-to-peak magnitude of 6 volts. At DC balance, this 6-volt triangular wave shape appears at the sensing bridge circuit.

The reference element used is a cold cathode voltage regulator tube. This tube was selected for its stable operating characteristics over wide ambient temperature ranges. It is necessary to add to the voltage reference circuit a high-impedance, high-voltage power supply to insure firing of the voltage reference tube during buildup and to insure constant ignition during low-voltage transients. This power supply is obtained from a winding on the buildup transformer. This arrangement provides isolation and, since this transformer is powered from the permanent magnet generator, positive voltage under main AC feeder fault conditions.

3-9 Saturating Amplifier

The amplifier is a four-stage transistor current amplifier. The four stages are connected in cascade, and a voltage of $\frac{1}{2}$ volt impressed at the input will cause all stages to saturate. The load resistances and power-supply voltages are so selected that if the generator exciter field is used as the fourth stage load, saturation of the amplifier stages will cause enough field current for the maximum excitation requirements of the AC generator. A one-volt power supply is used to back bias the second, third, and fourth amplifier stages when no input voltage appears at stage one. This assures no current leakage in the amplifier at elevated ambients.

The first-stage amplifier is connected to the output of the voltage-sensing bridge. At zero DC voltage, the first stage is driven from cutoff to saturation in an oscillatory manner by the 6-volt triangular wave shape. Any change in the average DC level across the sensing bridge causes a shift in the time between cutoff and saturation of the amplifier. This in

turn changes the average DC current applied to the exciter field, and hence a change in the generator output voltage. As is evident from the above description, the amplifier operates in one of two stages: the saturation condition where the transistor sees high current and low voltage, and the cutoff condition where the transistor sees no current and high voltage. Both of these states are compatible with the design objective of low dissipation of transistor power.

The amplifier stages of the voltage regulator during normal operation turn "on" and "off" at 1200 cycles per second. However, during heavy generator load switching, the amplifier, during the voltage transient, will remain in the full "on" or "off" condition for the period of the transient.

3-10 Power Supply

The power supply consists of a silicon rectifier bridge supplied with three-phase AC voltage from the permanent magnet generator mounted as an integral part of the brushless AC generator. The permanent magnet generator is capable of supplying the power necessary to operate the voltage regulator and control panel during all main AC generator faults, and is designed to be compatible with the voltage regulator and exciter field requirements. No transformers are necessary for voltage conversion in the power supply circuitry.

3-11 Buildup Circuit

During normal operation of the voltage regulator, the error signal to the amplifier is supplied from the AC line. During short-circuit conditions and for generator buildup, no AC line voltage exists. A small transformer rectifier is incorporated in the voltage regulator and supplies an error signal to the amplifier during the periods of low AC line voltage. This transformer receives its primary voltage from the permanent magnet generator. At all AC line voltages above 60 volts rms, the buildup circuit is electrically disabled. This action in no way affects the operation of the voltage regulator tube sustainer circuit.

All electronic components in the voltage regulator have been chosen with extreme care. Voltage and current rating of all the devices are at least 40% higher than values encountered at any condition that will be met during the life of the equipment.

3-12 The Supervisory or Control Panel

The Supervisory Panel is a transistorized supervisory panel (Fig. 3-4). The panel includes static sensing circuits for low-phase undervoltage protection, average voltage overvoltage protection, underfrequency protection, and feeder fault protection. The supervisory panel also performs

the control functions as follows: manual control by means of external three-position generator control relay is contained within the supervisory panel and is actuated by the control switch and by the fault protection system. The power ready relay supplies output power for operation of the main line contactor.

The Supervisory Panel also contains static logic circuits to perform necessary control and protective operations as desired. Static logic is also incorporated to prevent cycling of any control or protective circuit. As a design objective, circuitry upon failure will actuate the protective function in which the failure occurred.

All electronic circuitry has been designed to withstand the wide temperature limits (-55°C to +120°C) without damage or drift. Components were selected for reliability and low temperature drift. The circuitry was designed to be able to withstand the maximum amount of component drift encountered over wide ambient changes, without any temperature-compensating devices.

Control power for the supervisory panel is supplied from the system permanent magnet generator, which is mounted as an integral part of the generator. Its output is delta-connected, three-phase, 600-cycle AC. The permanent magnet generator voltage supplies the excitation system directly without voltage conversion transformers. In this system this voltage was considered too high for supervisory panel operation, and hence a voltage transformer is incorporated within the panel. Since permanent magnet voltage is directly proportional to speed, it was deemed necessary to include in the supervisory panel a regulated DC power supply. This is fed from the voltage transformer mentioned above.

Due to the high ambient operation required by this supervisory panel and to the temperature limitations of silicon semiconductor devices, it was necessary to design all circuits with minimum internal power dissipation. It was, therefore, decided that power levels would be kept low in all devices, and that all transistors would be used as switches. The transistors can be in only one of two states: "off," in which no current flows through the device and there is hence no power dissipation, and "on," in which the transistor is driven to saturation and the internal power dissipated depends on the current through the device and the saturation resistance of the device. All currents are kept as low as possible and the transistor types were selected for low saturation resistance. All transistor amplifiers used have a negative bias supply to assure no leakage at elevated operating ambients. All transistor circuits are designed around a transistor DC current gain of 10, and each component is checked at low ambient to assure this minimum gain.

3-13 Undervoltage and Voltage-Indicator Circuit

The undervoltage sensing circuit in the Control Panel is static in nature and senses the lowest phase of the three-phase, AC input voltage. Sensing is accomplished by rectifying each of the three AC phases and applying them to a diode "or" circuit. The lowest phase supplies a signal to a two-stage transistorized amplifier. The output of the first stage gives the undervoltage signal. The output of the second stage supplies a voltage-indicator signal. The undervoltage and voltage-indicator signals are then fed to the control panel logic circuits.

3-14 Speed Indicator

The speed indicator is a static voltage-sensing circuit which senses permanent magnet generator voltage. This voltage is proportional to generator speed. The signal from the speed indicator-sensing circuit is applied to the control panel logic circuit.

3-15 Underfrequency

The underfrequency circuit used in the Supervisory Panel is a transistorized counter-type circuit. It senses the permanent magnet generator frequency and, hence, sensing will not become inoperative during the main AC circuit fault conditions. The reference circuit used is a stable RC network. The underfrequency circuit compares the time between voltage cycles of the permanent magnet generator with a fixed timing signal. The output error signal obtained feeds a time delay circuit and then performs the necessary logic functions.

3-16 Overvoltage

The overvoltage-sensing circuit is a static circuit sensing average three-phase input voltage. The three-phase input magnitudes are added and applied to a two-stage transistor amplifier. Incorporated within this two-stage amplifier is an RC circuit designed to give the proper time-voltage characteristics to the overvoltage-sensing circuit. The output of this circuit is fed to the control panel logic circuit.

3-17 Control Panel Power Supply

The Control Panel contains its own regulated DC power supply. Its source of power is the system permanent magnet generator. The permanent magnet is rectified and supplied to a two-stage series voltage regulator. The output of this voltage regulator supplies the DC control power used within the control system. The rectified power supply used in the control is also capable of supplying control power for circuit breakers and other control devices.

3-18 Time-Delay Circuit

The time-delay circuits used in the Control Panel are completely static and use a temperature-stable RC network as the time-determining device. The circuit is designed to supply a constant current supply for the RC network. This assures repeatability in operation of the circuit. The time-delay circuit also employs the necessary components to assure its being nonintegrating in nature.

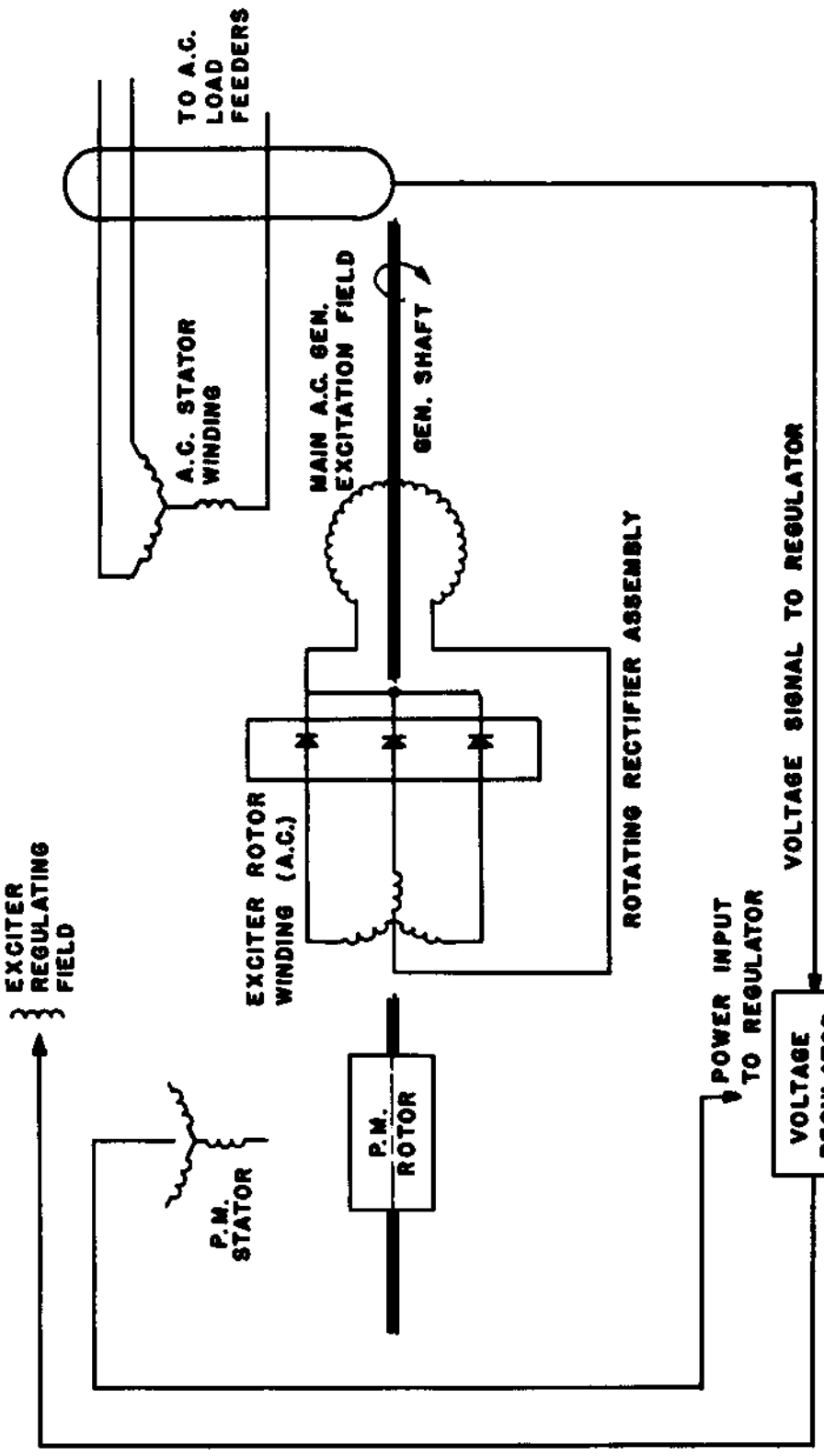

FIG. 3-1

BLOCK DIAGRAM OF EXCITATION SYSTEM

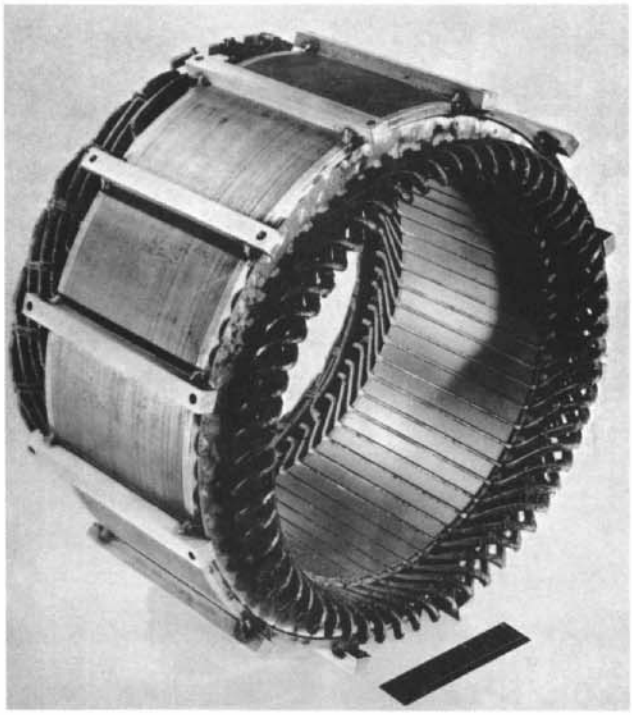

FIG. 3-2
STATOR WINDING ASSEMBLY

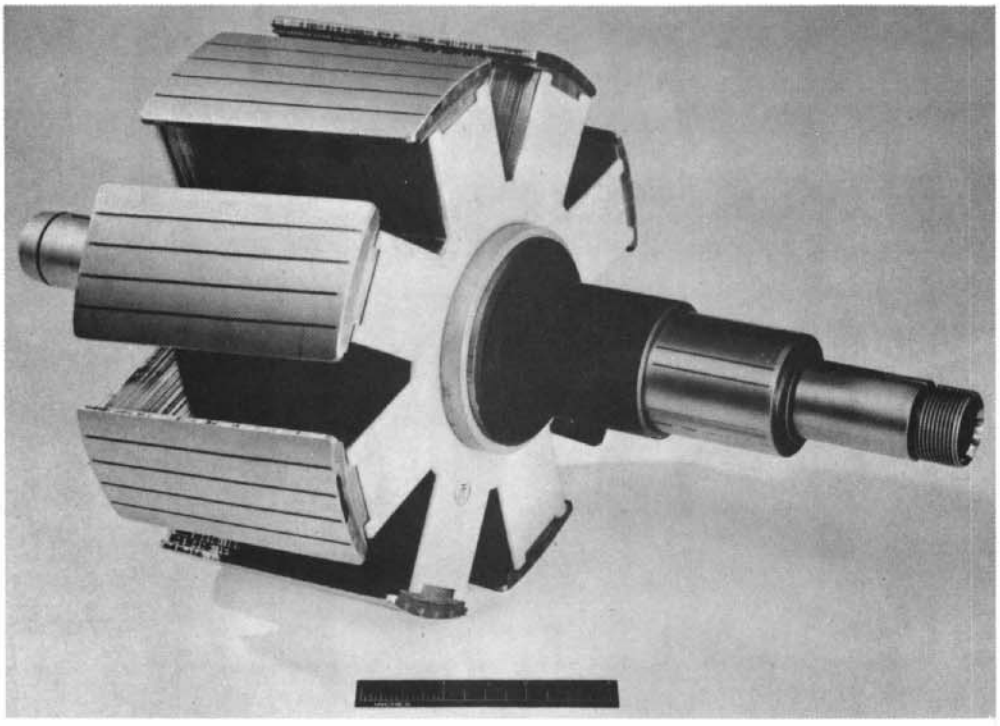

FIG. 3-3
SHAFT & FIELD CORE ASS'Y.

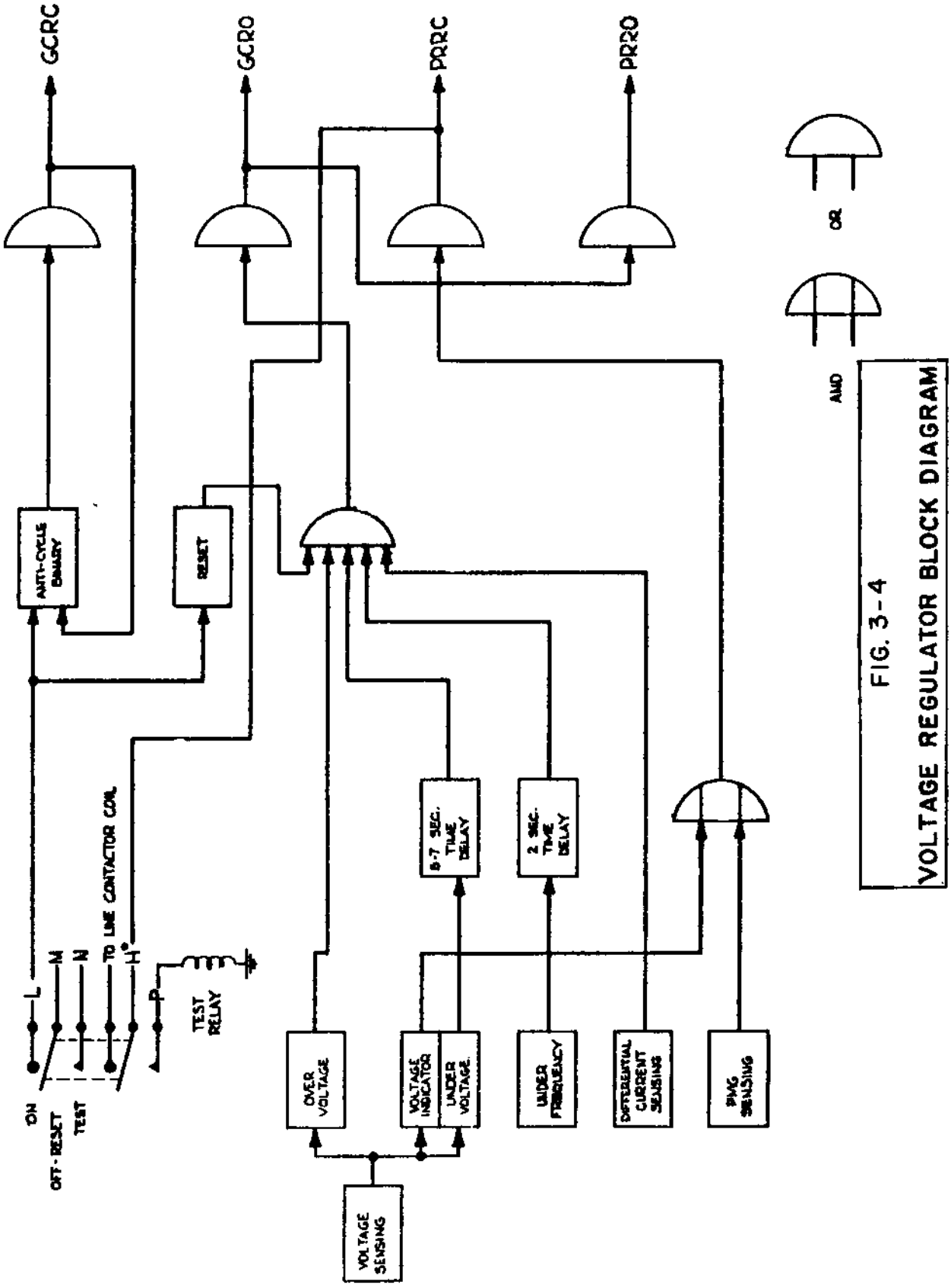

FIG. 3-4

VOLTAGE REGULATOR BLOCK DIAGRAM

4-0 RADIATOR

Currently the only obvious means of removing the heat of condensation from the mercury in a lunar environment is by radiation to space and to the lunar surface. Three radiator designs are presented. The first is shown in sketch form in Figs. 4-1 and 4-2. The heat transfer analysis outlined herein is based on this design. Design No. 2, per Figs. 4-11 and 4-12, is a foldout radiator concept, and design No. 3, per Figs. 4-13, is a wrap-around radiator concept. The engineering data pertaining to radiator No. 1 are listed below.

Heat Removal Rate	6.06 Mw
Flow Rate	22.675 kg/sec
Turbine Outlet Temperature	644°K
Turbine Outlet Pressure	1.3 atmos
Vapor Saturation Density at Turbine Outlet	0.0048 gm/cm^3
Vapor Mixture Density at Turbine Outlet	0.0054 gm/cm^3
Liquid Density at Radiator Outlet	12.66 gm/cm^3
Pressure Loss in Supply Tubes	0.0238 atmos
Pressure Loss in Condenser Tube	0.0136 atmos
Pressure Loss in Condensate Return	0.484 atmos
Isothermal Sonic Velocity at 371°C	15.5×10^3 cm/sec
Adiabatic Sonic Velocity at 371°C	20.1×10^3 atm/sec
Mean Radiator Temperature	638°K
Emissivity	0.90
Wing-radiating Efficiency	0.89
Fin-to-tube and Tube-to-tube Radiating Factor	0.978 VF (f-t) 0.848 VF (t-t)
Fin Effectiveness (actual)	0.873
Fin Type	Straight Triangular
Fin Width	4.750 cm
Fin Root Thickness	0.076 cm
Fin Material	Copper
Fin Thermal Conductivity	0.8764 cal/(sec)(cm)(°C)
Number of Radiator Wing and Angle of Separation	4 at 90°

Radiator Wing Length	22.0 m
Number of Sections per Wing	6
Number of Condenser Units per Section	30
Condenser Tube OD	2.540 cm
Condenser Tube Thickness	0.0889 cm
Condenser Tube Material	Steel
Condenser Tube Thermal Conductivity	0.0513 cal/(sec)(cm)(°C)
Supply Tube ID	10.160 cm
Supply Tube Wall Thickness	0.1270 cm
Total Radiator Weight	3700 kg
Total Radiator Specific Wt (elec)	3.7 kg/kwe

The radiator design is based on lunar environmental conditions and the temperature limitations of the turbine. The lack of substantial atmosphere on the moon has the most marked effect on a departure from earthly precedents in power plant designs. The surface density of the atmosphere of the moon has been measured[1] to be 2×10^{-13} of Earth's atmosphere. This near vacuum makes thermal radiation the only practical mode of transferring heat out of the thermodynamic cycle. The two most important considerations in this radiator design are minimum weight and reliability. Surface area is a function of such parameters as radiator surface temperature, surface emissivity, condensing coefficient, fin conductivity, fluid pressure losses, and mutual radiating inefficiencies. The single most influential parameter is temperature, since radiator surface is inversely proportional to the fourth power of the radiator temperature. For a radiator of minimum weight, the highest possible temperature is sought. However, to promote cycle efficiency, a paradoxically low temperature is also sought. The optimum conditions for maximum turbine energy per unit area of radiator occurs when the ratio of turbine to radiator temperature is approximately 0.75. The problem of troublefree longevity of the radiator is categorized into (1) the mechanical design of the system, which can be controlled; and (2) the problem of meteor penetration, which is a problem in probability.

The heat rejection is 6.06 Mw and the mass flow rate is 22.675 kg/sec. The outlet temperature of the turbine is 644°K with a vapor quality 9.5% by weight. Turbine vapor enters a toroidal distributing ring which directs the flow into the main supply lines. Vapor distribution to individual condenser tube units follows. Latent heat of the vapor is transferred to the inside surface of the tube, conducted to the tube and fin surface, and thermally radiated into space. Condensate now returns to the sump tank.

Figure 4-1 shows the geometric construction of the radiator. Extending from the main body of the plant are four wings perpendicular to each other and all mutually perpendicular to the lunar surface. Each wing is approximately 22 meters in length and is divided into six individual sections; a section is composed of thirty finned condensing tubes. Vapor supply and condensate returns are 10.16-cm and 5.08-cm diameter flexible hoses with corresponding wall thickness of 0.127 and 0.076 cm. All vapor and condensate lines are supplied with meteor bumpers.

An individual condenser unit is composed of a 2.54-cm OD steel tube with two straight triangular copper fins bonded metallurgically to its side; a full-scale drawing of this unit is shown in Fig. 4-2. A stainless steel tube wall thickness of 0.089 cm is considered sufficient for a two-year mercury corrosion life at 371°C. Fin width and root thickness are 4.750 and 0.076 cm, respectively. A thermal conductivity of 0.8764 cal/(sec)(cm)(°C) was used for the copper fins. The minimum condenser height is 457.2 cm. The condenser units are separated between copper fin ends; this separation allows for differential expansions and helps reduce stress problems.

Protection against coolant loss is provided by dividing the radiator into twenty-four independent sections. In the event of a meteor strike, cut-off valves at the inlet and outlet headers would temporarily remove the malfunctioning section from the main flow until repairs were made. Sensing of the penetration was assumed to be fast enough that only a small portion of the mercury would escape. A lunar mobile radiator repair unit constructed of dual-purpose parts taken from the rocket transportation vehicle was considered.

4-1 Heat Transfer

(a) Heat Transport

Heat was rejected from the LP-1 thermodynamic cycle by removing the latent heat of the mercury coolant, transferring the heat by conduction to the outer surfaces of the condensing unit, and thermally radiating the heat to space.

Heat rejection of the mercury working fluid will result in a near-isothermal radiator (see Fig. 4-3). The following situation exists. Radiant energy that leaves one radiator surface and "sees" another will be reflected; part of this reflected energy returns to the radiator surface from which it originated, where it again undergoes partial reflection. This process proceeds indefinitely. Effectively, a portion of the available sink medium has been removed for transferring radiant energy. This removal factor F_{12} of a surface 1 with respect to a surface 2 represents that fraction of the

total energy emitted per unit area of A_1 which is intercepted by A_2. This is represented by the following equation[5,6]

$$F_{12} = \frac{1}{A_1} \frac{1}{\pi} \int_{A_1} \int_{A_2} \frac{\cos \theta_1 \cos \theta_2}{s^2} \, dA_1 \, dA_2.$$

The calculation of radiation exchange between gray bodies was facilitated by an emissivity factor, F_e, which is based upon the sink and source geometric enclosure and the emissivities of the sink and source surfaces. This factor is slightly more complex than the geometrical factor F_{12}, and the information concerning this aspect of radiation transmission is limited to only a few simple geometrical shapes. The relationships that do exist, however, facilitate the solution of most of the problems that do arise in practice.[7]

Fin-and-tube radiations emitted and intercepted by configurations exactly as those proposed for the LP-1 designs have been investigated by Callinan and Berggren.[8] These radiation fin-to-tube and tube-to-tube inefficiencies are referred to by the author as fin-view-factors and tube-view-factors respectively. Fin and tube-view-factors are functions of distance along the fin width and are related to the diametrical size of the coolant tubes. A significant influence that should be noted was the effect of fin-view-factor on fin effectiveness. The product of mean fin-view-factor and fin effectiveness was considered to be the actual mean fin effectiveness for any particular fin width. The variations of mean fin-view-factor, fin effectiveness, and actual fin effectiveness are shown versus fin width in Fig. 4-4. The effect of poor fin and tube- view-factors near the tube-fin junction was markedly shown by noting the increase in weight required for very short fin widths (see Fig. 4-5).

A summary of the factors by which the heat transfer by radiation is affected is given in Table 4-1. These are called transmission efficiencies.

Table 4-1

TRANSMISSION EFFICIENCIES

(1)	Overall Radiation to Space	
	Geometric factor	1.00
	Emissivity factor	0.90
(2)	Geometric Factor for Mutual Wing Radiation	0.89
(3)	Fin-view-factor	0.978
(4)	Tube-view-factor	0.848
(5)	Fin Effectiveness	0.893
(6)	Actual Fin Effectiveness	0.873

(b) Fluid Flow

Vapor pressure is directly related to the temperature at which vapor condenses; reducing the vapor pressure reduces the condensing temperature. Recalling that radiator area is inversely proportional to the fourth power of the radiating temperature shows the high price that is paid for pressure losses. Radiating temperature should be maintained as high as possible. High pressure losses are prevented by the use of large piping and low flows. The supply pipe, however, cannot be too large or the dominant radiator weight will be the supply piping. In the LP-1 design, a compromise was made between the weight of large supply lines and the additional weight required for radiator area caused by a pressure-dependent temperature reduction. Due to pressure losses the reduction in the temperature of condensation of mercury vapor amounted to 3.8°C.

For small pressures losses, when $P_2/P_1 > 0.9$, the pressure loss of a two-phase compressible fluid in the supply tubing was satisfactorily evaluated by the conventional expressions for isothermal conditions:

$$\Phi = \sqrt{\frac{(\Delta P/\Delta \ell)_{TP}}{(\Delta P/\Delta \ell)_L}} \text{ and } X = \sqrt{\frac{(\Delta P/\Delta \ell)_L}{(\Delta P/\Delta \ell)_G}}$$

Here $(\Delta P/\Delta \ell)_{TP}$ denotes the pressure gradient for the two-phase flow, $(\Delta P/\Delta \ell)_L$ that of liquid flowing alone, and $(\Delta P/\Delta \ell)_G$ that of gas flowing alone. Functional relationships Φ and X were those usually reported by Lockhart and Martinelli.[7] The volume occupied by the liquid plus the volume occupied by the gas was taken equal to the volume of the pipe. A pressure of 0.0238 atmos was absorbed in the 10.16-cm ID radiator supply lines. The mass flow rate was 0.9447 kg/sec.

The pressure loss in the condensing unit was evaluated as

$$\Delta P = \Delta P_f + \Delta P_m + \Delta P_h \quad ,$$

that is,

$$\text{(Total pressure loss)} = \text{(frictional loss)} + \text{(momentum gain)} + \text{(head gain)} \quad .$$

Two-phase frictional losses for the condensing mercury coolant were evaluated by a friction multiplier supplied in a Kutateladze report.[15] The reasons for this choice over other popular types were that:

(1) the relationship agrees with the experimental two-phase flow of mercury; and

(2) other formulations break down at very high qualities and predict much higher values of two-phase friction than actually encountered.

The momentum gain in the condenser tube was directly proportional to the difference in the gas velocity, 22.4 m/sec entering the condenser, and the liquid velocity, 11.2 m/sec leaving. The pressure gained through elevation was neglected. A fairly good estimation of the vapor quality was made by assuming it varied linearly with distance. Pressure loss due to the condensing section was 0.0136 atmos. Kern[3] notes that a method of conservatively approximating condensing pressure losses may be simplified by taking one-half of the conventional pressure drop computed entirely on inlet conditions. The pressure loss by this method was 0.0154 atmos.

Mercury inventory or holdup in the condensing section was based on a momentum model of the type proposed by Levy.[14] The momentum model is not considered to be as conservative as that based on Lockhart-Martinelli predictions; however, the LP-1 model is believed to give a reasonably correct answer. One quickly realizes that the degree of optimism available to the designer in predicting the mercury inventory may vary widely - all gas to all liquid. Any finalized prognostications of this problem will eventually require an actual mockup and experimental support.

For a completely separated flow mechanism, each phase should satisfy a momentum equation of the Euler type. Consider an element $d\ell$ of the condensing tube with a two-phase mixture flowing downward as shown in Fig. 4-6. Writing a force balance on the gas phase, there is obtained

$$dF = PA_g + (P + \frac{dP}{2})\,dA_g - (P + dP)(A_g + dA_g) + \tau_i\, P_g\, d\ell + \frac{g}{g_c}\, A_g\, \rho_g\, d\ell,$$

and the momentum change causing this force is:

$$(1/g_c)(W_g + dW_g)(V_g + dV_g) - W_g\, V_g - V_g\, dW_g = dF \quad .$$

Assuming that

$$A_f \text{ (average)} = \frac{1}{2}\, A_f \text{ (exit)},$$

the final relationship is

$$\text{Mass of condensing coolant} = \frac{(\text{Mass flow rate})(\text{Length of condensing section})}{\text{Inlet vapor velocity}}$$

or

$$M = \frac{W\ell}{V_g} \quad .$$

For the LP-1 design conditions, an average mercury inventory of 6.36 gm is expected per tube.

(c) Emissivity

For most engineering purposes the usual assumption is made that total radiation may be expressed by a fourth-power temperature function modified by total values of emissivity, absorptivity, or transmissivity terms of the pertinent bodies. A total value of the absorptivity may be obtained from appropriate integration of the spectral distribution curves or from total radiation measurements. To determine this value, the spectral distribution of the incident radiation area is multiplied by absorptivity α_λ for the same wave lengths and divided by the area under the incident radiation. The equation for total absorptivity is

$$\alpha = \frac{\int_0^\infty \alpha_\lambda E_{\lambda_b} \, d\lambda}{\int_0^\infty E_{\lambda_b} \, d\lambda}$$

Also, the ratio of the total emissive power of any body to the total emissive power of a black body at the same temperature is called the emissivity ϵ and is numerically equal to the absorptivity. The following are generalized statements concerning the emissivity of a surface:

1. Highly polished metals have low emissivities.
2. The emissivity of most substances increases with increases in temperature.
3. Most nonmetals have high emissivities.
4. The emissivity of any surface varies widely with the condition of the surface.

The peroration then is that it will be necessary to apply a high-emissivity coating to the metallic surfaces of the radiator. An evaluation, however, of this high-ϵ coating has not been fully investigated. Some of the evaluations to be made are:

1. the additional temperature reduction due to the poor high-ϵ thermal conductivity;

2. efficaciousness of the high-ϵ material bond to the metallic surface; and

3. the high-ϵ coat reaction to the lunar environment.

A value of ϵ equal to 0.90 was assumed for the coating material, and the coating was also assumed to be thin and in good contact with the metallic surfaces. These assumptions are felt to be slightly optimistic but not impossible.

(d) Condensing Heat Transfer

Differences in Nusselt's film theory arise when the mechanism of condensing is dropwise rather than filmwise. Metallic heat transfer media, characterized by dropwise condensation, have been noted to differ widely from Nusselt's predictions. For example, the General Electric Company[13] has satisfactorily used values of 0.2034 and 0.4068 [cal/(sec)(cm^2)(°C)]in designing their mercury power plants; these values correspond to 3-6% of what the theoretical Nusselt relationship predicts.

Two independent reports from Bonilla[13] and Kutateladze[10] agree that heat flux is practically independent of temperature difference ΔT for dropwise condensation of mercury vapor, that is, for $q'' = h\Delta T$ and $h \propto \Delta T^{-1}$. Their agreement as to the value of the heat flux was also good.

The LP-1 heat transfer coefficient based on these published reports indicates that sufficient area could be supplied in the 457.2-cm long condenser unit to condense the coolant and remove some heat for subcooling. A reduced gravity of one-sixth earth's has been included in the calculations; however, all the implications of the reduced gravity on condensate removal are not clearly understood.

Reduced gravity will affect the manner in which condensate breaks away from the surface on which it was formed. This condensing mechanism is briefly described as follows. A vapor pressure, corresponding to the condensation surface temperature, establishes a differential pressure which produces a vapor flow normal to the condensing surface. Mercury condensate collects in droplets until it is sufficiently increased in size to break away towards its gravitational attraction.

Admixtures of noncondensible gases in the mercury vapor can produce a vapor gas boundary that prevents condensation at a specified temperature. The adverse effects of these noncondensible gases can engender a serious problem once the LP-1 is in operation. Details of a gas-venting system which prevents admixtures has not been worked out in detail for the LP-1 design.

Other pertinent observations on mercury condensation reported in the literature include: (1) mercury condensation and heat transfer rate are almost independent of the condensing tube position relative to the horizontal plane, and (2) pressure increases have been noted to increase the heat transfer rate.

(e) Fins

The two most important considerations of a radiator design are to obtain a minimum radiator weight and troublefree longevity. Finning lowers the number of condenser tubes required for heat rejection, and a fewer number of condenser tubes reduces the probability of radiator puncture. Fins penetrated by meteors have very little of their heat transfer area removed and the concern for coolant is somewhat reduced.

Criteria used for obtaining the best fin width for the LP-1 radiator were based on obtaining a minimum weight for a specified thickness of condenser tube. The tube thickness, based on corrosion rate, was 0.089 cm. Figure 4-5 shows the variations in radiator weight as a function of fin width; minimum weight of 3,700 kg occurred at a fin width-to-tube diameter ratio of 1.87. The reasons for the choice of fin parameters follow:

(1) A fin root thickness of 0.076 cm was selected primarily because of ease of construction.

(2) Copper finning material was used because of its high thermal conductivity.

(3) A triangular fin profile was chosen for its high fin effectiveness per unit weight and for its constructual simplicity.

Necessity dictates, however, that final radiator calculations must include a factor for puncture probability. When reasonably accurate data become available on the frequency, density, size and velocity of meteors penetrating a suitable LP-1 site, the best fin criteria will then be based on a minimum weight for an allowable number of punctures. If the meteor flux is high, extensive finning will be required; for low fluxes, less finning will be required. A quantitative comparison of the number finned and nonfinned, one-inch diameter tubes required is given in Fig. 4-7. This estimate, however, is low for large fin widths because, as the number of units increases, the length of the supply lines increase and the pressure losses increase; these pressure reductions in turn require more radiator units. An estimate, based on condenser units alone, shows the wing length requirements for finned and nonfinned condenser units based on similar centerline spacings (see Fig. 4-8).

Selection of a particular design of fin profile for space applications depends primarily on its effectiveness at a minimum weight. Profiles which require the least cross-sectional area to dissipate a given heat rate at optimum dimensions for the rectangular, triangular, and inverse parabolic profiles are given by Schneider[11] and are shown in the following equations:

$$A_R = \frac{0.252}{h^2 k} \left(\frac{q_0}{T_0}\right)^3 , \qquad \text{(Rectangular)}$$

$$A_T = \frac{0.174}{h^2 k} \left(\frac{q_0}{T_0}\right)^3 , \qquad \text{(Triangular)}$$

and

$$A_{IP} = \frac{0.167}{h^2 k} \left(\frac{q_0}{T_0}\right)^3 . \qquad \text{(Inverse Parabolic)}$$

Notice the optimum rectangular fin area requires 51% more material to dissipate the same heat rate as the optimum parabolic fin having a least profile area, and the optimum triangular fin profile area requires only 4% more material than the parabolic consideration. These equations also show that the required weight of the fin is proportional to the specific weight ρ^{-1} of the material used and inversely proportional to the thermal conductivity k, i.e. weight is proportional to $\rho^{-1}k^{-1}$. Where weight is premium, materials such as copper, silver, and aluminum should be considered as a supplemental material to iron and stainless steel.

Optimum Dimensions for Straight Triangular Fin

The optimum semithickness of the triangular profile is given by the equation

$$\delta_{opt} = (4\, A^2 h_r / \lambda^2_{opt}\, k)^{1/3}$$

and thus the optimum width ω_{opt} is given by

$$\omega_{opt} = A / \delta_{opt} ,$$

where

λ_{opt} = 2.6188 (root determined by trial and error)

A = Profile area

h_r = Surface heat transfer coefficient

k = Thermal conductivity

ω = Profile width

δ = Profile semithickness.

Fin performance is defined as the ratio of the total heat dissipated by the fin to that which would be dissipated if the entire fin surface were at T_0. The effectiveness of the straight triangular fin, $e = q_a/q_0$, is given by the equation

$$e = (1/\zeta)\, I_1(2\zeta)\, I_0(2\zeta) \quad ,$$

where

$$\zeta = (\omega^{3/2})\, h_r/kA.$$

Radiant Surface Heat Transfer Coefficient

A simplified surface heat transfer coefficient for a radiating body may be obtained by equating the following equations:

$$Q = \epsilon\sigma(T_r^4 - T_s^4)A$$

and

$$Q = h_r A(T_r - T_s) \quad ,$$

to produce

$$h_r = \epsilon\sigma(T_r^4 - T_s^4)/(T_r - T_s) \quad .$$

For $\epsilon = 1.0$ and $T_s = 0°K$, there is found

$$h_r = \sigma T_r^3 \quad .$$

(f) Solar Radiation

The problem of LP-1 solar radiant-heat exchange is of importance in the control system design of the nuclear power plant. This problem is treated as a nonsteady-state problem since the position of the sun varies with time.

Net energy, Q(net), emitted from the LP-1 surfaces may be expressed as

$$Q(\text{net}) = Q_a + Q_m - Q_s \quad ,$$

where

Q_s = energy received by the radiator surfaces directly from the sun

Q_m = energy emitted to the surface of the moon

Q_a = energy emitted to outer space.

The amount of radiation that a body will absorb depends upon its temperature, amount of surface, surface finish, and the angle at which the rays strike the surface.

Direct energy from the sun, Q_s, which is absorbed by the LP-1 radiator wing surface is given by the equation[12]

$$dq_s = \epsilon_{sr}\, t_r\, F_{s(1-2)}\, T_s^4\, dA_r \quad (\text{cal/sec}) \quad ,$$

where

ϵ_{sr} = absorptivity of the radiator wing surfaces for solar radiation

t_r = transmissivity of the lunar surface atmosphere

dA_r = element of radiator surface area

$F_{s(1-2)}$ = solar configuration factor

T_s = temperature of the sun ~ 5,500°K.

For flat surfaces, $F_{s(1-2)}$ is equal to $(r/R)^2 \cos \theta$ where r = radius of the sun, R = distance from the sun to the surface, and θ = angle between the sun's rays and the normal to the surface.

The value of cos θ may be determined by the equation

$$\cos \theta = \cos |\xi_1 - \xi_2| - \sin \xi_1 \sin \xi_2 (1 - \cos |\Psi_1 - \Psi_2|) \quad ,$$

where

ξ_1 = angle between the sun and the lunar surface vertical

ξ_2 = angle between the radiator surface normal and the lunar surface vertical (90°)

Ψ_1 = azimuth angle of the sun

Ψ_2 = azimuth angle of the radiator normal to the lunar surface.

The value of $|\xi_1 - \xi_2|$ must be less than 90 degrees, whereas the value of $|\Psi_1 - \Psi_2|$ must be less than 90 degrees or greater than 270 degrees for the radiator surfaces to see the sun. Angles different from these indicate the radiator surface does not see the sun and does not receive any direct solar radiation.

For a description of the angles pertinent to the determination of cos θ, see Fig. 4-9; also notice that the magnitude and time variations of cos θ are a function of the LP-1 site location.

The immediate incidence of solar energy on any particular wing will be a function of (1) time variance of the magnitude of cos θ and (2) the quantity of shadowing that perpendicular wings produce on each other. Fig. 4-10 was used to illustrate the probable magnitude and time variation of solar energy on the four LP-1 radiator wings during a typical lunar day.

(g) Generator and Reflector Heat Rejection

In addition to the required heat rejection for the thermodynamic cycle, the generator and reflector control shell heat generation is to be considered. Four methods are available for removing this heat. They are:

1. A refrigeration system which would allow for operation of a generator at a lower temperature than the radiator-condenser. The unfavorable characteristics of such a system include a penalty because of a high specific weight and the deterioration of the refrigerant in a nuclear radiation environment.

2. A gaseous medium for transporting the heat from the generator and reflector shells to a radiator similar to the mercury coolant rejection system. The mercury condensing radiator rejects heat almost isothermally at a high temperature and has good working fluid heat transfer characteristics; however, the gas radiator would have a comparatively poor heat transfer coefficient and would have temperature differences between inlet and outlet conditions. Unless high gas temperatures can be obtained, which means a high generator temperature, the gas radiator appears to be unfavorably heavy.

3. A high-temperature generator (750-800°F) that would be ducted or ported would utilize the returning condensate to carry away the heat. This method of removing heat sounds plausible, but the electrical characteristic changes of such a system have not been fully investigated.

4. A system that would operate at a sufficiently high temperature to radiate its heat to outer space with a minimum of conveyor mechanisms. Temperatures of 1000-1800°F would be a reasonable range to consider for these self-radiators and definitely for future state-of-the-art concepts.

The conclusions are that (1) and (2) result in unfavorable weight systems but can be made to work for the LP-1 generator and reflector heat removal conditions. These methods will utilize a reasonably sized auxiliary radiator if this radiator can be maneuvered so as to orient itself and to eliminate the solar and lunar surface thermal effects.

4-2 Discussion of the Analysis

The turbine contribution to the overall system weight is very small, but the ability of the turbine to function at high temperatures greatly affects the size of the dominant weight - the radiator. Two simple relationships exemplify the problem of minimization of radiator weight. They are: (1) for maximum work per unit area, radiator temperature is approximately $\frac{3}{4}$ of turbine inlet temperature, and (2) radiator area is inversely proportional to the fourth power of the radiating temperature. Maximizing the system temperature minimizes the radiator weight, and obtaining a high system peak temperature becomes a problem of maximizing the high-temperature capabilities of the turbine. These high temperature quests are primarily associated with a reduction in radiator weight and must be carefully evaluated with the other system components, e.g., the reactor, and turbine and generator, which favor a low temperature.

For purposes of turbine reliability, the present LP-1 design was based on a realistic peak turbine temperature of 538°C. The resulting 371°C turbine outlet temperature, thus approximate radiating temperature, was considered very low by present aero-space standards. As a result of this low temperature of heat rejection, the LP-1 specific weight was approximately twice that of some published advanced state-of-the-art space reactor designs. However, noting that peak operating temperatures of 2000°F were common for the advanced systems immediately indicates where and why the LP-1 and advanced system specific weights differ so widely.

A further refinement for the radiator analysis will include the effect on meteoroids with respect to vulnerable radiator area. The effect of meteor vulnerability on radiator size is a function of site location and radiator design specifications. Data concerning meteoroid frequency and their penetrating power can be correlated with the radiator thicknesses, material density, and vulnerable area to resolve a value for the probability of radiator puncture. This analysis would help evaluate the cost of radiator specific weight if additional protection is considered.

For a specified temperature, the two-phase mercury system is lighter and less vulnerable to meteor incident than a single-phase inert gas system. However, the price paid for this choice are the usual problems inherent in most high-temperature liquid metal systems, namely, material transport, erosion, and corrosion.

4-3 Discussion of Meteors

The frequency of some interplanetary meteoric impacts[2] was recorded during the flight of Pioneer I. Eleven low momentum impacts were made during the first nine hours, which gave a mean flux of $9 \times 10^{-3}\ m^{-2}\ sec^{-1}$ in the momentum range from 3×10^{-4} to 10^{-2} (gm)(cm)/sec; only one count was observed in the momentum class above 10^{-2}(gm)(cm)/sec. During the flight of Pioneer II, the results of meteor impact were considerably different. During a one-minute interval, sixteen strikes were made, indicating a flux of $6.1\ m^{-2}\ sec^{-1}$. An estimate of the density of low-momentum matter in interplanetary space has been placed at $10^{-7}/m^3$. This meteoric density was obtained by assuming the mean velocity to be 4×10^4 m/sec.

Designing a radiator for zero penetration is impossible. The thickness of radiator tubes required to stop a certain size of meteor during a particular time interval is a function of the diameter of the meteor, frequency of occurrence of meteor impact, meteor density, velocity of the meteor, radiator material density, and sonic velocity of the radiator material. To design a radiator for an arbitrary number of penetrations would mean that a reliable valving system must be incorporated into the design to absorb the loss of a percentage of radiator area and working fluid. If the system were not reliable one hundred per cent of the time, a single puncture could be catastrophic to the radiator system. Quantitative knowledge of the distribution, density, and size of the meteoric matter penetrating the lunar surface is still very vague. This last statement is exemplified by the flux data between Pioneer I and II, which was shown to vary as much as 1000. The idea of deciding on a tube condenser thickness based on meteor incidents with the present data would only result in a euphoric design. Therefore, tube wall thicknesses for LP-1 were not considered a function of probable puncture; however, a low vulnerable area was maintained. Meteor penetration is recognized to be a very serious problem, and it was not neglected for simplicity.

4-4 Alternate Radiator Design No. 2

Foldout Type Radiator

This design (see Fig. 4-11) consists of four basic sections, each of which contains 25 concentric radiator elements, which in transit nest against the reactor vessel and are unfolded at the site. A unit radiator element is comprised of an inlet header at the upper end, 2.54 cm thick by 10.2 cm high, an outlet header at the lower end, 2.54 cm thick by 5.08 cm high, and a series of radiator tubes (see Fig. 4-12) assembled between these headers. Since the arc lengths of the headers vary with the radial position, the innermost is the shortest and contains the least number of tubes, whereas the outermost is the longest and contains the largest number of tubes. Each side of the units contains a structural

channel which provides additional rigidity to the unit and provides a surface to assemble the hinges which connect adjacent radiator segments. Hinge pins assembled to the innermost segment engage hinge sockets welded to the reactor vessel, thus providing a pivot for the radiator quadrants to open outward on the lunar site. Since each radiator element is a movable unit, mercury flow between adjacent elements is achieved by modified swivel joints. To unfold a radiator section, a conveyor rail is attached to the swivel in the upper head of the reactor. This rail is hinged for storage during transit and is opened on the site. A series of bipod supports provide lateral bracing.

Roller assemblies containing hanging bars are connected to sockets on the outside of the radiator outlet manifolds as the radiator is pulled out on this conveyor. Each radiator quadrant contains eight sets of adjustable bipod support braces equispaced along the length of the radiator. These supports nest in the radiator for transit, yet may be opened and lengthened on the site to provide the necessary side supports. The conveyor hangers are then disconnected and the conveyor moved 90° to the next radiator section where the operation is repeated. This same method is used for the third and fourth sections. The conveyor can then be dismantled or left in place as the situation demands.

All liquid and gas lines are preassembled so that the radiator is ready for operation when all sections are unfolded. Projections on the inlet and outlet headers extend beyond the headers. To these projections are assembled the flexible hoses which connect with the reactor. The four upper hoses connect to four modified 10-cm solenoid valves which, in turn, are connected to the four mercury vapor riser ducts. The four lower hoses are connected to four 3.80-cm solenoid valves which, in turn, are connected to the four mercury condensate return lines extending below the reactor. Thus, any malfunction in one wing can be isolated by actuating the inlet and outlet valves, and the system can still operate at reduced power.

The radiator unit in outermost position is used to cool the hydrogen gas from the compressor and also can be isolated by solenoid valves interposed between the radiator hoses and the inlet and outlet openings at the lower end of the reactor. An opened radiator quadrant is 473 cm high by 2305 cm long and is supported at 288-cm intervals. The radiator tubing per Fig. 4-12 is presumed to be made of 5% chromium-1/2% molybdenum alloy steel. Tests now in progress, however, indicate the possibility of using a titanium alloy. If proven feasible, the use of this material would effect a 45% weight saving.

4-5 Radiator Design No. 3

This design (see Fig. 4-13) consists of four basic sections, each containing 67 horizontally assembled tubing units. The unit is a tubular material supplied as a flat ribbon that can be inflated at a pressure of about 85 atmos into conventional tubing with integral fins. The tubing material is assembled into headers which, in turn, connect through solenoid valves to the outlet and inlet lines of the reactor. Since this material is essentially a flat ribbon in its initial state, the four sections can be concentrically wrapped around the reactor, thus providing a reactor radiator package of about 183-cm diameter for rocket transit.

Vertical and horizontal braces, plus bipods similar to those used on radiator design No. 2, provide the necessary support. The base is similar to that described for radiator design No. 2 except that the cylindrical column is divided into two sections which contain bearings that permit the reactor plant to rotate as the radiator is unwrapped.

To open up the radiator, four conveyor rails extend radially from the upper end of the reactor. These rails are hinged for storage during transit, and are unfolded and assembled to the center pivot point on the site. As in radiator design No. 2, bipods are provided for bracing the conveyor. A motor-driven or manually operated winch device provides the mechanical force required to perform the unwrapping operation. Dividers in the vertical inlet and outlet headers permit the four lower tubes to be used for the gas-cooling circuit, the remainder of the tubes being used in the mercury circuit. The basic tube cross section, when expanded, is the same as that specified for design No. 2; the lengths, however, will be different. The comments made on p. 75 regarding the use of titanium alloy also applies to this design.

4-6 Nomenclature

A	area
D	hydraulic diameter
E_{λ_b}	monochromatic emissivity of a black body
e	actual fin effectiveness
F	force
F_e	emissivity factor
F_{12}	geometrical factor
F_s	solar configuration factor
f	friction factor
g	acceleration due to local gravity

g_c	gravitational constant
h	convection heat transfer coefficient
h_r	surface heat transfer coefficient for radiation
$I_n(X)$	modified Bessel function of order n
K	thermal conductivity
ℓ	length
M	mass
P	pressure
Q	total heat
q	heat generation
q_0	rate of heat dissipation of entire surface is at T_0
q"	heat flux
s	distance between two surface elements
T	temperature
T_0	absolute temperature at fin root
t_r	transmissivity of lunar surface atmosphere
V	velocity
v_f	view factor
W	flow rate
α	total absorptivity
δ	fin profile semi thickness
ϵ	emissivity
ϵ_{sr}	absorptivity of the radiator wing surface for solar radiation
θ	angle between beam and normal to the radiator surface
λ	wave length
ξ	angle of beam
ρ	density
τ_l	local tractive force
ω	fin width
σ	Stephan Boltzman constant

Subscripts

a	outer space
b	black body
f	liquid; friction
G	gas phase
g	gas
h	head
IP	inverse parabolic
L	Liquid phase
l	length
m	moon
o	initial
R	rectangular
r	radiator
s	sun
T	triangular
TP	two phase fluid

4.7 References to Radiator Section

1. Elsmore, B., Radio Observations of Lunar Atmosphere, Philosophical Mag., 2(8th Series), 1040-6 (1957).
2. 1958 NASA/USAF Space Probes, Vol. 2, Payload and Experiments, NASA Memo 5-25-59W, June 1959, p. 59
3. Kern D. G., Process Heat Transfer, McGraw-Hill Book Co., Inc., New York, N.Y. (1950), pp. 272-273.
4. Baker, R. H., Astronomy, D. Van Nostrand Co., Inc., New York, 6th Ed., 1956.
5. Giedt, W. H., Principles of Engineering Heat Transfer, D. Van Nostrand Company, Inc., Princeton, New Jersey, January, 1957.
6. Yakob, M., Heat Transfer, John Wiley and Sons, Inc., New York, 1957.
7. McAdams, W. H., Heat Transmission, McGraw-Hill Book Co., Inc., 3rd Ed. (1954).

8. Callinan, J. P. and Berggren, W. P., Some Radiator Design Criteria for Space Vehicles, Journal of Heat Transfer, 81(Series C), 237 (Aug. 1959).

9. Liquid Metals Handbook, Sodium-NaK Supplement, TID 5277, 1955.

10. Kutateladze, S. S., Heat Transfer in Condensation and Boiling, AEC Translation 3770, Second Edition, (Aug. 1959).

11. Schneider, P. J., Conduction Heat Transfer, Addison-Wesley Publishing Company, Inc., Reading, Massachusetts (1955).

12. Brown, A. J., and Marco, S. M., Introduction to Heat Transfer, McGraw-Hill Book Company, Inc. New York, Second Edition, 1951.

13. Misra, B., and Bonilla, C. F., Heat Transfer in the Condensation of Metal Vapors: Mercury and Sodium up to Atmospheric Pressure, HEAT TRANSFER - LOUISVILLE, Chemical Engineering Progress Symposium Series, 52(No. 18), pp. 7-21 (1956).

14. Levy, S., Steam Slip - Theoretical Prediction from Momentum Model, Transactions of ASME Journal of Heat Transfer, 82(No. 2), 113 (1960).

15. Kutateladze, S. S. et al., Liquid Metal Technology, Supplement to Atomnya Energia, No. 2. (1958).

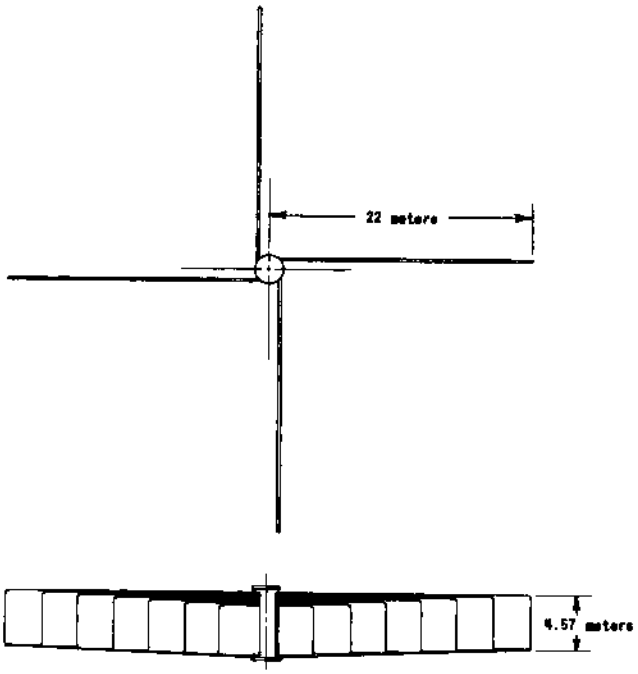

FIG. 4-1
GEOMETRIC ARRANGEMENT OF DESIGN #1 RADIATOR WINGS

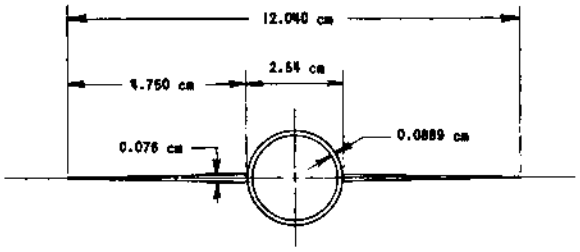

FIG. 4-2
TRIANGULAR FINNED CONDENSER UNIT

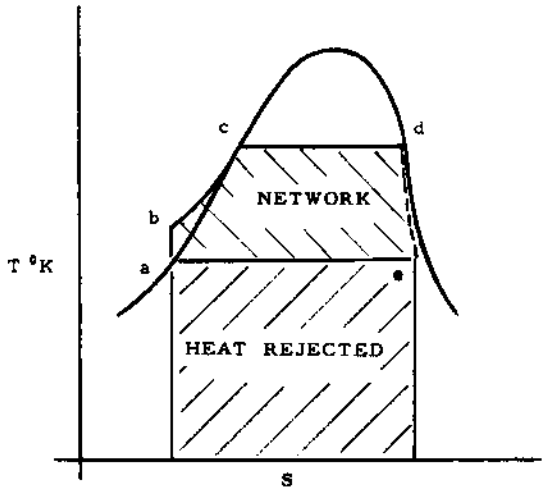

FIG. 4-3
TEMPERATURE-ENTROPY DIAGRAM

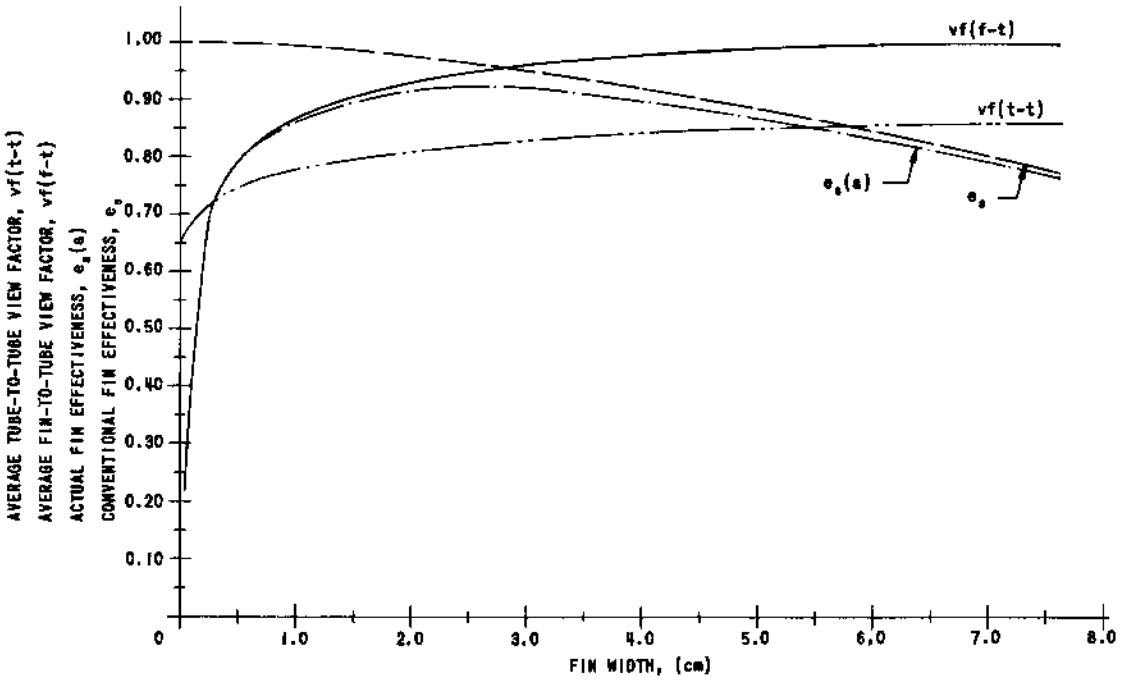

FIG. 4-4
FINNED CONDENSER TUBE PARAMETERS Vs. FIN WIDTH

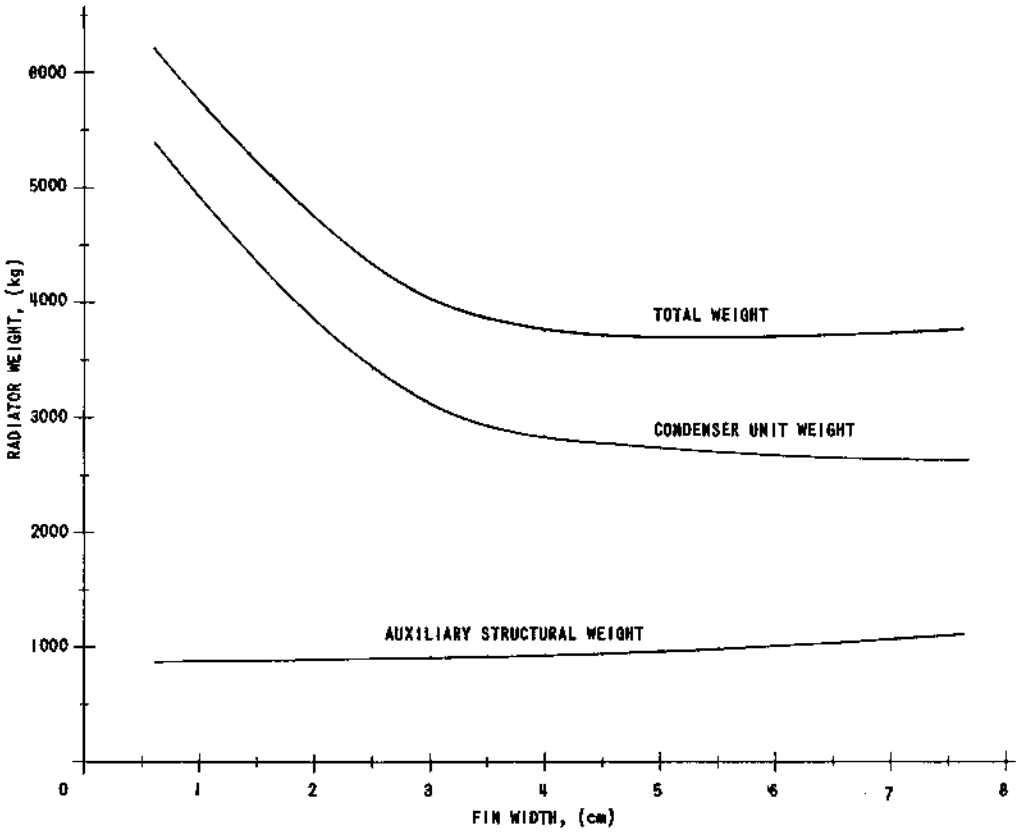

FIG. 4-5
RADIATOR WEIGHT Vs. FIN WIDTH

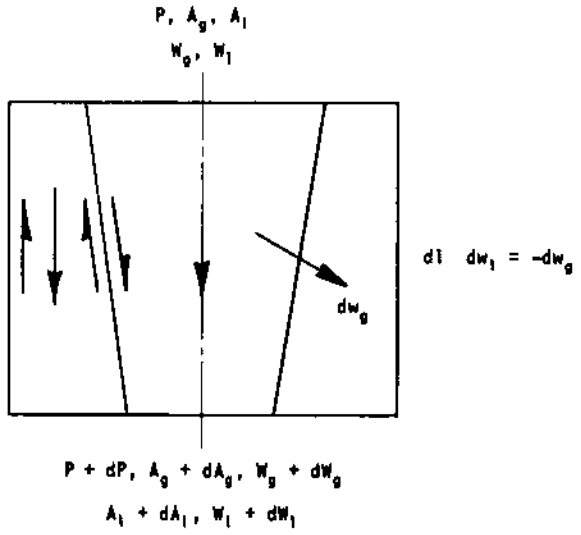

FIG. 4-6
HOLD-UP MODEL OF MERCURY CONDENSATE

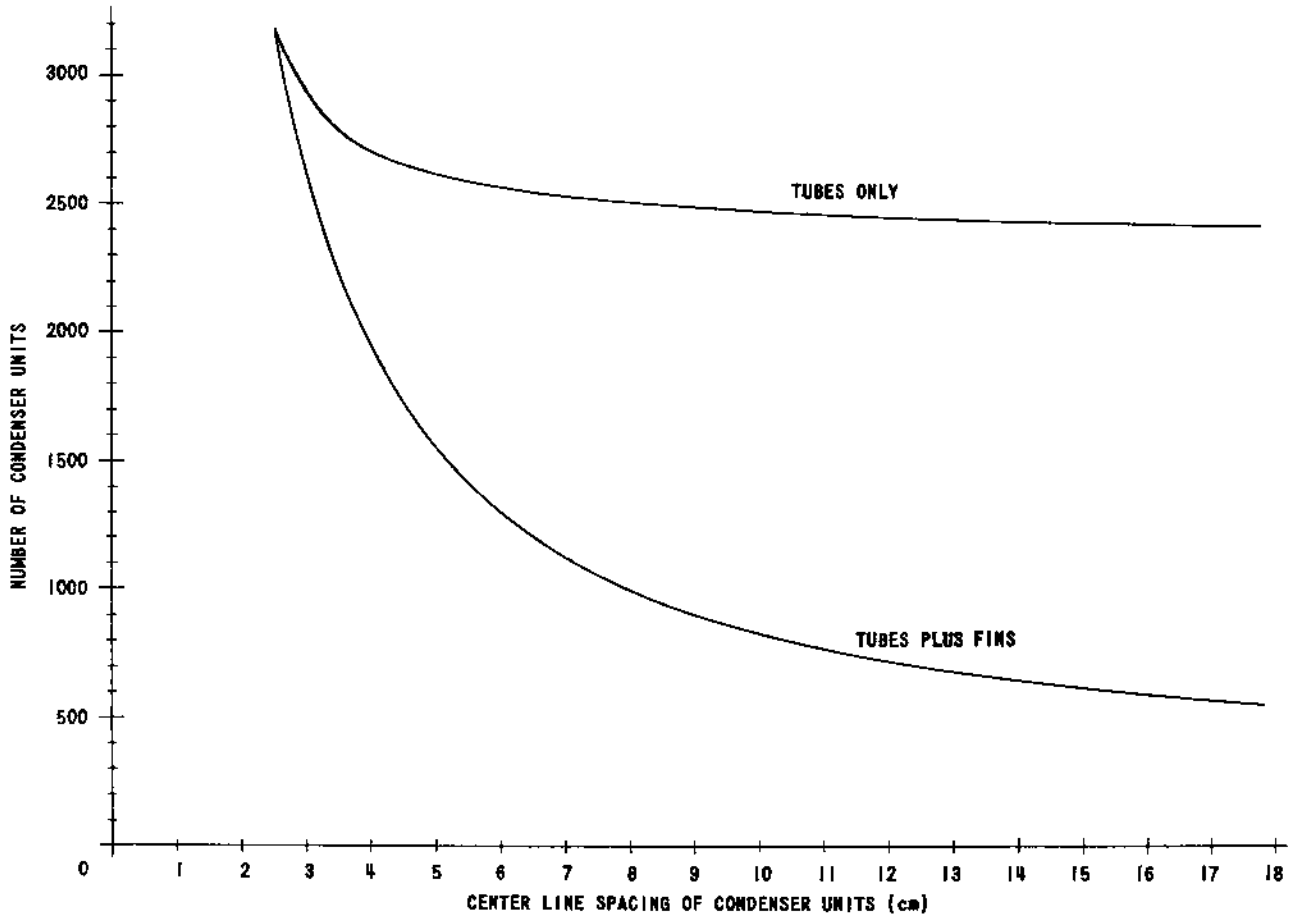

FIG. 4-7
NUMBER Vs. CENTER LINE SPACING OF CONDENSER UNITS

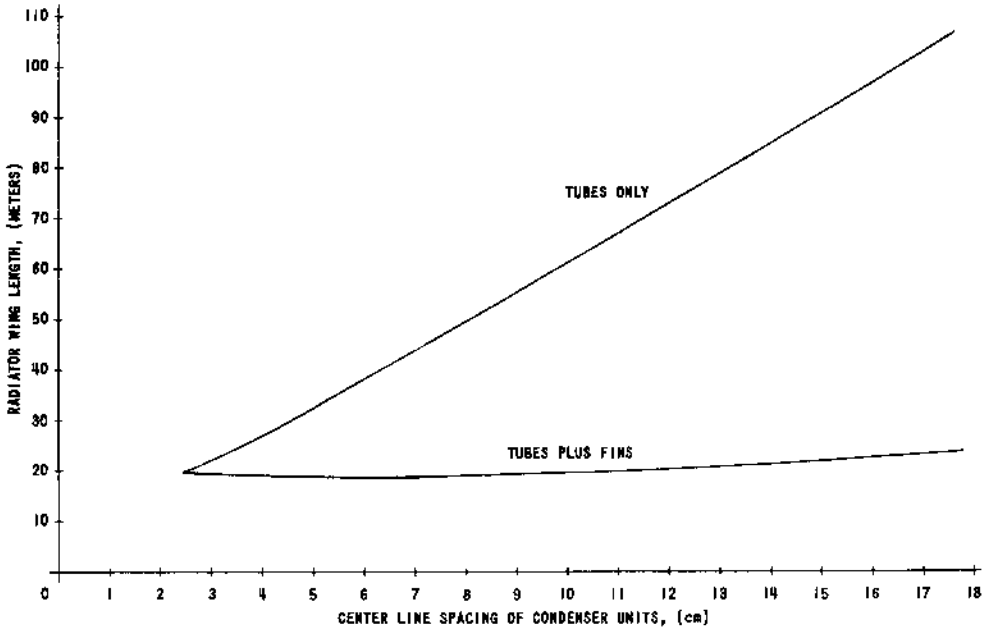

FIG. 4-8
RADIATOR WING LENGTH Vs. CENTER LINE SPACING OF CONDENSER UNITS

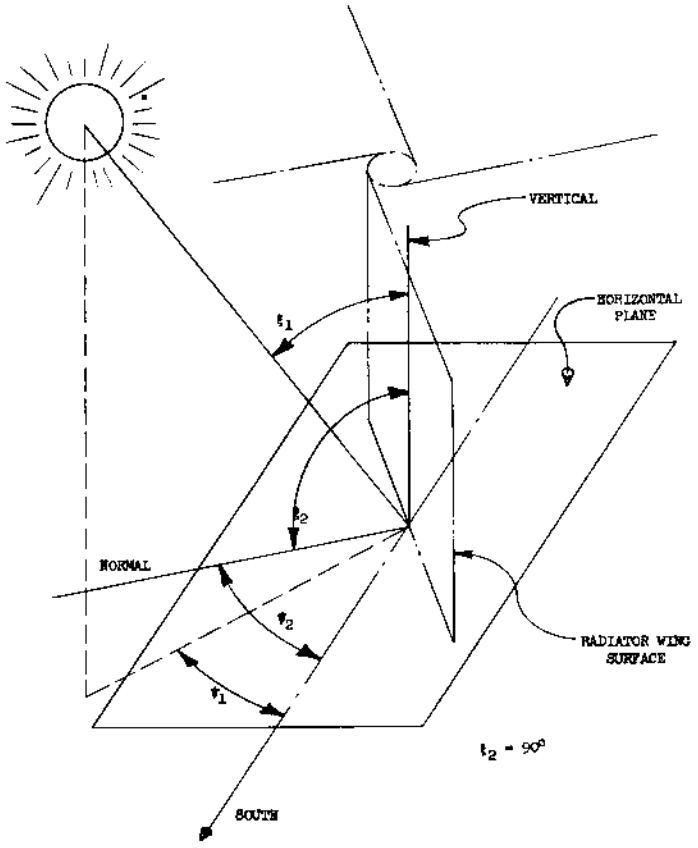

FIG. 4-9
θ-ANGLE BETWEEN THE SUN'S RAYS AND THE NORMAL TO THE RADIATOR SURFACE

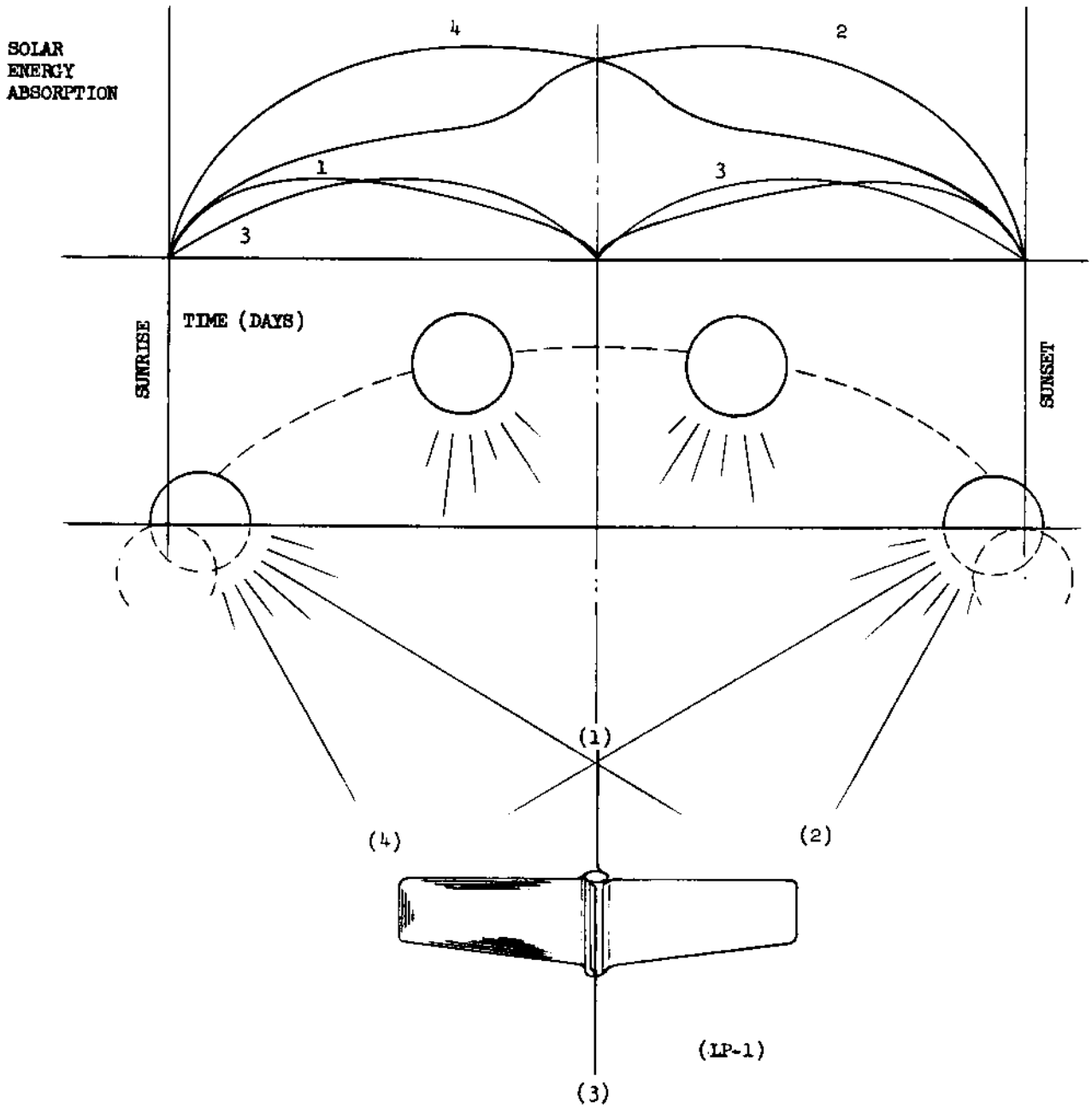

FIG. 4-10
VARIATION IN ABSORPTION OF SOLAR ENERGY DURING A TYPICAL LUNAR DAY

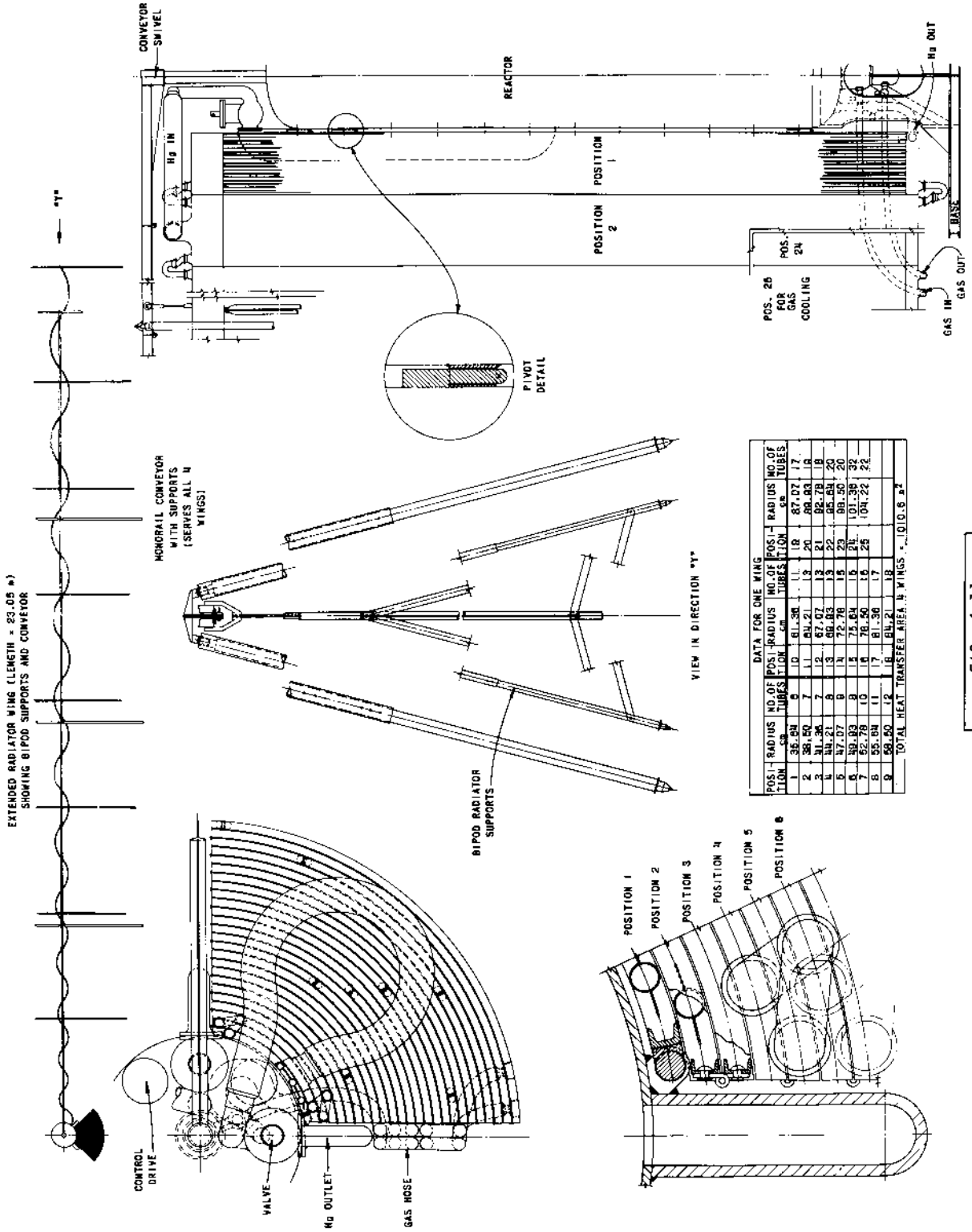

POSITION	RADIUS cm	NO. OF TUBES	POSITION	RADIUS cm	NO. OF TUBES	POSITION	RADIUS cm	NO. OF TUBES
1	36.84	6	10	61.36	11	18	87.07	17
2	38.50	7	11	64.21	13	20	88.83	18
3	41.36	7	12	67.07	13	21	92.78	18
4	44.21	8	13	69.93	13	22	95.64	20
5	47.07	8	14	72.78	15	23	98.50	20
6	49.93	8	15	75.64	15	24	101.36	32
7	52.78	10	16	78.50	16	25	104.22	22
8	55.64	11	17	81.36	17			
9	58.50	12	18	84.21	18			

DATA FOR ONE WING

TOTAL HEAT TRANSFER AREA 4 WINGS = 1010.6 m^2

FIG. 4-11
RADIATOR DESIGN #2

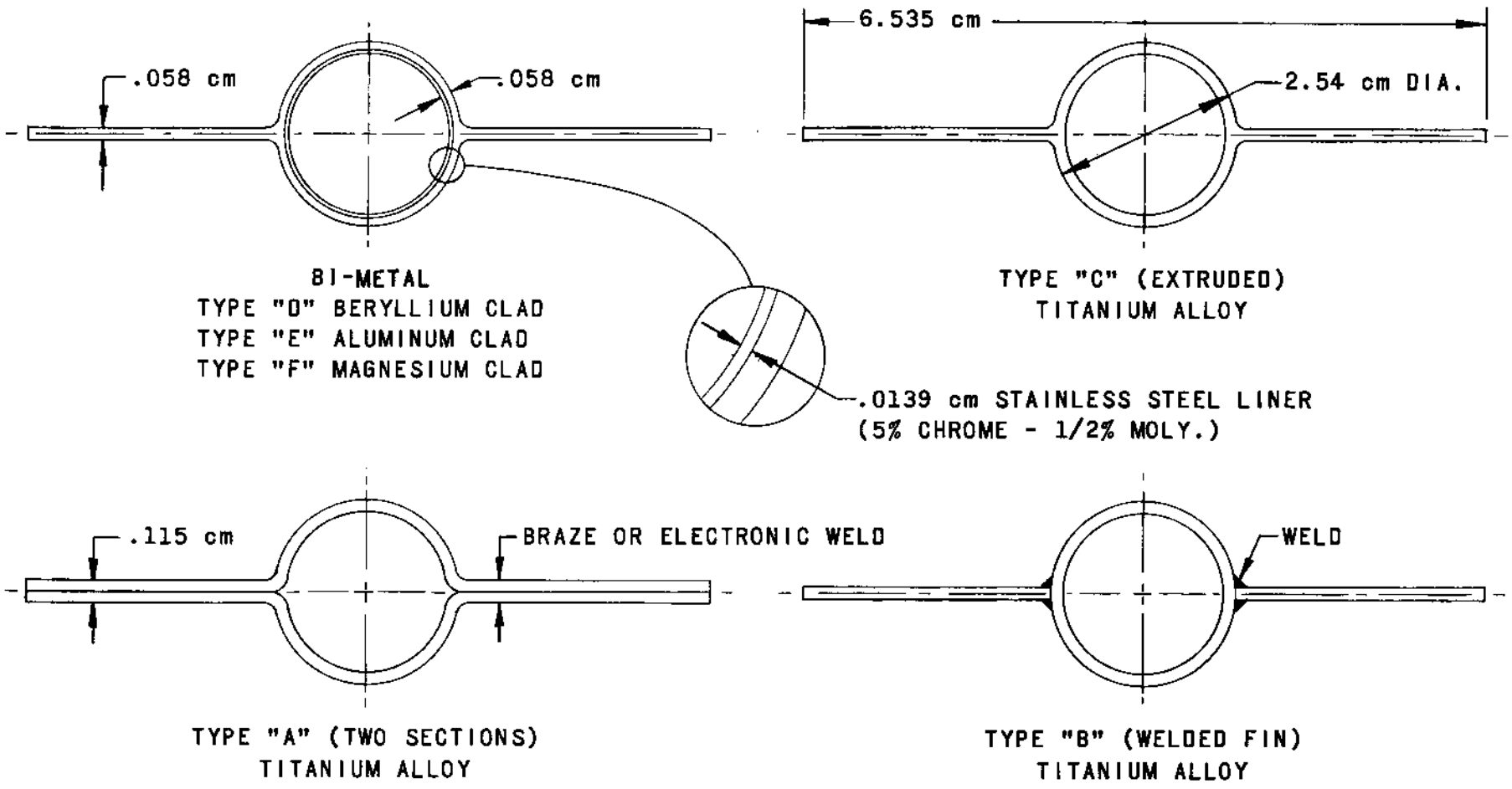

NOTES:

TUBE I.D. TO CONTAIN MERCURY AT 371 °C AND 6.86 ATMOS.

TYPE "D" "E" AND "F" MAY BE FABRICATED THE SAME AS TYPE "A"

FIG. 4-12
RADIATOR TUBE DESIGN # 2

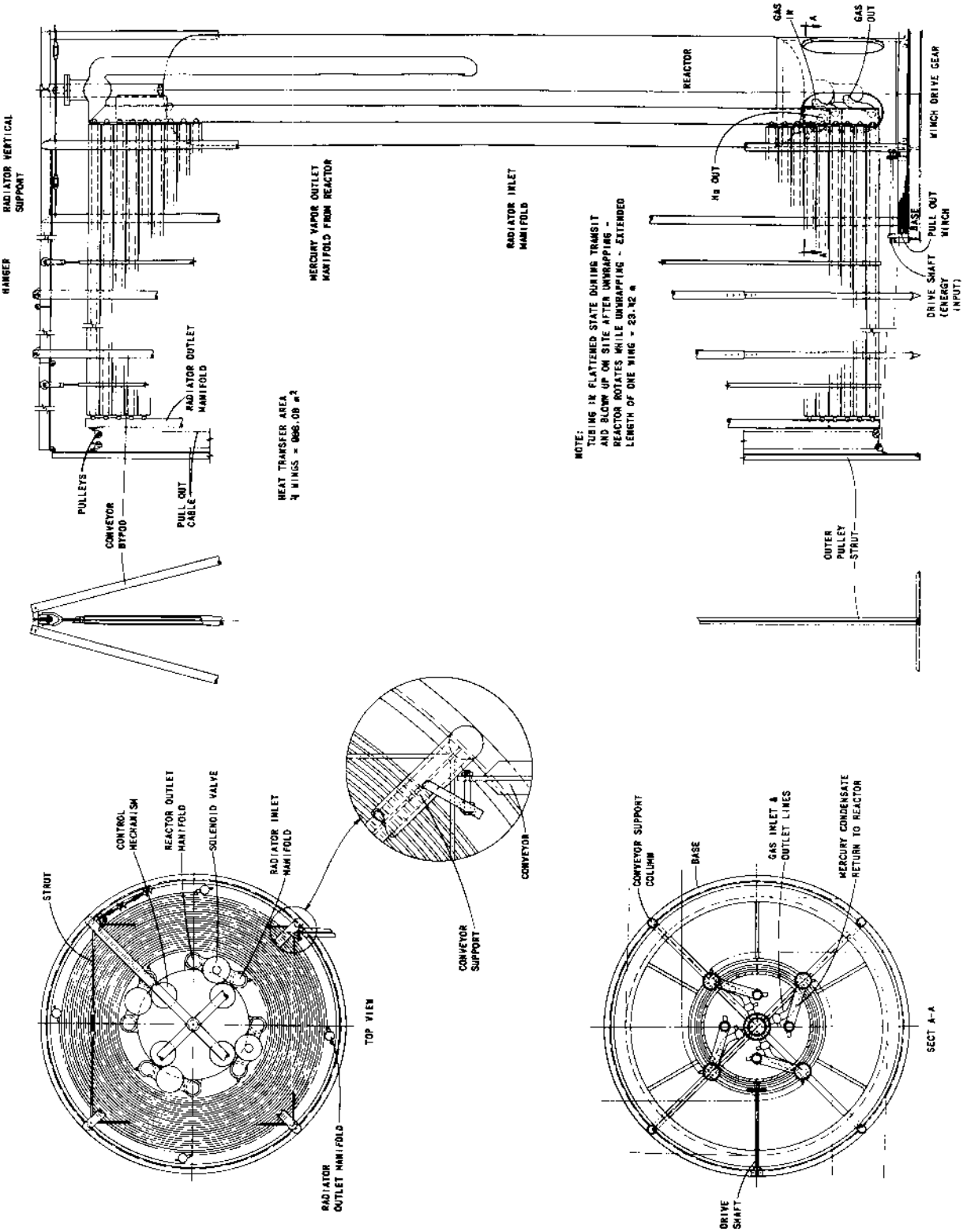

FIG. 4-13
RADIATOR DESIGN #3

5-0 PUMPS AND COMPRESSOR

5-1 Recirculating and Condensate Pumps

Two mercury pumps (see Fig. 2-1) are required in the system: the recirculating pump to provide circulation in the reactor, and the condensate pump to take the mercury from the condenser and return it to the reactors.

The circulating pumps handle a large volume of mercury at low pressure ratio, and the condensate pump handles a small volume at a high pressure ratio. Since the output of both pumps goes to the inlet header of the reactor, their impellers are integral with separate inlets and a common volute, thus saving weight and space for piping and casing.

A radial flow impeller is used for the condensate pump because of the large pressure ratio and small volume of mercury. A mixed flow impeller is used for the recirculating pump because of the small pressure ratio and large volume of mercury.

The integral impeller unit is mounted on an extension of the main turbine shaft; thus the weight and loss of efficiency entailed in intermediate-energy converters is saved. Also, a shaft seal is eliminated, because the pump and turbine casings are integral.

The characteristics of these two pumps are as follows:

	Condensate Pump	Circulatory Pump
Type	Radial	Mixed flow
Flow, kg/sec	22.68	56.94
Head, cm of Hg	1097	293
Inlet pressure, atmos	1.27	11.9
Outlet pressure, atmos	14.0	14.0
Inlet temp, °C	371	576
Pressure Ratio	11.8	1.2
Speed, rpm	6,000	6,000
Pump power, kw	3	10
Weight of both impellers and volute, kg	68	

5-2 Hydrogen Compressor

Hydrogen is used to cool the windings of the main generator and the windings and bearings of the auxiliary motor because a gas possessing good physical properties for heat transfer by convection is required to remove

the heat from the main generator windings. Hydrogen also has the highest ratio of specific heats of any gas. This property makes it desirable as a working medium in gas compressors where weight and volume are at a premium.

The cooling system consists of an axial flow compressor (see Fig. 5-1) for circulating the hydrogen and a radiator for removing the heat from the hydrogen. The compressor is also on an extension of the main shaft. Information pertaining to the compressor is tabulated below.

Type of compressor	axial with air foil type blades
Number of stages	6
Working medium	hydrogen
Flow of Hydrogen	15 kg/min
Pressure at inlet	6.8 atmos
Pressure ratio	1.2
Temperature of Hydrogen entering	66°C
Head per stage cm of H	28.7×10^4
Compressor work	19.25 kw
Speed	6000 rpm
Flow number	0.42
Pressure number	0.553
Throttling number	0.32
Specific speed	1.001
Avg. dia. of blade tips	21.6 cm
Avg. blade height	1.0 cm
Number of blades per wheel	64
Material	aluminum
Weight	27 kg

5-3 Radiator

The radiator removes the heat from the hydrogen cycle by radiating it to space. It is identical in construction to the main condensing radiator. The temperature of space is considered to be absolute zero.

Temperature leaving the radiator	10°C
Temperature entering the radiator	84°C
Temperature entering the machinery	10°C
Temperature leaving the machinery	66°C
Flow	15 kg/min

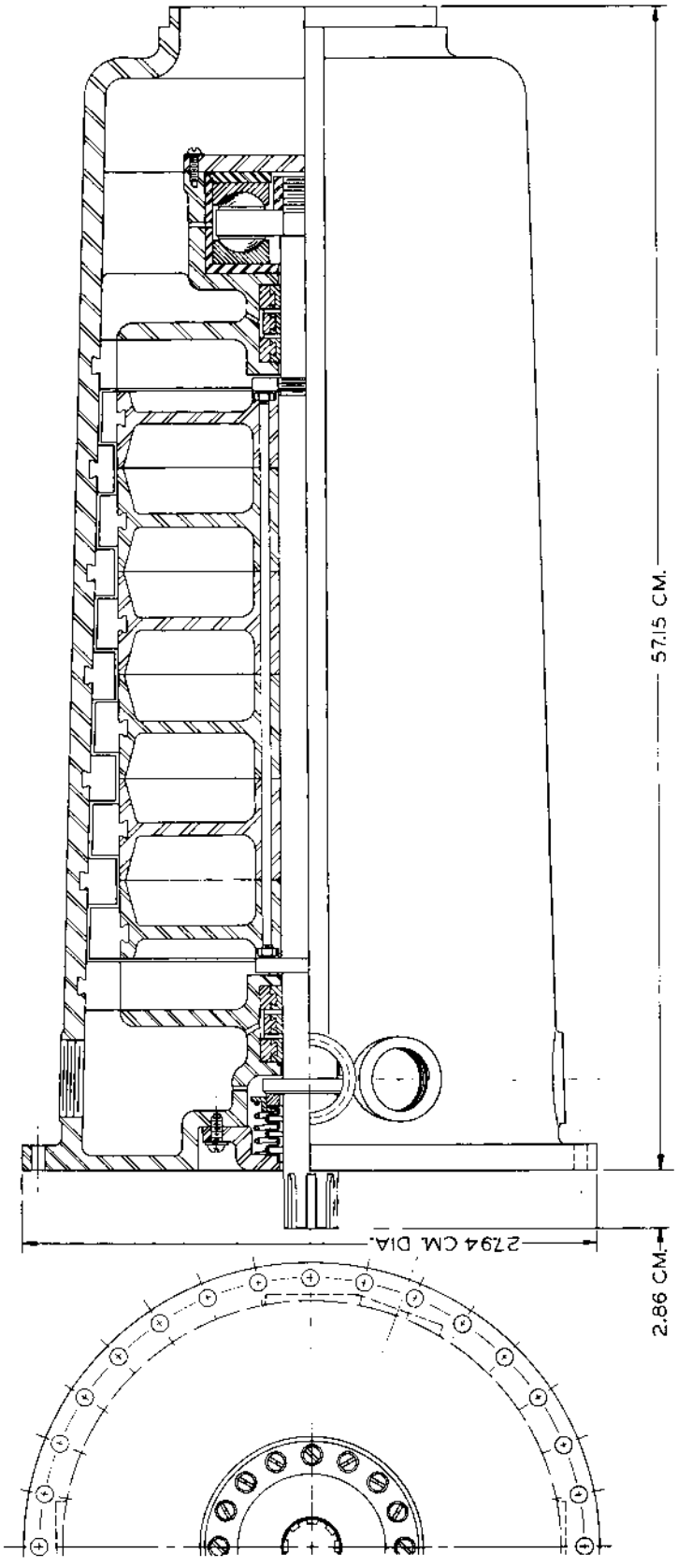

FIG. 5-1
CROSS SECTION OF
HYDROGEN COMPRESSOR

6-0 CYCLE FLUID

An ideal fluid for the Rankine cycle should have the following properties:

1. The latent heat of vaporization should be large and the heat capacity small relative to each other. This condition is exemplified in the temperature-entropy diagram of Fig. 6-1.

The effect of Cycle A on Cycle B would be negligible and the efficiency of the Rankine cycle (A and B) would essentially be that of Carnot Cycle B.

2. The critical point should be above the highest operating temperature to allow the temperature of heat addition to Cycle B to be increased to the highest possible value that the materials can withstand.

3. The vapor pressure at the highest operating temperature should be low. High pressure increases design costs and produces maintenance problems.

4. The vapor pressure at the lowest operating temperature should be higher than atmospheric pressure, thus preventing a mixture pressure increase. This mixture pressure of exhaust for the turbine greatly controls the work output.

5. The entropy of the saturated vapor should not change markedly with change in pressure. However, the angle should not be such that the vapor is in the superheat region as it enters the condenser or becomes wet in passing through the turbine.

6. The properties of the fluid should be conducive to high rates of heat transfer to engender minimum surface areas and temperature differences.

7. This ideal fluid should be low in cost, stable, nonexplosive, and noncorrosive under all conditions of operation.

The nature of the fluid which satisfies these desirable characteristics is shown in part in the temperature-entropy diagram of Fig. 6-2.

The ideal Rankine fluid shows that the properties of the working fluid are intimately related to the output of the Rankine cycle.

Of particular interest are the high-temperature coolants which occasionally result in high operating pressures. These high-pressure coolants produce excessive penalties with respect to system weight due to stress

considerations. Conversely, low-pressure coolants result in excessive penalties of weight due to a high specific volume requirement. Water and mercury are examples of working fluids which violate excessive pressure requirements. Bismuth and lead have excessive specific volumes due to their low pressures. While rubidium, sodium, and potassium offer advantageous high-temperature cycles, their temperature ranges are not concomitant with long turbine life. Past experience dictates that mercury be used as the working fluid because its feasibility has been proven in many commercial power plants.

The physical properties of mercury which are of interest in this investigation are shown on Figs. 6-3 to 6-14.

Additional pertinent information on physical properties is listed below.

Gas constant	4.108 atmos. $cm^3/°K$ gm
Volume increase on fusion	3.6%
The heat of fusion	2.80 cal/gm
Fusion temperature	-38.9°C

For details and further reference, see original sources.[1,2,3]

6-1 Uranium-Mercury System

(a) The Constitutional Diagram

The uranium-mercury system has been studied by Wilson[4] and by Frost,[5] with virtually identical results. The essential difference was that Frost studied the system by sealing samples and allowing the pressure to rise, while Wilson worked at a pressure of 1 atmos. The pressure-temperature diagram of Fig. 6-3 is that of Frost. Since data above the boiling point of mercury (358°C) were obtained by means of a sealed system, the pressure varied and was as high as several hundred atmospheres.

A diagram by Wilson is identical, except that mercury vapor was in equilibrium with the uranium-mercury compounds and with uranium above the boiling point of mercury.

This is a very difficult system to study. A special means of preparing alloys is necessary, the high vapor pressure of mercury presents a special problem, and the intermetallic compounds are pyrophoric in nature and, therefore, require special techniques in handling.

It is of interest that Wilson and Frost used the same method of alloy preparation. Essentially, it consisted of hydriding uranium, dehydriding under vacuum, and reacting mercury with the resulting uranium powder.

(b) Crystallography

Tabulated crystallographic data for UHg_2, UHg_3, and UHg_4 are available from the works of Rundle.[6] Frost has reported similar information for UHg_2 and UHg_3 but was unable to obtain a more certain analysis of the UHg_4 structure. According to Frost, UHg_2 is close-packed hexagonal with a = 4.934 Å and c = 3.503 Å, whereas UHg_3 is close-packed hexagonal with a = 3.320 Å and c = 4.875 Å. The UHg_3 structure is reported to be a random structure.[1]

It has been reported[2] that the unit cell volumes of these compounds, within the limit of accuracy of the work, are equal to the additive atomic volumes. This equivalence is interpreted to mean that the binding is purely metallic in nature.

Phase	Type	Dimensions, Å	Number of Molecules	Density, g/cm³		Space Group	Remarks
				X-ray	Other		
Delta (UHg_2)	Hexagonal	a = 4.99 ± 0.01 c = 3.23 ± 0.01	1	15.29	15.3	C6/mmm	C32-type, AlB_2 structure
Epsilon (UHg_3)	Hexagonal	a = 3.327 ± 0.005 c = 4.888 ± 0.005	½	14.88			
Zeta (UHg_4)	Bcc	a = 3.63	2	14.5			Tentative analysis

6-2 Mercury Corrosion

Our present knowledge concerning the resistance of engineering materials to mercury at elevated temperatures can be attributed almost entirely to the efforts of A. J. Nerad and his associates in connection with the development of the mercury-vapor turbine by the General Electric Company. They were concerned chiefly with ferrous alloys. In most cases, only equilibrium solubility data are available upon which to judge the resistance of other materials to attack by mercury (see Table 6-1).

Early, short-time experiments near the normal boiling temperature of mercury indicated that iron and steels were practically unaltered by mercury. However, over long periods of operation it was found that the inside tube walls in the cooler zones of large mercury-vapor boilers became plugged with a crystalline deposit of iron.

Dynamic laboratory tests were carried out in hundreds of so-called "harps," wherein mercury was circulated by thermal convection through the heating of one leg and the cooling of the top and other leg of a closed loop of pipe. Most tests were carried out at 650°C and some tests at as

high as 800°C, and the 10°C temperature differences which were maintained between the hot and cold zones resulted in very slow flow of the mercury (approximately 3.05 cm/sec). In the following discussions where resistance to flowing or dynamic mercury is referred to, it will be understood that the specimens were tested in these harps.

Studies in these systems were made of the rate of attack by mercury as a function of alloying elements in the steel, of additives to the liquid metal, and of such variables as time and temperature. It was found that some low-alloy steels, e.g., Sicromo 5S (4-6 chromium, 0.45-0.65 molybdenum, and 1-2 silicon), had better resistance to attack by mercury than low-carbon steel. However, of even greater importance was the discovery that the controlled addition of certain elements (titanium and magnesium) to the mercury resulted in negligible attack on even low-carbon steel.

(a) Mechanism of Attack on Steels by Mercury

Whereas ferrous alloys are practically unaltered by mercury in static systems, they are drastically attacked in dynamic systems where mercury flows very slowly and where even slight temperature gradients exist. A theoretical discussion of the differences in the mechanism of attack by mercury and that by NaK has been offered by Epstein.[3]

The attack on steels by mercury appears to be largely governed by a solution mechanism whose rate is determined by the rate of diffusion of iron in mercury. Since attainment of equilibrium solubility of iron in the liquid boundary layer is extremely rapid, the rate of attack is determined by the rate of diffusion of the dissolved iron from the solid-liquid interface into the bulk of the liquid. The most recent information indicates that the equilibrium solubility of iron in mercury is very low, but that an appreciable temperature coefficient of solubility exists - the solubility varies from 0.015 ppm at 25°C to 0.96 ppm at 700°C. Unlike the case for iron in NaK, calculations for dynamic systems, taking the flow rate of mercury into account and assuming that equilibrium solubility is achieved in both the hot and cold zones, give rates of attack on steel that are in good agreement with experimental observations.

At 500°C and above, the rate of attack increases approximately by a factor of 5 for every 100°C rise in the mercury temperature. For example, the rate of attack (based on weight changes) on low-carbon steel in a harp test increased from 5 mpy at 500°C to 560 mpy at 800°C.

(b) Effect of Alloying Elements in Low-carbon Steel

A large number of tests were made in an effort to develop low-alloy steels which would resist attack by flowing mercury. Selected test data are given in Table 6-2. The following discussion is based almost

entirely on these data. Low-carbon steels have good resistance to attack by flowing mercury below about 400°C, limited resistance up to about 540°C, and poor resistance at higher temperatures.

Alloying elements which, when added in small amounts, make low-carbon steels more resistant to attack by mercury in dynamic systems include chromium, silicon, titanium, and possibly molybdenum, whereas aluminum shows little promise. Various combinations of these elements in small amounts, especially of chromium, silicon, and molybdenum, result in several steels which have good resistance to attack by flowing mercury up to about 600°C.

Chromium, in amounts as low as 0.2 and 0.4 wt-%, increased the resistance of low-carbon steel to attack by dynamic mercury by a factor of about 6. A 4 wt-% chromium addition was much less effective, probably because of the formation of nonadherent chromium oxide films. Averages of a large number of harp tests, as well as long-time exposures in operating mercury boilers, resulted in weight losses of a 5 wt-% chromium steel which were half those of low-carbon steel.

The addition of 0.5 wt-% molybdenum to low-carbon steel had little, if any, influence on its ability to resist attack by dynamic mercury, but a 20 wt-% molybdenum addition reduced the attack by mercury at 650°C to a negligible amount.

Additions of 1, 2, and 3 wt-% silicon to low-carbon steel were uniformly successful in lowering the rate of attack by flowing mercury at 640°C by about a factor of 10.

Titanium additions of 1 and 2 wt-% to low-carbon steel resulted in a four to fivefold increase in the resistance to attack by flowing mercury.

The resistance of low-carbon steel to attack by dynamic mercury was somewhat improved by the addition of small amounts of aluminum plus chromium; however, in general, the benefits were not so great as those derived from chromium additions alone. The best of these alloys was a commercially available Nitralloy, not nitrided, containing 1.23 wt-% aluminum and 1.49 wt-% chromium, which had limited resistance to attack by flowing mercury (4 mpy) at 650°C, better than a tenfold improvement over ordinary low-carbon steel. The equilibrium solubility of iron from Nitralloy was found to be practically the same as that found when pure iron was exposed to mercury.

Low-alloy steels containing 4 to 6 wt-% chromium, 0.45 to 0.65 wt-% molybdenum, and 1 to 2 wt-% silicon (Sicromo 5S or Croloy 5-silicon), which are used in mercury boilers, were found to be about

20 times as resistant as low-carbon steel to attack by flowing mercury over a wide temperature range. Steels containing greater amounts of chromium and molybdenum were found to have even better resistance to attack by mercury.

The high-chromium ferritic stainless steels had good resistance to attack by static mercury at 550°C, but these steels were not tested in harps. The chromium-nickel austenitic stainless steels showed poor resistance to attack by dynamic mercury at 650°C. Other high-nickel ferrous alloys, however, resisted attack by static mercury at 550°C.

(c) Effect of Additives to the Mercury on Attack on Ferrous Metals

Attack by mercury on ferrous alloys can be reduced to negligible amounts by the addition of an inhibitor to the mercury, the best of which is titanium, as indicated by the data listed in Table 6-3.

The presence of 10 ppm titanium dissolved in the mercury reduces the rate of attack on ferrous metals at 650°C to an inappreciable value, and as little as 1 ppm titanium is similarly effective at 4550°C. Zirconium, chromium, nickel, and aluminum are also effective as inhibitors, but larger concentrations are required. Copper, lead, and tin in mercury increase its attack on low-carbon steel.

In addition to the presence of an inhibitor, it was found desirable to have a wetting agent present in the mercury. Its function is twofold: (1) to reduce oxides on steel surfaces in order that wetting and optimum heat transfer may be realized, and (2) to react with the free oxygen, nitrogen, and water vapor in the mercury in order to keep the inhibitor active. Wetting agents must, therefore, have a greater affinity for oxygen and nitrogen than both the inhibitor material, titanium, and iron.

The alkaline earths, especially magnesium and calcium, have been found to be very effective wetting agents and do not have any deleterious effects. Magnesium is preferred on the basis of low cost and higher solubility in mercury. Approximately 20 ppm magnesium is required at 650°C to effectively tie up free oxygen, thereby allowing titanium to remain active as an inhibitor.

The alkali metals, especially sodium, are less satisfactory as wetting agents. They tend to form compounds, such as $Na_2O \cdot Fe_2O_3$, which are both insoluble in mercury and resistant to reduction. This material tends to plug openings in dynamic systems and can be very troublesome.

(d) Nonferrous Metals

The dearth of experimental evidence that is available makes it difficult to judge nonferrous metals as containing materials for mercury at elevated temperatures. The only metals tested in dynamic harp systems were molybdenum, tungsten, and Stellite. Several metals have been tested in static mercury, but the results are only qualitative and may be misleading if used as a basis for the design of dynamic systems. Solubility data, much of it at room temperature only, are also available; however, experience regarding mercury attack on ferrous metals indicates that these data are probably of limited usefulness to the designer of an engineering system. However, sufficient experimental evidence is available to indicate that tungsten, molybdenum, chromium, and beryllium can be considered for long-time use in contact with mercury at elevated temperatures.

Although the available information is very meager, there is reason to believe that the following elements might resist attack by mercury at elevated temperatures: tantalum, columbium, silicon, and titanium. The following can be used at times to contain mercury at low temperatures, but they have limited resistance to attack by mercury at elevated temperatures: nickel, Inconel and Monel, copper and copper-base brazing alloys, cobalt and Stellite, platinum, manganese, and zirconium.

Several elements are relatively soluble in mercury, including aluminum, bismuth, cadmium, cerium, gold, lead, magnesium, silver, tin, and zinc. Alloys containing appreciable amounts of these elements, especially in the free state, are not recommended for use with mercury.

(e) Nonmetals

In the laboratory, mercury is ordinarily handled in glass. From free-energy considerations it is evident that ceramic materials can be expected to withstand attack by mercury. The negligible solubility of carbon in mercury at its normal boiling point indicates that graphite might also be used as a containing material.

6-3 Enthalpy-entropy Diagram and Thermodynamic Properties

The enthalpy-entropy diagram for mercury is shown on Fig. 6-15.

The thermodynamic properties of mercury are shown on Fig. 6-16.

6-4 References

1. ATL-118 (appendix D), Evaluation of Mercury-cooled Breeder Reactors, American-Standard, Sept. 1959.
2. BMI-1000, Compilation of U.S. and U.K. Uranium and Thorium Constitutional Diagrams, Battelle Memorial Institute (July 1955).
3. Liquid-Metals Handbook, NAVEXOS P-733, Atomic Energy Commission Department of the Navy, Washington, D.C. (June 1955).
4. Wilson, A. S., Ahmann, D. H., and Baldwin, R. R., unpublished (October 1945).
5. Frost, B. R. T., The System Uranium-Mercury, (AERE-M/R 1208) J. Inst. Metals, 82 (9), 456-462 (1954).
6. Rundle, R. E., and Wilson, A. S., The Structures of Some Metal Compounds, (AECD-2388) Acta Cryst., 2, 148-150 (1949).

TABLE 6-1
RESISTANCE OF MATERIALS TO LIQUID MERCURY

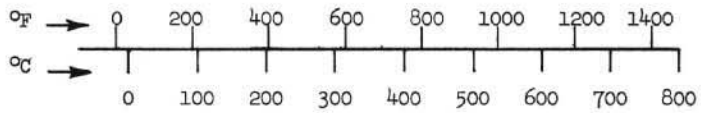

Ferrous Metals

Ferrous Metals (Ti and Mg in Hg)	◗
Low-C Steel	◗
Low-C Steel + 0.1 to 4 Al	D
Low-C Steel + < 4 Cr	D
5 Cr Steel	◗
Low-C Steel + 0.5 Mo	D
Low-C Steel + 20 Mo	D
Low-C Steel + 1 to 3 Si	D
Low-C Steel + 1 to 2 Ti	D
Low-C Steel + < 2 Al + < 2 Cr	D
Nitralloy (1.23 Al + 1.49 Cr)	D
Low-C Steel + 5.7 Cr + 1.2 Cu	D
Low-C Steel + < 4.5 Cr + < 4.5 Mo	D
Low-C Steel + 5.7 Cr + 1.2 W	D
Low-C Steel + 15 to 20 Mo + 3 Si	D
Low-C Steel + 8 Cr + 0.5 Al + 0.3 Mo	D
Sicromo 5S (5 Cr, 0.5 Mo, 1.5 Si)	◗
Low-C Steel + 5.5 Cr + 6.4 Mo + 1.4 Si	D
Types 304 and 310 S.S. (Cr, Ni)	D
High Ni-Fe and Ni-Cr-Fe Alloys	S
Ferritic Stainless Steels (Cr)	S

Nonferrous Metals

Tungsten	D
Molybdenum	SD
Chromium	S
Beryllium	S
Ta, Cb, Si, Ti, V	
Ni, Cu and their alloys	
Cobalt and Stellite	
Pt, Mn, Zr	
Al, Bi, Cd, Ce, Au, Pb, Mg, Ag, Sn, Zn	

Non-Metals

Glass
Ceramics
Graphite (C)

Resistance Ratings:

(These ratings refer to liquid-metal resistance only - not to temperature - dependant mechanical strength or metallurgical stability. See text for further discussion)

Good - Consider for relatively long time use
Limited - Short time use only
Poor - No structural possibilities
Unknown - Information inadequate

◗ - Dynamic mercury harp and industrial boiler tests.
D - Dynamic mercury harp tests.
S - Static mercury tests.

Table 6-2

DYNAMIC "HARP TESTS ON FERROUS ALLOYS IN MERCURY"

Material	Major Alloying Elements, wt %	Time of Test, hr	Maximum Harp Temp., °C	Rate of Attack (Weight Change Data)	
				mg/cm²/month	mils/year
Low-C steel (mild steel)	0.2 C	*	482	- 7	4
		*	538	-15	9
		*	593	-37	22
			649	-88	53
Low-C steel (+Al)	0.1 Al**	162	625	-28	17
	0.2 Al**	48	650	-18	11
	0.5 Al**	257	625	-64	40
	1 Al**	95	620	-52	32
	4 Al**	113	630	-69	43
	4 Al**	48	650	- 7	4
Low-C steel (+Cr)	0.2 Cr**	46	650	-13	8
	0.5 Cr**	138	615	- 7	4
	4 Cr**	138	625	-23	14
5 wt % Cr steel	5 Cr	*	482	- 3	2
		*	538	- 7	4
		*	593	-17	10
		*	649	-42	25
Low-C steel	0.5 Mo**	161	670	-86	53
(+Mo)	20 Mo**	64	650	< - 0.5	< 0.3
Low-C steel	1 Si**	67	640	- 7	4
(+Si)	2 Si**	107	640	-11	7
	3 Si**	67	640	- 7	4
Low-C steel	1 Ti**	329	620	- 9	6
(+Ti)	1 Ti**	329	675	-39	24
	2 Ti**	329	625	- 7	4
	2 Ti**	329	640	-15	9
Low-C steel	0.1 Al, 0.1 Cr**	136	625	-46	29
(+Al+Cr)	0.5 Al, 0.5 Cr**	137	630	-37	23
	2 Al, 2 Cr**	48	620	-44	27
	2 Al, 2 Cr**	142	650	-13	8
Nitralloy	1.23 Al, 1.49 Cr	165	650	- 7	4
(not nitrided)		2	615	6	4
Low-C steel (+Cr+Cu)	5.7 Cr, 1.2 Cu**	161	670	- 8	5
Low-C steel	0.5 Cr, 0.5 Mo**	140	650	- 6	4
(+Cr+Mo)	4.5 Cr, 4.5 Mo**	140	640	- 6	4
	4.9 Cr, 0.5 Mo	161	670	-86	53
Low-C steel (+Cr+W)	5.7 Cr, 1.2 W	100	660	-26	16
Low-C steel	15 Mo, 3 Si**	89	655	- 1	0.6
(+Mo+Si)	20 Mo, 3 Si**	88	655	< - 0.5	< 0.3
Low-C steel (+Al+Cr+Mo)	0.5 Al, 8 Cr, 0.3 Mo**	140	650	- 1	0.6
Low-C steel	4.6 Cr, 0.5 Mo, 1.23 Si**	140	640	- 6	4
(+Cr+Mo+Si)	4.6 Cr, 0.45-0.65 Mo, 1-2 Si (Sicromo 5S or Croloy 5 Si)	*	482	- 0.3	0.2
		*	538	- 0.80	0.5
		*	593	- 1.8	1.1
		*	649	- 4	2.5
	5.5 Cr, 6.4 Mo, 1.4 Si**	280	588	- 0.7	0.4
		982	620	- 0.8	0.5
		111	650	- 0.8	0.5
Low-C steel (+Al+Cr+Mo+Si)	0.8 Al, 5 Cr, 0.5 Mo, 0.9 Si**	450	650	-64	38
Type 304 S.S.	18 Cr, 8 Ni	460	652	-32	20
Type 310 S.S.	25 Cr, 20 Ni	400-500	650	-77	47

*Average of a large number of laboratory tests as well as samples from large-scale boiler operations, exposures of up to 10,000 hr.

**Alloys made in G.E. laboratory by melting portions of a single low-carbon steel billet and adding desired alloying elements.

Table 6-3

EFFECT OF ADDITIVES IN MERCURY ON THE RATE OF ATTACK ON LOW-CARBON STEEL

Additive	Time, hr	Temp., °C	Rate of Attack*	
			mg/cm²/month	mils/year
None	Testing periods ranging from 40 to 175 hr	482	- 6.5	4
None		649	- 88	53
None		800	- 990	560
0.1 wt% Sn		640	-4200	2590
1 wt% Cu		650	- 360	222
1 wt% Pb		650	- 280	173
10 wt% Pb		700	- 280	173
1 wt% Na		650	- 80	49
0.25 wt% Al		650	- 0.6	0.37
0.25 wt% Cr		600	<- 0.5	<0.3
1 wt% Ni		600	<- 0.5	<0.3
0.0001 wt% Ti	Tests of 100 to 2000 hr	454	<- 0.5	<0.3
0.001 wt% Ti		538	<- 0.5	<0.3
0.04 wt% Zr		625	<- 0.5	<0.3
0.02 wt% Zr		625	- 1	0.66

*There is evidence that the rate of attack does not change appreciably with time.

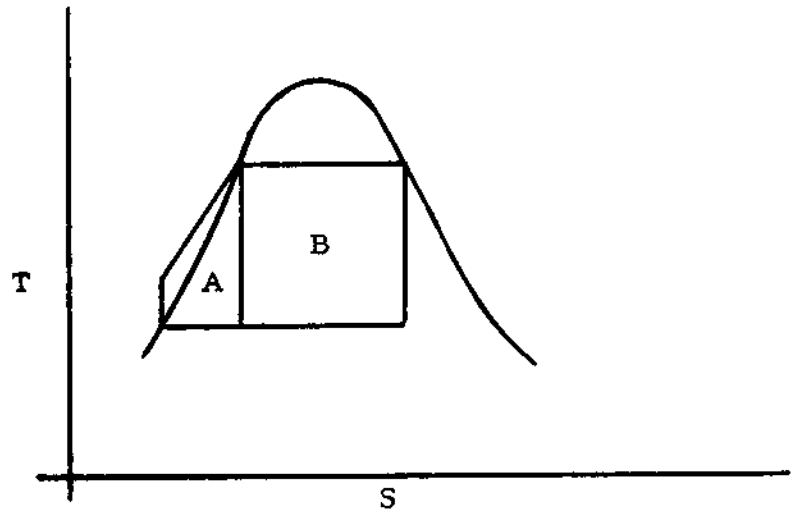

FIG. 6-1
THE RANKINE CYCLE

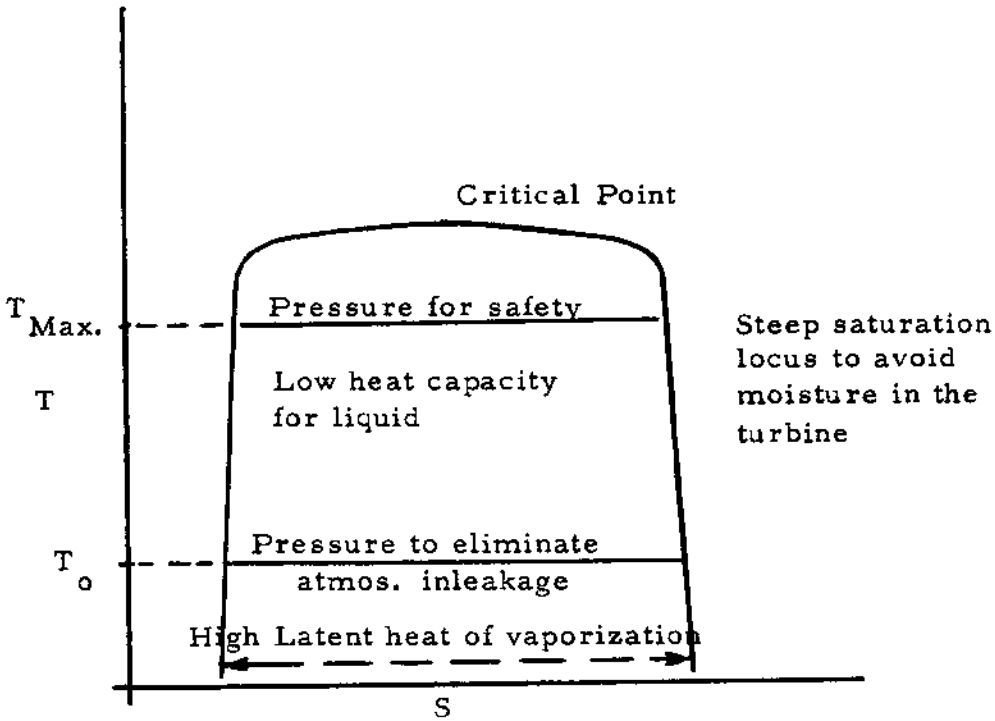

FIG. 6-2
THE CHARACTERISTICS OF AN IDEAL FLUID

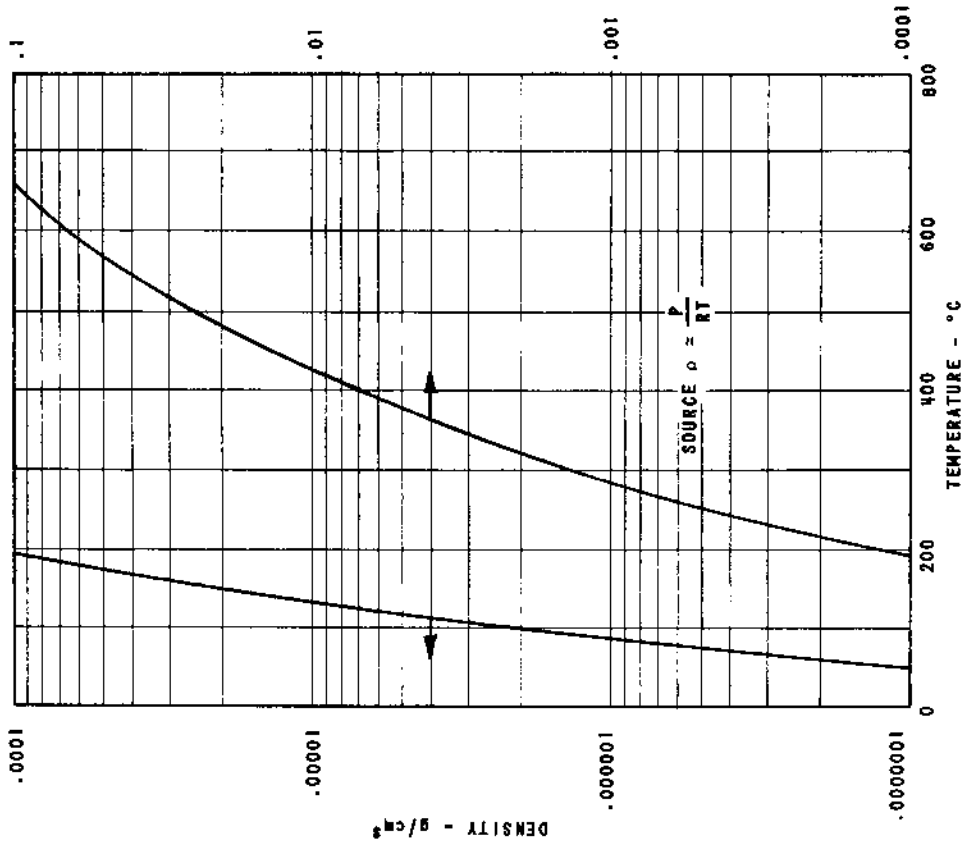

FIG. 6-4
MERCURY VAPOR DENSITY AT SATURATION CONDITIONS

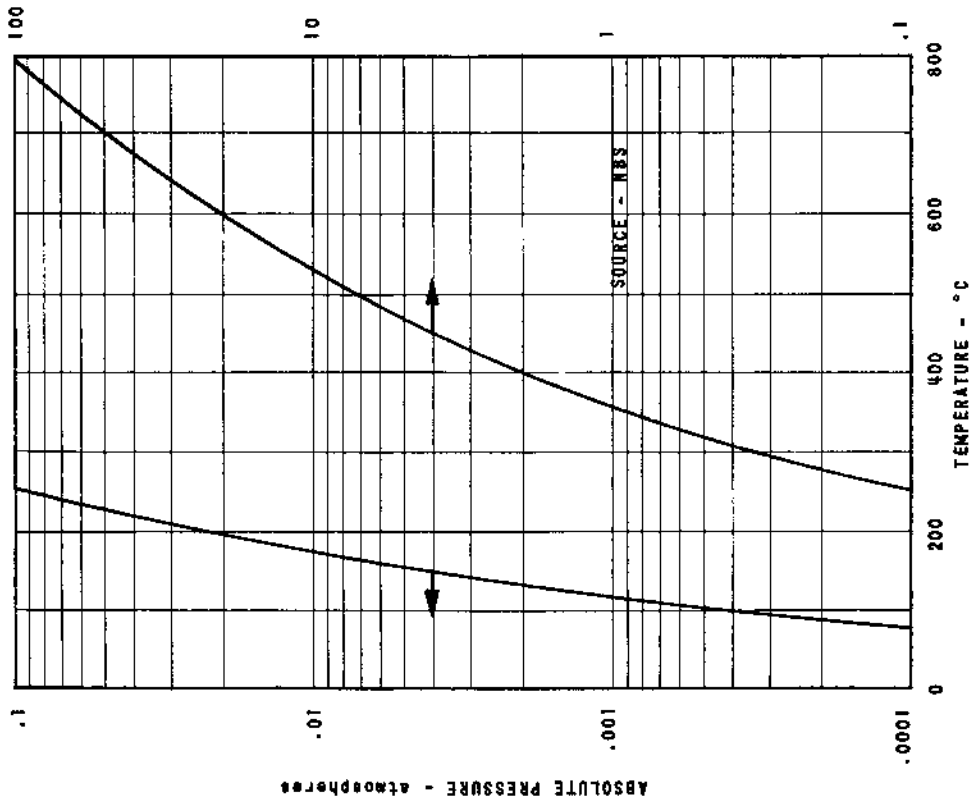

FIG. 6-3
MERCURY SATURATION PRESSURE

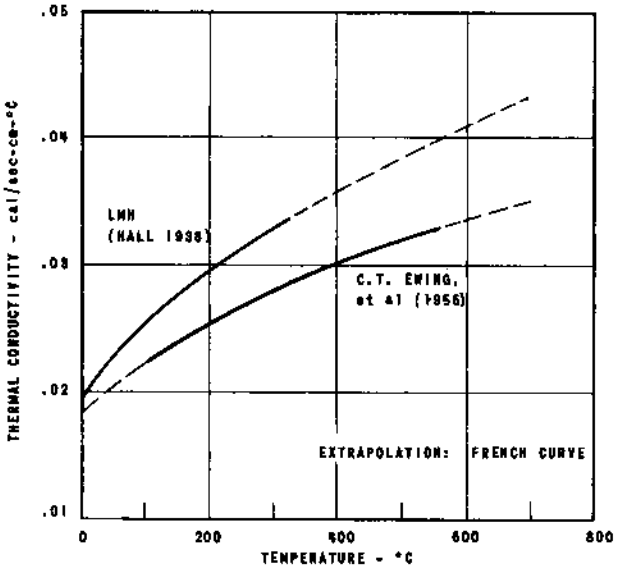

FIG. 6-5
THERMAL CONDUCTIVITY OF LIQUID MERCURY

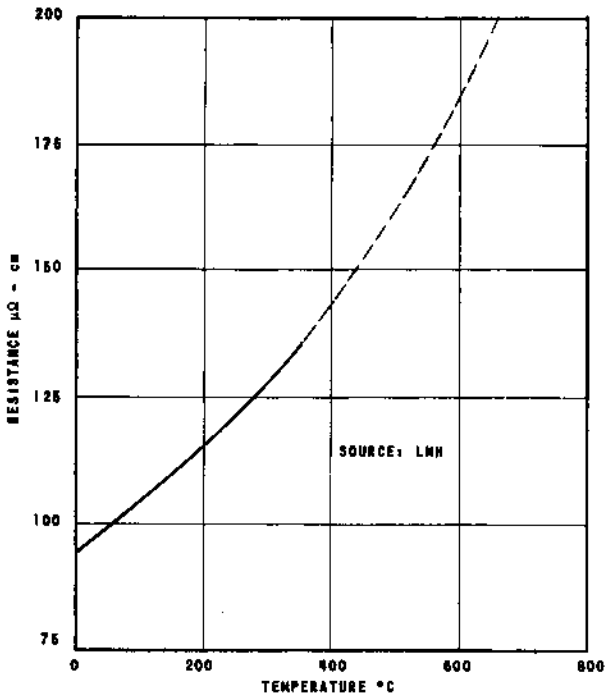

FIG. 6-6
ELECTRICAL RESISTIVITY OF LIQUID MERCURY

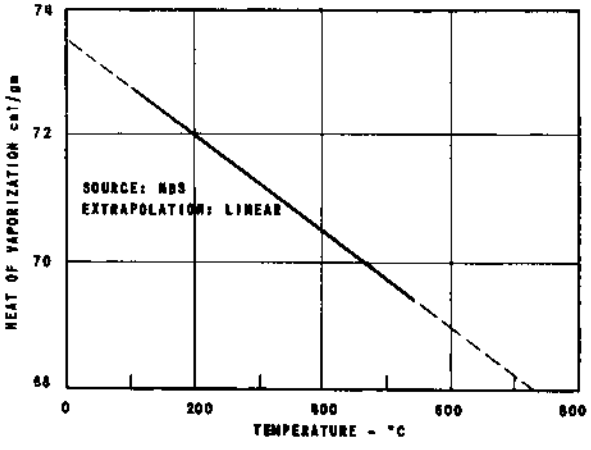

FIG. 6-7
MERCURY HEAT OF VAPORIZATION

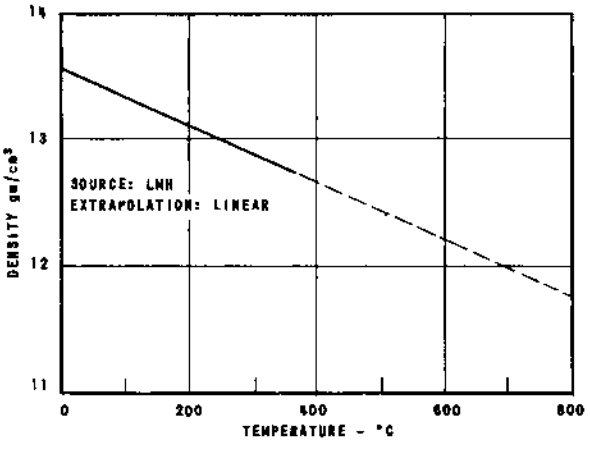

FIG. 6-8
DENSITY OF LIQUID MERCURY

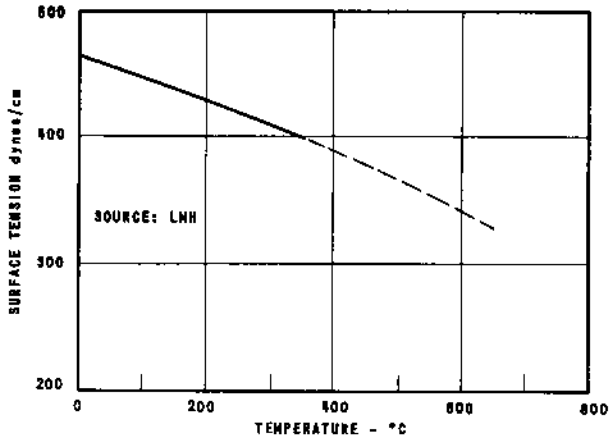

FIG. 6-9
SURFACE TENSION OF MERCURY

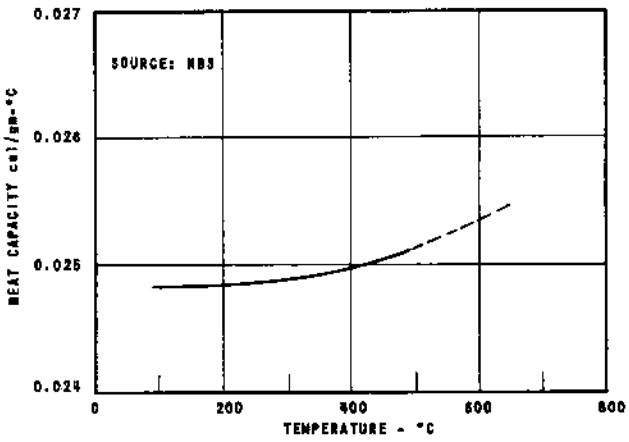

FIG. 6-10
HEAT CAPACITY OF MERCURY VAPOR

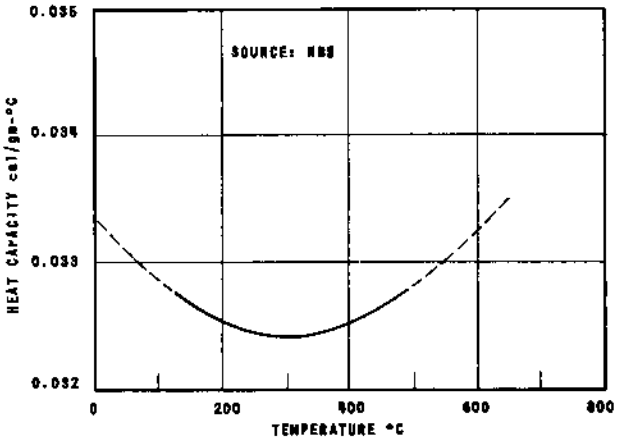

FIG. 6-11
HEAT CAPACITY OF LIQUID MERCURY

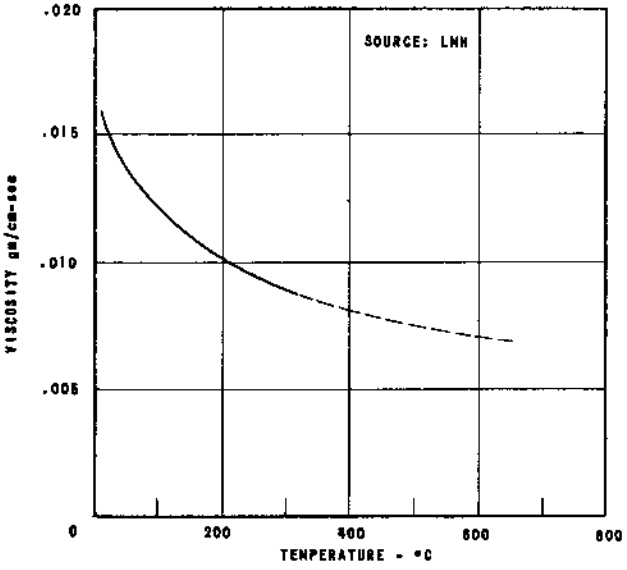

FIG. 6-12
VISCOSITY OF LIQUID MERCURY

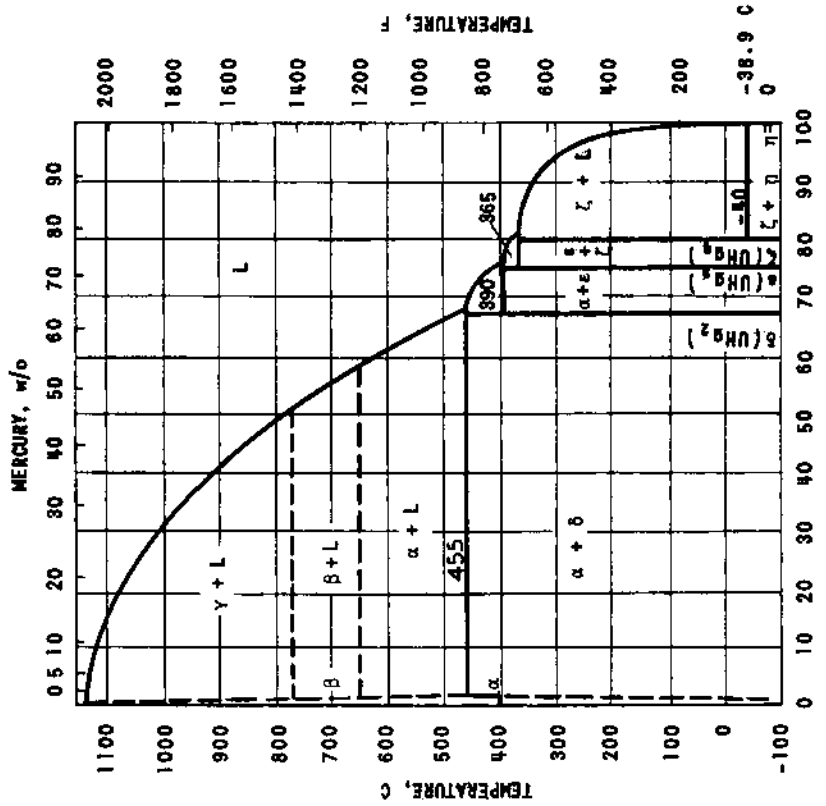

FIG. 6-14
CONSTITUTIONAL DIAGRAM
OF U-Hg SYSTEM

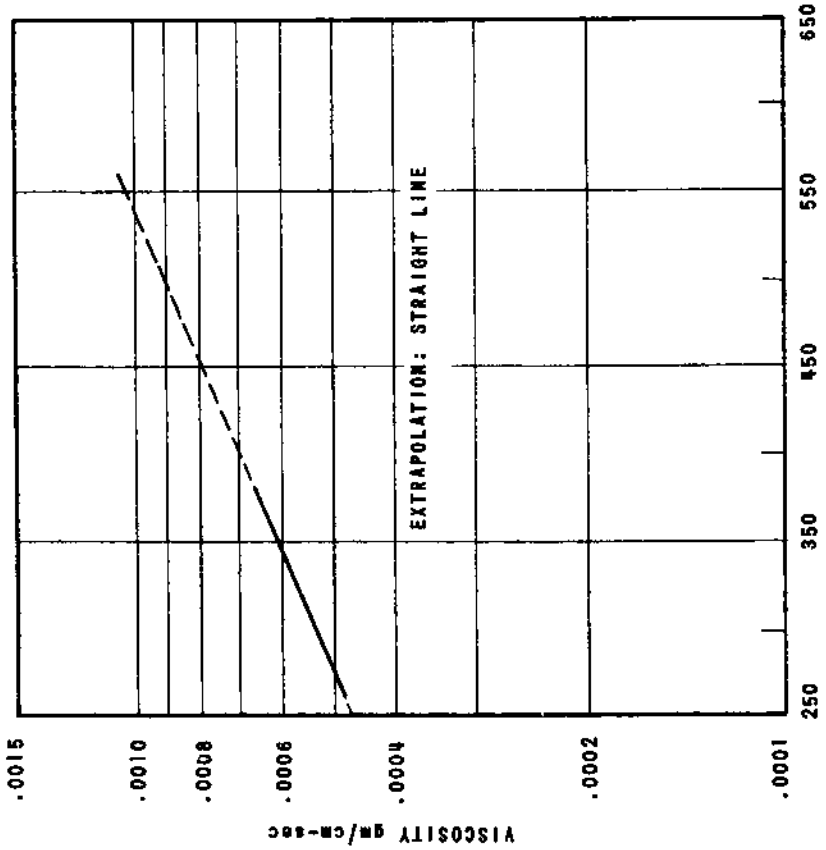

FIG. 6-13
VISCOSITY OF MERCURY VAPOR

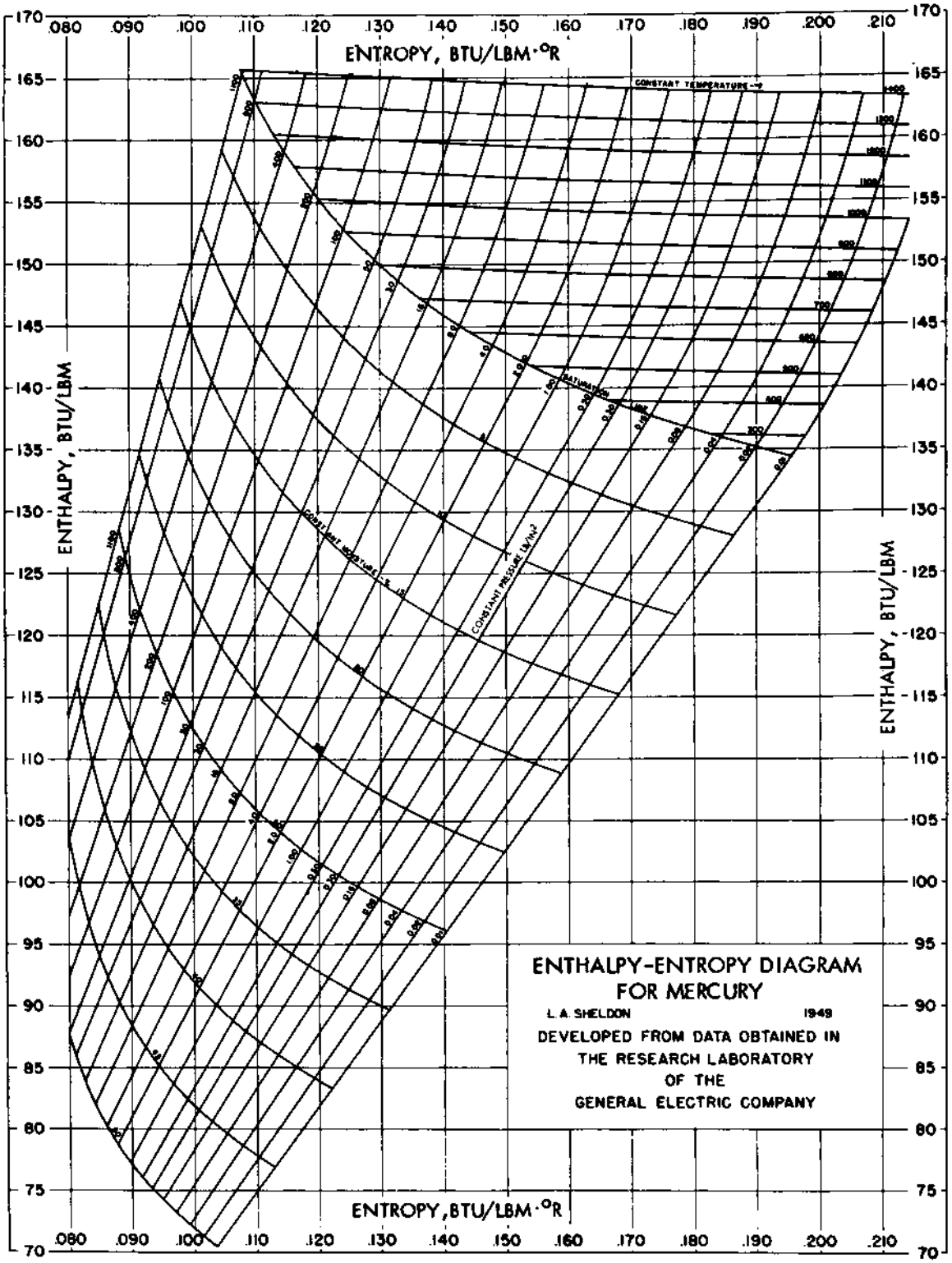

FIG. 6-15

ENTHALPY-ENTROPY DIAGRAM FOR MERCURY.
(COURTESY OF GENERAL ELECTRIC CO.)

Figure 6-16

THERMODYNAMIC PROPERTIES OF MERCURY: PRESSURE TABLE

Pressure (lb/in.^{2})	Temp (^{0}F)	Enthalpy (Btu/lb$_m$)			Entropy Btu/(lb$_m$)(^{0}R)			Specific Volume of Saturated Vapor (ft^3/lb)
		Saturated Liquid	of Evapo-ration	Saturated Vapor	Saturated Liquid	of Evapo-ration	Saturated Vapor	
0.010	233.57	6.668	127.732	134.400	0.01137	0.18428	0.19565	3637
0.020	259.88	7.532	127.614	135.146	0.01259	0.17735	0.18994	1893
0.030	276.22	8.068	127.540	135.608	0.01332	0.17332	0.18664	1292
0.040	288.32	8.463	127.486	135.949	0.01386	0.17044	0.18430	986.0
0.050	297.97	8.778	127.442	136.220	0.01427	0.16821	0.18248	799.0
0.075	316.19	9.373	127.361	136.734	0.01504	0.16415	0.17919	545
0.100	329.73	9.814	127.300	137.114	0.01561	0.16126	0.17687	416
0.200	364.25	10.936	127.144	138.080	0.01699	0.15432	0.17131	217.3
0.300	385.92	11.639	127.047	138.686	0.01783	0.15024	0.16807	148.6
0.400	401.98	12.159	126.975	139.134	0.01844	0.14736	0.16580	113.7
0.500	415.00	12.568	126.916	139.484	0.01892	0.14511	0.16403	92.18
0.600	425.82	12.929	126.868	139.797	0.01932	0.14328	0.16260	77.84
0.700	435.23	13.233	126.825	140.058	0.01965	0.14172	0.16137	67.45
0.800	443.50	13.500	126.788	140.288	0.01994	0.14038	0.16032	59.58
0.900	451.00	13.740	126.755	140.495	0.02021	0.13919	0.15940	53.40
1.00	457.72	13.959	126.724	140.683	0.02045	0.13814	0.15859	48.42
2.00	504.93	15.476	126.512	141.988	0.02205	0.13116	0.15321	25.39
3.00	535.25	16.439	126.377	142.816	0.02302	0.12706	0.15008	17.50
4.00	557.85	17.161	126.275	143.436	0.02373	0.12434	0.14787	13.38
5.00	575.7	17.741	126.193	143.934	0.02430	0.12188	0.14618	10.90
6.00	591.2	18.233	126.124	144.357	0.02477	0.12002	0.14479	9.26
7.00	604.7	18.657	126.065	144.722	0.02516	0.11846	0.14362	8.04
8.00	616.5	19.035	126.011	145.046	0.02551	0.11712	0.14262	7.12
9.00	627.3	19.381	125.962	145.343	0.02583	0.11588	0.14171	6.39
10	637.0	19.685	125.919	145.604	0.02610	0.11483	0.14093	5.81
20	706.0	21.864	125.609	147.473	0.02800	0.10779	0.13579	3.09
30	750.6	23.277	125.407	148.684	0.02918	0.10361	0.13279	2.14
40	784.4	24.345	125.255	149.600	0.03004	0.10068	0.13072	1.648
50	812.1	25.203	125.131	150.334	0.03070	0.09839	0.12909	1.348
60	835.7	25.940	125.024	150.964	0.03127	0.09652	0.12779	1.144
70	856.4	25.585	124.931	151.516	0.03175	0.09493	0.12668	0.998
80	874.8	27.159	124.849	152.008	0.03218	0.09356	0.12574	0.885
90	891.5	27.680	124.774	152.454	0.03255	0.09234	0.12489	0.797
100	906.8	28.152	124.706	152.858	0.03290	0.09127	0.12417	0.725
110	921.0	28.596	124.641	153.237	0.03321	0.09027	0.12348	0.667
120	934.3	29.005	124.582	153.587	0.03350	0.08938	0.12288	0.617
130	946.6	29.390	124.526	153.916	0.03377	0.08855	0.12232	0.575
140	958.3	29.748	124.474	154.222	0.03401	0.08778	0.12179	0.538
150	969.4	30.090	124.424	154.514	0.03425	0.08707	0.12132	0.507
160	979.9	30.415	124.376	154.791	0.03447	0.08640	0.12087	0.478
170	989.9	30.724	124.331	155.055	0.03468	0.08577	0.12045	0.453
180	999.5	31.018	124.288	155.306	0.03488	0.08518	0.12006	0.431
190	1008.8	31.290	124.249	155.539	0.03506	0.08464	0.11970	0.410
200	1017.2	31.560	124.209	155.769	0.03523	0.08411	0.11934	0.392
225	1038.0	32.204	124.115	156.319	0.03565	0.08287	0.11852	0.354
250	1057.2	32.784	124.029	156.813	0.03603	0.08178	0.11781	0.322
275	1074.8	33.322	123.950	157.272	0.03637	0.08079	0.11716	0.297
300	1091.2	33.824	123.876	157.700	0.03669	0.07989	0.11658	0.276
350	1121.4	34.747	123.740	158.487	0.03725	0.07828	0.11553	0.241
400	1148.4	35.565	123.620	159.185	0.03775	0.07688	0.11463	0.215
450	1173.2	36.315	123.509	159.824	0.03820	0.07566	0.11386	0.194
500	1196.0	37.006	123.406	160.412	0.03861	0.07455	0.11316	0.177
600	1236.8	38.245	123.221	161.466	0.03932	0.07264	0.11196	0.151
700	1173.3	39.339	123.058	162.397	0.03993	0.07102	0.11095	0.132
800	1306.1	40.324	122.910	163.234	0.04047	0.06961	0.11008	0.118
900	1336.2	41.226	122.775	164.001	0.04095	0.06837	0.10932	0.106
1000	1364.0	42.056	122.649	164.705	0.04139	0.06726	0.10865	0.098
1100	1390.0	42.828	122.533	165.361	0.04179	0.06625	0.10804	0.090

7-0 DYNAMICS

The control and dynamic stability of this power plant are especially important, since it will have to operate with automatic controls for a period of two years. Only a qualitative discussion can be included in this report.

The control loop as presently conceived is shown in Fig 7-1. Primary control is based on the system output voltage. This system has the advantage that the steady-state error of the system is unaffected by reactor internal feedback gain, and thus the system is free of any drift of the output voltage or frequency, and the feedback gains need only be known approximately to design the system for the required accuracy.

Inclusion of an anticipatory feedback derived from a wattmeter-circuit measurement of actual power consumed by the load minus a neutron-density measurement of power generated in the core enables the system to regulate almost instantaneously against a full-scale load transient. With the system operating in steady state at the proper output voltage and frequency, but at zero output load, full load can be instantly applied and the voltage and frequency will hold constant within 1%. This is possible only because of the fast response inherent in the reactor, which can be safely utilized with proper control loop design. That this is possible can be seen from the following sequence of events.

Consider the system to be operating at normal output voltage and frequency but at zero load current. Full-load current is suddenly switched on. The kinetic energy already in the rotating system provides the power immediately required. The auxiliary feedback path senses this change of consumed power and, by virtue of a sufficiently high gain in the auxiliary loop, immediately increases neutron density by an amount equivalent to the change in consumed power. Thus, by the time the loss of kinetic energy of the system has resulted in opening of the throttle valve, the power generated in the reactor is already set at that pressure which will be required to maintain the required pressure at the turbine input.

The dynamic characteristics of the reactor depend upon the interaction of the internal feedbacks which are in the reactor by design and the reactivity imposed by the movement of the reflector in response to power changes.

A change in power level initiates the movement of the reflector. The internal feedbacks modify the effort of the reflector to adjust the reactor to the desired power level.

The dynamics of the reactor are then dependent upon the designer. The worth and movement of the reflector must be matched to the characteristics of the internal feedbacks so as to return the reactivity multiplication factor to one as swiftly and smoothly as possible after a change in the operating conditions of the reactor.

The significant sources of feedback are considered to be those due to a change in the number of atoms of uranium per unit volume of core and to the variation in density of the boiling mercury.

The variation of reactivity due to a change in the volume of the core were determined by calculations at static state conditions to be

$$\Delta k/k = A(\Delta \ell/\ell)$$

$$\Delta k/k = B(\Delta r/r)$$

$$\Delta k/k = C(\Delta \bar{\rho}/\bar{\rho})f(t) \quad .$$

The structural arrangement of this core is quite similar to that of EBR-I, Mark III; therefore, it is assumed that the mechanical characteristics will be the same and that they will modify the feedback due to volume change in the same manner.

The reactor with its feedback mechanisms is considered to constitute a closed loop system which will respond in some nonlinear manner to a variation in reactivity caused by an induced movement of the reflector.

The solution of the equations which comprise this system are the reactor kinetics, the equations which define temperature distribution in the fuel and structure as a function of time, the equations which define the nonlinear movement of the fuel rods in response to the thermal forcing functions, and the equations which relate a disturbance of dynamic equilibrium of the boiling mercury to reactivity. The two last groups of equations are unique to this particular reactor.

7-1 Equations

All of the equations defining the concomitant physical phenomena which significantly affect internal feedback in the reactor during the period of perturbation are derived from analysis of the physical characteristics of the core.

The equations which describe the phenomena fall into five categories:

(a) neutron kinetics;
(b) heat transfer in metals;
(c) elasticity in metals;
(d) nonlinear mechanics of metal expansion; and
(e) dynamics of boiling mercury.

(a) Neutron Kinetics

$$\frac{dn}{dt} = \frac{-\beta n(t) + k_{ex}(t)\,(1-\beta)n_0}{\ell} + \sum_{i=1}^{6} \lambda_i C_i \qquad \text{Eq. 7-1}$$

$$\frac{dC_i}{dt} = \frac{\beta_i n(t) + k_{ex}(t)\,\beta_i n_0}{\ell} - \lambda_i C_i \quad ; \quad (i = 1 \rightarrow 6) \qquad \text{Eq. 7-2}$$

$\ell = 1 \times 10^{-7}$ sec

Keepin Constants

i	β_i	λ_i
1	0.000234	0.0127
2	0.001377	0.0318
3	0.001257	0.1153
4	0.002760	0.3110
5	0.000974	1.4000
6	0.000228	3.8700

(b) Heat Transfer in Metals

Heat generated in the uranium by fission flows to the surface of the uranium by conduction. It continues through the nongenerating steel cladding by conduction and, at the outer surface of the steel, is transferred to the mercury by convection and conduction.

It is assumed that the curves of power vs. the distance along the longitudinal and radial axes do not change shape and that the level of power varies directly as the neutron density.

The basic equations of heat flow for this particular arrangement are considered to be:

1. Radial temperature distribution in the uranium

$$c_p \rho \frac{\partial T(r,t)}{\partial t} = k \left[\frac{\partial^2 T(r,t)}{\partial r^2} + \frac{1}{r} \frac{\partial T(r,t)}{\partial r} \right] + \frac{n}{n_0} q(t) \quad . \qquad \text{Eq. 7-3}$$

Heat is assumed to be generated uniformly and no account is taken of the effect of axial flow of heat.

2. Radial temperature distribution in the steel cladding

$$c_p \rho \frac{\partial T(r,t)}{\partial t} = k \left[\frac{\partial^2 T(r,t)}{\partial r^2} + \frac{1}{r} \frac{\partial T(r,t)}{\partial r} \right] + 0 \quad . \qquad \text{Eq. 7-4}$$

3. Heat transferred from the surface of the steel cladding to liquid Hg

$$Q = hS \frac{(T_{s1} - T_{Hg1}) - (T_{s2} - T_{Hg2})}{\ell n \left(\frac{T_{s1} - T_{Hg1}}{T_{s2} - T_{Hg2}} \right)} \quad . \qquad \text{Eq. 7-5}$$

It was not feasible to attempt a continuous solution of these fundamental equations of heat flow with an analog computer. It was necessary to resort to a step solution of the thermal equations. The fuel rods were sectionalized into cylindrical shells of thickness ΔR and length ΔZ (see Fig. 7-2). The average conditions in each cylindrical element were summed over the volume of a rod. The average temperature in an element of volume $2\pi r_1 \Delta z_j$ was determined from the time-dependent heat balance on the element:

Storage = generation + entering - leaving.

The inlet mercury temperature to element ΔZ_i is the outer mercury temperature from the element ΔZ_{i-1}. Log mean temperature differences were used between steel and Hg in computing the convection heat transfer. The convection heat transfer rate in each fluid phase of the mercury is a function of velocity, the geometry of the flow channel and the temperature of the materials involved in the heat transfer.

A rod was not assumed to be homogeneous but bimetallic, the steel being a nongenerating conductor and playing a significant part in the calculation of $\Delta\ell/\ell$ and $\Delta r/r$.

(c) Elasticity in Metals

The radial spacers between the rods assure that the center lines of the rods remain essentially in the same relative position and that the force of thermal expansion is expressed as strain energy in the metals of the core. As the temperatures of the metals increase, there is compression of the rods and spacers, but stretching of the structure containing them. Concurrently, the volume of the uranium increases, the volume of mercury decreases, the velocity of the mercury increases, the convection heat transfer rate increases, the microscopic cross sections of isotopes change, and there is a Doppler effect. All of these apparently have little effect upon reactivity, except for the changes in the number of atoms of uranium and mercury per unit volume of core.

The effect of axial expansion is that of increasing the length of the rods and of the structure. The rods at the center of the core will try to expand more than the rods at the periphery. Any plane which was perpendicular to the center line of the core axis at the steady-state condition,

except that plane through the peak of the neutron buckling along the axis will appear as a surface of revolution during the change in power and possibly after.

The actual expansion of any rod is dependent upon thermal conditions, and the restraining effect occasioned by contact with adjacent rods or shell, as each rod attempts to move through the compacted bundle of rods.

The amount of restraint depends upon the interface contact pressure between adjacent longitudinal elements. This pressure is due to manual clamping and to restrained radial thermal expansion. Throughout the range of temperature the coefficient of expansion of stainless steel is greater than the equivalent coefficient of expansion of the bimetallic rod.

The coefficient of expansion of stainless steel is nearly constant over the range of temperatures to which it is subjected, but the coefficient of uranium varies widely over the range of temperature. The coefficient of uranium is expressed as a function of temperature in the model.

The restraining effect of the cladding upon the radial and axial expansion is considered first and then the effect of the radial spacers.

The uranium rod is clad with a drawn-on steel tube. The absolute temperatures in the uranium are higher than those in the steel, and the coefficient of expansion of the uranium is approximately three times that of the steel. The uranium will be in compression and the steel in tension. Strain-energy methods are used to determine how much the uranium can expand against the restraining influence of the steel. Equilibrium exists when the strain energy of the uranium equals the strain energy of the steel, and the increase in length and diameter of the uranium and steel will be that concomitant with this condition.

The clad rod presents a three-dimensional problem in elasticity. However, in the interest of simplicity it is treated as a two-dimensional and an axial strain problem.

The expansion of the uranium in the bimetallic rod provides all of the driving force and part of the retarding force associated with the movement of the uranium.

Since there are radial spacers associated with each rod and since the bundle of rods is initially clamped by a circumferential band, the center lines of the rods remain essentially in their same relative position and the energy of thermal expansion is converted to strain energy in the metal of the core.

The radial movement of the uranium, retarded only by the steel cladding, is determined from the condition that the increase in radius of the steel must equal the decrease in the outer radius of the uranium.

The difference in radius (δ) of the uranium and steel from that which it would have been if both rod and cylinder were permitted to expand fully is determined by equating the strain energy in each:

$$V_u = V_s$$

$$V = \frac{1}{2E}(\sigma_r^2 + \sigma_t^2) - \frac{\nu}{E}\sigma_r\sigma_t + \frac{1+\nu}{E}\tau_{rt}^2 \quad , \qquad \text{Eq. 7-6}$$

where

V = Strain energy

τ = Shear stress

$\sigma_{r,t}$ = Radial and tangential stress

ν = Poisson ratio

A = Cross-sectional area of rod or cylinder

E = Modulus of elasticity .

The boundary conditions are that σ_r is the pressure at the interface of the uranium rod and steel cylinder and that the derivative of σ_r with respect to r is zero at the center of the uranium rod:

$$\left(\frac{\Delta r}{r}\right)_s = (\alpha\Delta T)_s + \delta \qquad \text{Eq. 7-7}$$

$$\left(\frac{\Delta r}{r}\right)_s = \frac{A[(\alpha\Delta T)_u - (\alpha\Delta T)_s - \delta] - \delta + B(\alpha\Delta T)_s}{AB} \qquad \text{Eq. 7-8}$$

where

$$A = r[1 + \alpha(T_{t=0} - 27°C) - \delta]_u$$

and

$$B = r[1 + \alpha(T_{t=0} - 27°C)]_s \quad .$$

The quantity, $\Delta r/r$ provides a clamping force in the core and blankets which is a function of the thermal conditions in the reactor.

The summation of $\Delta r/r$ is $\Delta R/R$.

The axial movement of the uranium retarded only by the steel cladding is determined in a similar manner.

The coefficients of thermal expansion of uranium and steel are different ($\alpha_u > \alpha_s$). Therefore, an increase in temperature produces compression in the uranium and tension in the steel.

The unit elongation of both metals must be the same on this basis:

$$X_f = \frac{\Delta \ell}{\ell} = \frac{(\alpha AE \Delta T)_u + (\alpha AE \Delta T)_s}{(AE)_u + (AE)_s} \quad . \qquad \text{Eq. 7-9}$$

The effect of the radial spacers is that of holding the relative spacing of the fuel rods nearly constant. As the rods tend to bend or buckle, they are restrained by these radial spacers. The structural system of the core is statically indeterminate, and the shape of the center line of a rod is that concomitant with energy equilibrium. The contact pressure between a steel spacer and fuel rod causes a much greater relative decrease in diameter of the spacer and, thus, greater stress. The spacers would be the first to be compressed beyond the elastic limit as the temperature gradient increased. As long as the temperature gradient is such that the spacers are not compressed beyond their yield point, the bundle of cylinders will return to its original position with point contact between parallel cylinders. If the rod is restrained, reactive couples (M) along the length of the rod try to reduce the curvature due to nonuniform heating (see Fig. 7-3).

The strain energy in a spacer rod is the sum of that due to the bending moment and that due to the radial pressure. If two elastic objects with convex surfaces are pressed against each other in the direction of their common normal, their respective surfaces become flattened and high local stress is present. In the case of the rod and spacer the contact surfaces are narrow rectangles of a width 2a which is a function of strain energy in the rods:[5]

$$a = 1.522\sqrt{\frac{Pr_1r_2}{E(r_1 - r_2)}}^{(1)} \quad . \qquad \text{Eq. 7-10}$$

This rectangle of width 2a is the contact surface with adjacent rods and structure. Here r_1 is the radius of the rod and r_2 is the radius of the spacer.

The pressure P is determined from a synthesis of test results. It was a question of determining how tight was tight.

(d) Nonlinear Mechanics

If the heterogeneous assembly of materials comprising the core and blankets and contained in the stainless steel shell expanded freely, the axial movement of a rod would be given by $X_f = \Delta \ell$, but there is mechanical restraint so the movement is some other value X, which is X_f retarded in time and modified in magnitude.

An oscillation of the forcing functions causes this assembly of materials to expand and contract alternately. The mechanical restraints in the form of friction phenomena constitute the damping in the forced oscillation of a redundant elastic structure.

Since bowing and elastic buckling are obviously of little consequence in this particular reactor, some nonlinear effects are due to mechanical restraints and friction phenomena.

The mechanical restraints are due to friction between rods moving relative to each other and to their containing structure. The normal force in the friction phenomena is partially due to initial manual clamping, a relatively small effect, and to radial thermal expansion.

When the bundle of rods becomes hot, there is a random thermal distortion and contact between adjacent rods and between rods and structure. Since the bundle of rods is clamped circumferentially, an increase in $\Delta r/r$ of each rod further increases the normal forces at the surfaces of contact and thus increases the resistance to relative movement of rods and structure. Thus the free response to thermal forcing functions is modified.

It would be impractical to try to take into account the exact movement of every unit volume of the core. Therefore, a dynamically equivalent model of core must be used. It is considered that the dynamic characteristics of the variations in core dimension can be simulated by analogy to a single rod in a tightly bound bundle of rods. While this is not a refined analogy physically, it is considered to be a good dynamic simulation and the constants associated with the equivalent friction phenomena are plausible.

A rod is represented by a series of segments of mass m separated by springs which represent the modulus of elasticity of the rod (Fig. 7-4). The force of thermal expansion is manifest as a change in the equilibrium length of the springs. The movement of each mass is retarded by the friction force dragging on its surface. The equation of motion of a mass m is considered to be that of a simple harmonic oscillator with static and sliding coulomb friction forces added:

$$m\ddot{X} = (gEA/\ell)\,(X_f - X) - c\dot{X} - F - F_r \qquad \text{Eq. 7-11}$$

For $0 < \dot{X} < \epsilon$:

$$F_r = \mu_0 N \quad ; \quad F = 0 \quad .$$

For $\dot{X} > \epsilon$:

$$F_r = 0 \quad ; \quad F = \mu N \quad .$$

(e) Dynamics of Boiling Mercury

The density of a boiling mixture in the core of a forced-circulation reactor depends upon the fluid dynamic conditions existing in the system. Any disturbance to the equilibrium of the system results in a variation of the density of the mixture and thus in the reactivity which feeds back on the signal which disturbed the equilibrium. The vapor is separated from the mixture leaving the reactor. The vapor passes through the turbine, is condensed, and returned to the inlet of the reactor through a common channel.

The fluid dynamic system (Fig. 7-5) is a closed circuit consisting of conductors in parallel and in series, with a pump in a single line which closes the circuits. The sum of the pressure differentials around any closed circuit in the system must be zero for steady-state flow.

The pump in this single line assures that the total flow around the circuit will be the same, but the flow will not be stable nor properly proportioned in the parallel conductors unless they are designed correctly. There are as many degrees of freedom in the system as there are parallel conductors. Fluid stability in the parallel conductors, and especially in those in which heat transfer is occurring, requires that features be designed into the reactor so that any tendency toward instability will damp out.

The design procedure is that of postulating a likely physical system, creating a mathematical model of it, and then preparing an electronic analog of this model. The describing function of the system can then be determined and the physical features of the postulated system changed until the system has the desired dynamic characteristics.

The simplified equations for a single, heated, parallel conductor in the reactor are set forth. The equation for the other geometrically identical parallel conductors will vary only in the amount of heat generation. The equations for each external circuit are written because there are differences in their physical characteristics.

The equations for the dynamic model are:

Liquid heating section

$$Q = hN\pi D Z_f \text{ (L.M.T.D.)} \qquad \text{Eq. 7-12}$$

(L.M.T.D. = ℓn mean temperature difference)

with

$$Z_f = \frac{W_T \bar{c}_p (T_{sat} - T_1)}{h\pi D(\text{L.M.T.D.})} \quad . \qquad \text{Eq. 7-13}$$

Boiling section

$$W_5 h_{f5} + (1 - \chi_3)\, W_3 h_{f3} = W_1 h_{f1} \qquad \text{Eq. 7-14}$$

$$(h_{f2} - h_{f1})\, W_2 = q'' \pi D Z_f \qquad \text{Eq. 7-15}$$

where

$$\chi = q'' \pi D Z_{fg} / W_3 h_{fg} \qquad \text{Eq. 7-16}$$

$$\alpha_3 = \frac{1}{\frac{V_g / V_f}{(\chi_3 / 1 - \chi_3)(\rho_f / \rho_g)} + 1} \qquad \text{Eq. 7-17}$$

$$\frac{W_3}{2 g_c A_c^2 \rho_f^2} \left[\sum N_i \right] - \frac{g}{g_c} (Z_{fg})(\rho_f - \bar{\rho}_{fg}) - \frac{\Delta P}{\rho_f} = 0 \quad . \qquad \text{Eq. 7-18}$$

The pressure difference ΔP is determined as a function W_T from the pump characteristic curve.

$$\bar{\rho}_b = \left(1 - \frac{\alpha_3}{2}\right) \rho_f \qquad \text{Eq. 7-19}$$

$$N_1 = f \frac{\ell}{D} \rho_f \frac{A_c}{A_d} \qquad \text{Eq. 7-20}$$

$$N_2 = \rho_f \left[1 - \frac{A_c}{A_d} + K \right] \qquad \text{Eq. 7-21}$$

$$N_4 = 2 \Psi \rho_f^2 \qquad \text{Eq. 7-22}$$

$$\Psi = \frac{(1 - \chi_3)^2}{(1 - \alpha_3)\rho_f} + \frac{\chi_3^2}{\alpha_3 \rho_g} - \frac{1}{\rho_f}$$

$$N_5 = \rho_f \bar{R} \left(\frac{f}{D_c} \right) Z_{fg} \qquad \text{Eq. 7-23}$$

$$N_6 = 2 \rho_f \left(\frac{A_c}{A_p} \right) \left\{ \chi_3^2 \frac{\rho_f}{\rho_g} \left(\frac{A_c}{A_p \alpha_p} - \frac{1}{\alpha_3} \right) + (1 - \chi_3)^2 \left[\frac{A_c}{A_p (1 - \alpha_p)} - \frac{1}{1 - \alpha_3} \right] \right. \qquad \text{Eq. 7-24}$$

$$N_7 = \frac{\rho}{(1 - \alpha_3)\rho_f} \left(\frac{A_c}{A_s} \right)^2 \qquad \text{Eq. 7-25}$$

$$N_g = \rho_f R \left(\frac{\ell_r}{D_r}\right) f \qquad \text{Eq. 7-26}$$

$$R = 1 + \left(1 - \frac{\rho_g}{\rho_f}\right) \frac{\rho_f}{\rho_g} X$$

$$\bar{R} = \frac{1}{Z_{fg}} \int_0^{Z_{fg}} 1 + \left(1 - \frac{\rho_g}{\rho_f}\right) \frac{\rho_f}{\rho_g} X$$

Condensing Section

$$q_{net} = q_a + q_m + q_s \qquad \text{Eq. 7-27}$$

$$q_s = C_1 T_s^4 \qquad \text{Eq. 7-28}$$

$$q_m = C_2 \left(T_r^4 - T_m^4\right) \qquad \text{Eq. 7-29}$$

$$q_a = C_3 \left(T_r^4 - T_s^4\right) \qquad \text{Eq. 7-30}$$

$$\left(\frac{dP}{d\ell}\right)_f = - \frac{fG^2(1 - \chi)^2}{\rho_f D(2g)} \qquad \text{(Tubes)} \qquad \text{Eq. 7-31}$$

The transport lags (Fig. 7-5) around the fluid dynamic circuits are:

Path		τ
1 → 2	heating liquid mercury to saturation temperature	$\tau_{1-2} = Z_f/V_\ell$
2 → 3	boiling mercury (liquid to vapor)	$\tau_{2-3} = Z_{fg}/V_{fg}$
3 → 4	reactor to condenser (vapor)	$\tau_{3-4} = \ell_{3-4}/V_f$
4 → 5	condensing mercury (vapor to liquid)	$\tau_{4-5} = \ell_{4-5}/V_{fg}$
5 → 6	condenser to pump (liquid)	$\tau_{4-5} = \ell_{4-5}/V_\ell$
3 → 6	reactor to pump (liquid)	$\tau_{3-6} = \ell_{3-6}/V_\ell$
6 → 1	pump to reactor (liquid)	$\tau_{6-1} = \ell_{6-1}/V_\ell$

The above 31 equations constitute the mathematical model of the reactor only. The additional equations necessary to define a model of the entire power plant are not included in this report.

7-2 Nomenclature

A	area; constant
B	constant
C	concentration of neutron precursors; constant
C_f	constant of proportionality
c	viscous damping coefficient
C_c	critical viscous damping coefficient
c_p	specific heat
D	equivalent diameter; diameter of rod
E	modulus of elasticity
F	kinetic friction force; fission products
F_c	constant normal force
F_r	static friction force
f	frequency, Fanning friction factor
G	mass flow
g	acceleration due to gravity
g_c	gravitational constant
h	heat transfer rate; enthalpy
h_{fg}	heat of vaporization
K	loss coefficient; constant
k	thermal conductivity; reactivity; spring constant
k_{ex}	excess reactivity
l	neutron lifetime; length
M	reactive couple
m	mass
N	total normal force; number of rods
n	neutron density
P	pressure; power
Q	total heat
q	heat per unit volume per unit time; total heat
q"	heat flux
R	radius of a region; two-phase friction force multiplier; thickness

r	radius of a rod
S	surface for heat transfer
T	temperature
t	time
U	uranium
V	strain energy; velocity
W	mass flow
X	restrained motion of mass; wt-% of vapor
X_f	free motion of m
x	x/ℓ; vapor
x_f	x_f/ℓ
Z	total length of a rod
α	coefficient of expansion; μ_0/u; vol-% of vapor;
β	fraction of delayed neutrons
δ	Δr concomitant with V; relative jump
ϵ	an arbitrary velocity
λ	decay constant
ζ	damping ratio
μ	kinetic friction coefficient
μ_0	ratio friction coefficient
ρ	density
σ	stress (plain) surface tension
ν	Poisson ratio
τ	stress (shear); time constant; transport lag.

Subscripts

a	lunar surface
fg	boiling phase
c	core
d	downcomer
f	liquid phase
g	vapor phase

m	moon
r	upper reflector; radiator; radial
s	separator; surface; steel; space; sun
T	total
t	tangential
u	uranium
$^{1,2,3,}_{4,5}$	points in fluid circuit (see Fig. 7-5)

7-3 References

1. Nádai, A., Placisity, McGraw-Hill Book Company, Inc., New York, (1931) p. 242.
2. Chesnut, H., and Mayer, R. W., Servomechanisms and Regulating System Design, John Wiley and Son, Inc., New York, (1951).
3. Bode, H. W., Network Analysis and Feedback Amplifier Design, D. Van Nostrand Company, Inc., Princeton, N. J., (1945).
4. Evans, W. R., Control-System Dynamics, McGraw-Hill Book Company, Inc., New York, (1954).
5. Truxall, J. G., Automatic Feedback Control System Synthesis, McGraw Hill Book Company, Inc., New York, (1955).

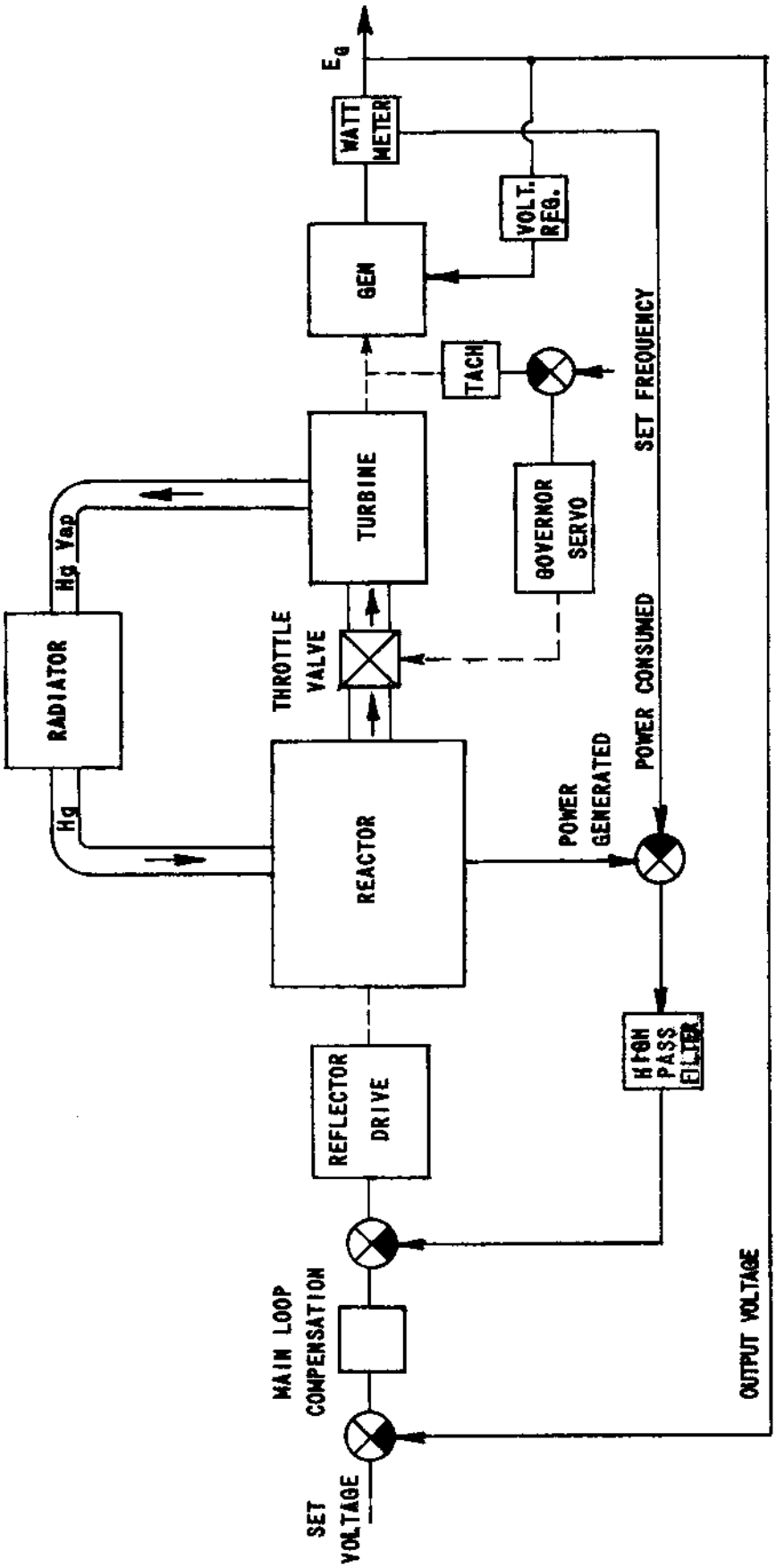

FIG. 7-1
BLOCK DIAGRAM OF CONTROL SYSTEM

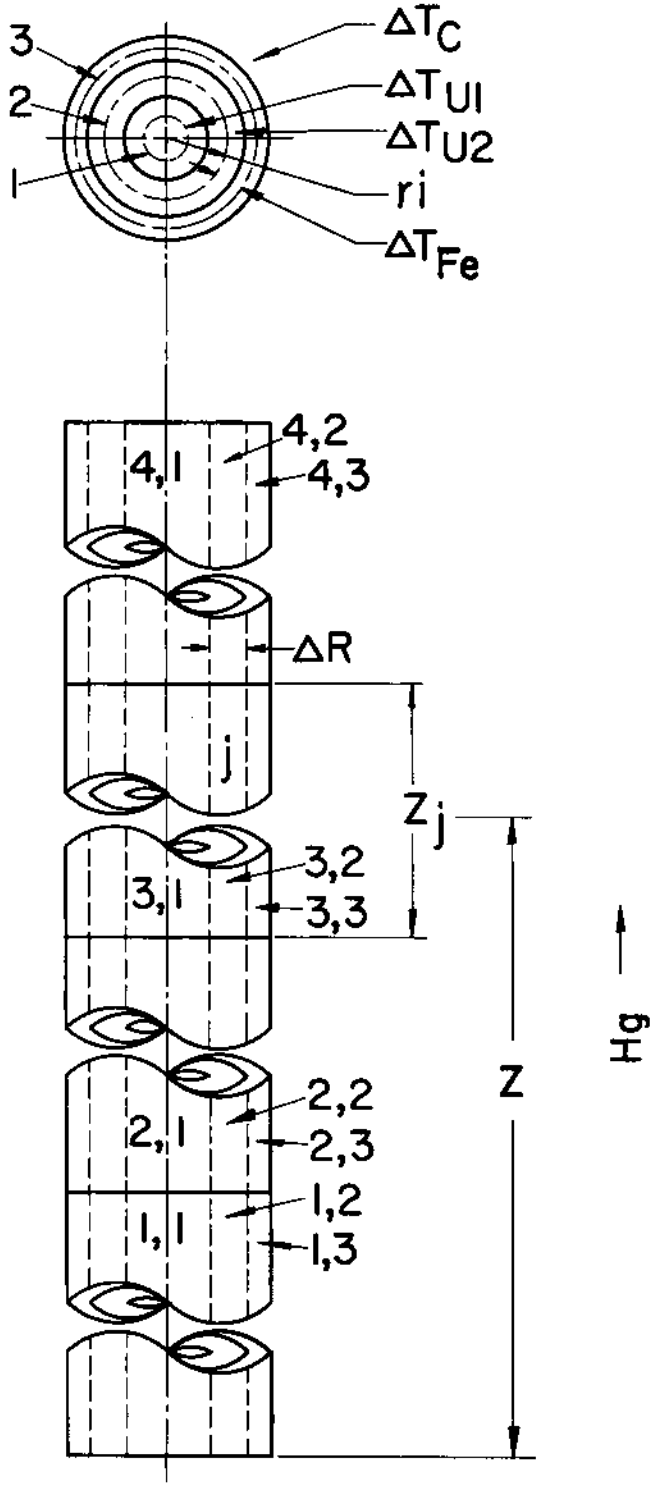

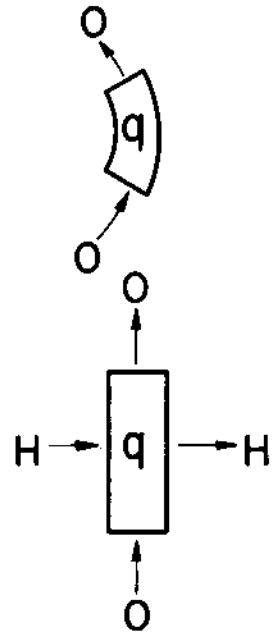

ELEMENT ij ΔRXΔZ

FIG. 7-2
VOLUMETRIC DIVISION
OF A FUEL ROD

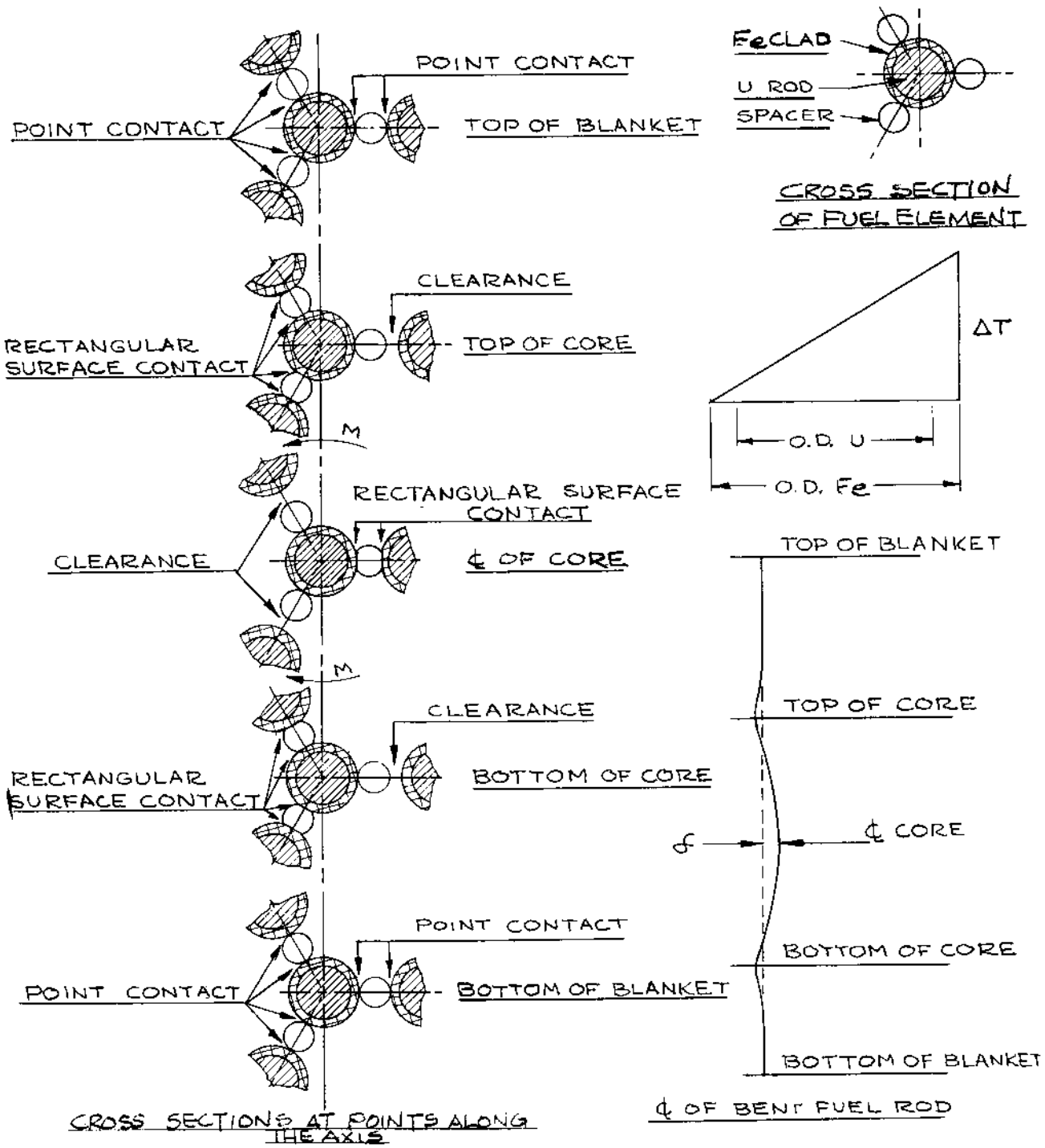

FIG. 7-3
EFFECT OF TEMPERATURE GRADIENTS ON THE LATERAL MOVEMENT OF FUEL RODS

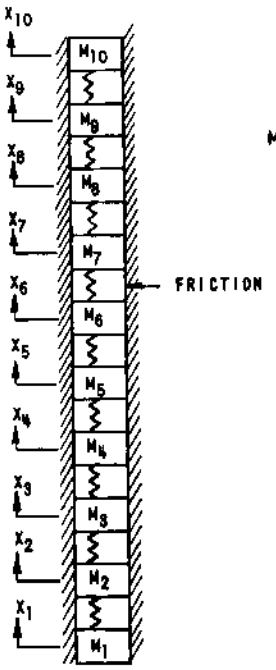

$$M\ddot{x} = \frac{gEA}{\ell}(X_f - X) - C\dot{X} - F - Fr$$

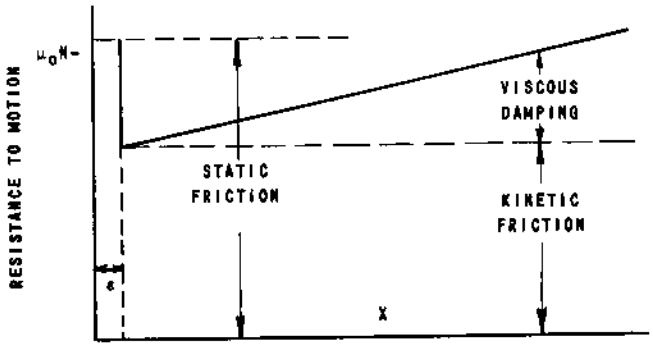

FIG. 7-4
EQUATION OF MOTION OF A FUEL ROD

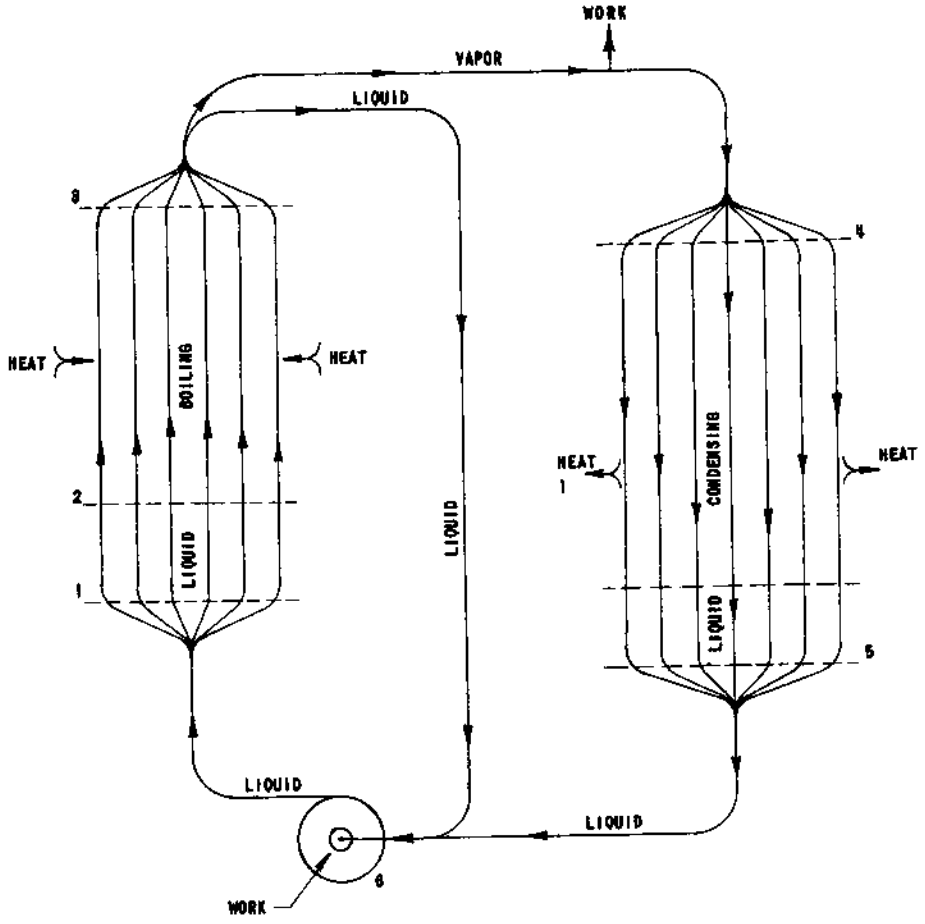

FIG. 7-5
DYNAMIC SYSTEM OF THE FLUID

8-0 WEIGHTS

The weights of the power plant are listed in Fig. 8-1 and are stated in three ways. Column one is based on the entire plant being made of 5% chromium-1/2% molybdenum steel alloy. As stated elsewhere in this report, this material is well proven for use with mercury. Column two is the same as column one except that the radiator and associate manifolds are based on the use of titanium alloy. Whether or not this may be used in contact with mercury at the operating conditions of pressure and temperature will depend upon the results of a long-term program now in progress. If its use is possible, a weight saving of 1878 kg will result. The third column is based on the use of a titanium pressure vessel lined with steel and a radiator using magnesium tubing with a steel liner (Fig.4-12 type "F"). If proven practical, this concept will result in a weight saving of 3008.2 kg over the steel plant in column one. In all three concepts the base and supporting structure are made of magnesium alloy.

A detailed analysis of all components can result in further weight reductions.

FIG. 8-1

POWER PLANT WEIGHTS
(Radiator Design No. 2 Used as an Example; All Weight in Kilograms)

	1 All Steel, Except Mg Base and Supports	2 Steel Reactor Ti Radiator Mg Base	3 Combination Steel and Ti Reactor, Mg-clad Radiator, Mg Base
REACTOR			
Pressure Vessel, Ducts, Grids, Separation Plates, and Misc. Hardware	1062.2	1062.2	920.0
Core	686.5	686.5	686.5
Reflector Controls and Operating Mechanisms	637.8	637.8	574.0
Turbine and Pumps	318.0	318.0	318.0
Generator	454.0	454.0	409.0
Compressor	27.0	27.0	24.0
Reactor Total	3185.5	3185.5	2931.5
Base and Radiator Scaffold	133.0	133.0	133.0
RADIATOR			
Radiator Tubes	3450.8	1929.0	1052.0
Manifolds	807.0	451.0	451.0
Misc. Hardware	429.7	429.7	429.7
Valves and Hoses	477.0	477.0	477.0
Radiator Total	5164.5	3286.7	2409.7
Mercury Inventory	1315.0	1315.0	1315.0
Total Plant Weight	9798.0	7920.2	6789.2
Weight, kg/kwt	1.225	.990	.849
Weight, kg/kwe	9.798	7.920	6.789

9-0 SITE

Man's first space frontier will be the Moon. For this task, an enormous expenditure of energy has been directed to eliminate as many unknowns as possible. Some geological considerations for locating a "best" area for establishing lunar bases have been reported by the U.S. Geological Survey and the Army Engineers. A compilation of lunar photographs was used as the basis for this first study. Further geological studies will include the "hard" and "soft" landing of lunar probes for data reporting. Other future lunar probes that orbit the moon will be utilized to observe micrometeorite particles in a gravitational environment other than Earth's and to study the blocking effect that Earth has on the passage of particles from various directions in space toward the moon.

From earth, meteoric phenomena have been observed which help in the LP-1 site selection. We observe the frequency of meteors on Earth to be approximately four times greater in the dawn than in the evening. The lunar site should be so located that during the Earth evening it would be facing the Earth. This position protects the site during the Earth morning when the forward side of the Earth is slightly more exposed to meteoric bombardment (see Fig. 9-1).

Meteor showers and swarms are generally named for the positions of the radiants they produce among the constellations. Meteor showers occur only where the orbit of the swarm crosses the Earth's orbit and when the Earth and swarm arrive coincidently on that path (see Fig. 9-2). This occasion determines the date of the shower. Examples of this dating would be the two meteor showers that are associated with Halley's comet; they are the Eta Aquarids in May and the Orionids in October. For more examples of meteor showers, their intensity, and their penetrating power, see Tables 9-1 and 9-2. Early lunar space investigations should determine accurately the direction and intensity of the majority of expected showers that intersect the Earth-moon orbit; with this information it can be determined on which moon hemisphere the site would be safest from meteor incident.

Lunar power station television communication with Earth will provide a visual record during the expedition. Television transmission waves travel in straight lines; this requirement also places the site on or near the side of the moon, always facing Earth.

From a radiator safety view point, a minimum meteoroid flux appears to be the criterion to use in the site selection for the U.S. LP-1 power station. Unless there are unforeseen reasons, it appears the LP-1 will be located in the area indicated on Fig. 9-3. A choice site in this area could be the level terrain of Mare Imbrium, Mare Serenitatis, or Mare Crisium.

Table 9-1

METEOR DATA

Name	Date of Maximum	Mean Hourly Rate at Maximum	Duration (days)
Nocturnal			
Quadrantids	Jan. 3	100[r]	2
Lyrids	April 21	10[v]	2
Perseids	Aug. 12	50[v]	12
Giacobinids	Oct. 10	1,400[r]	0.2*
Orionids	Oct. 19	15[v]	10
Taurids	Nov. 3-10	10[v]	27
Leonids	Nov. 16	10[v]	5**
Geminids	Dec. 12	60[v]	5
Ursids	Dec. 22	10[v]	1
Daylight			
-Aquarids	May 4	10[r]	10
Piscids	May 7	30[r]	9
Arietids	June 4	60[r]	6
-Perseids	June 6	40[r]	15
54-Perseids	June 26	30[r]	8
-Taurids	July 3	40[r]	10
-Orionids	July 12	50[r]	5
-Geminids	July 12	60[r]	5
-Geminids	July 12	30[r]	5
-Aurigids	July 25	20[r]	11

*Giacobinids show appreciable display only occasionally (about once in every 12 years)

**Leonids show occasional concentrated displays (periodicity 33 years ?) Hourly rate given is the normal one.

r = from radar observations v = from visual observations

Table 9-2

THE PENETRATING POTENTIAL OF METEOROIDS

Meteor Visual Magnitude	Total Kinetic Energy (ergs)	Mass (gm)	Radius (cm)	Probable Encounter per 24 hr	Penetration in Al (cm)
0	1.0×10^{13}	1.25	0.46	1.2×10^{-8}	10.9
1	4.0×10^{12}	0.50	0.34	3.1×10^{-8}	8.0
2	$.6 \times 10^{12}$	1.98×10^{-1}	0.25	7.7×10^{-8}	5.9
3	6.3×10^{11}	7.9×10^{-2}	0.18	2.0×10^{-7}	4.3
4	2.5×10^{11}	3.1×10^{-2}	0.14	4.9×10^{-7}	3.2
5	1.0×10^{11}	1.2×10^{-2}	1.0×10^{-1}	1.2×10^{-6}	2.3
6	4.0×10^{10}	5.0×10^{-3}	7.4×10^{-2}	3.1×10^{-6}	1.7
7	1.6×10^{10}	2.0×10^{-3}	5.4×10^{-2}	7.7×10^{-6}	1.3
8	6.3×10^{9}	7.9×10^{-4}	4.0×10^{-2}	2.0×10^{-5}	0.93
9	2.5×10^{9}	3.1×10^{-4}	2.9×10^{-2}	4.9×10^{-5}	0.69
10	1.0×10^{9}	1.2×10^{-4}	2.2×10^{-2}	1.2×10^{-4}	0.51
11	4.0×10^{8}	5.0×10^{-5}	1.6×10^{-2}	3.1×10^{-4}	0.37
12	1.6×10^{8}	2.0×10^{-5}	1.2×10^{-2}	7.7×10^{-4}	0.27
13	6.3×10^{7}	7.9×10^{-6}	8.6×10^{-3}	2.0×10^{-3}	0.20
14	2.5×10^{7}	3.1×10^{-6}	6.3×10^{-3}	4.9×10^{-3}	0.15
15	1.0×10^{7}	1.2×10^{-6}	4.6×10^{-3}	1.2×10^{-2}	0.11

9-1 Bibliography

1. C. A. Tobias, Radiation Hazards in High-altitude Aviation, J. Av. Med. 23, 345 (1952).
2. H. J. Schaeffer, Theory of the Protection of Man in the Region of the Primary Cosmic Radiation, J. Av. Med., 25, 338 (1954).
3. L. R. Shepherd, The Possibility of Cosmic Ray Hazards in High Altitude and Space Flight, J. Brit. Interplan. Soc. 12, 197 (1953).
4. S. F. Singer, Cosmic-ray Effects at High Altitudes, J. Av. Med. 27, 111 (1956).
5. G. Grimminger, Probability that a Meteor Will Hit or Penetrate a Body Situated in the Vicinity of the Earth, J. Appl. Phys. 19, 947 (1948).
6. H. W. Ovenden, Meteor Hazards to Space Stations, J. Brit. Interplan. Soc. 10, 275 (1951).
7. F. L. Whipple, Meteoric Phenomena and Meteorites in Physics and Medicine of the Upper Atmosphere, edited by C. S. White and O. O. Benson, Univ. of New Mexico Press, Albuquerque (1952).
8. E. J. Öpik, Theory of the Formation of Meteor Craters, Pub. Obs. Astron. Univ. Tartu, 28, 1 (1936).
9. E. J. Öpik, private communication (April 1956).
10. G. K. Wehner, Sputtering by Ion Bombardment in Advances in Electronics and Electron Physics, Vol. VII, Acad. Press, Inc., N.Y., (1955).
11. J. C. Slater, The Effects of Radiation on Materials, J. Applied Phys. 22, 237 (1951).
12. D. S. Billington and S. Siegel, Metal Progress, 58, 847 (1950).
13. M. J. Swetnick, private communication (April 1956).
14. M. T. Simnad, Radioisotopes in the Study of Metal Surface Reactions in Solutions, in Properties of Metallic Surfaces, Inst. of Metals, London (1953).
15. S. F. Singer, Measurements of Interplanetary Dust in Earth Satellites - Their Scientific Uses, Univ. of Mich. Press, Ann Arbor (1956).
16. H. Bonke at 10th Anniv. Mtng. of Upper Atm. Rocket Research Panel, Ann Arbor, Mich, Jan. 1956; even suggested the advisability of charging the satellite up to a very high potential by artificial means.
17. H. Broida, Stabilization of Free Radicals at Low Temperatures, Conf. on Unstable Chem. Species, N. Y. Acad. of Sci. (March 1956).

18. S. F. Singer, Studies of a Minimum Orbital Unmanned Satellite of the Earth (MOUSE) Part I. Geophys. and Astrophys. Applications, Astronautica, Acta, 1, 171 (1955).

19. 1958 NASA/USAF Space Probes (Able 1), Space Technology Laboratories, Volume 1, Summary, Final Report (February 18, 1959).

20. P. J. Coleman, C. P. Sonett and A. Rosen, (Space Technology Laboratories), Ionizing Radiation at Altitudes of 3500 Kilometers to 36,000 Kilometers - Pioneer I, Bull. Amer. Phys. Soc., 4 (4) (Series 2), 223 (1959) (Abstract).

21. J. W. Lindner, Geophysical and Astrophysical Studies, Exploration of the Terrestrial Radiation Belt, Applied Physics Department, Research and Development Division, Space Technology Laboratories, TR-59-0000-0652 (March 18, 1959); revised June 15, 1959.

22. J. A. Van Allen, and L. A. Frank, Radiation around the Earth to a Radial Distance of 107,400 km, Nature, 183, 430-434 (1959).

23. N. L. Baker, Radiation Can be Avoided, Missiles and Rockets (January 5, 1959), pp 13-14.

24. NASA Theoretical Division Discussion (March 26, 27, 1959), Science, 129, 1012-1013 (1959).

25. R. Jastrow, Van Allen Discovery Most Important, Missiles and Rockets, 5 (30), 43-47 (1959).

26. E. Clark, Sun May be Origin of Van Allen Radiation, Aviation Week, 70, (13), 26-27 (1959).

27. R. A. Imobersteg, Review of Outer Space Environment. Part 1. Radiation Environment in Space, General Electric Company.

28. S. N. Vernov, A. Ye. Chudakov, P. V. Vakulov, and Yu. I. Logachev, The Study of Terrestrial Corpuscular Radiation and Cosmic Rays during the Flight of the Cosmic Rocket, Doklady Akademii Nauk SSSR, 125 (2), 304-307 (1959).

29. J. A. Van Allen, and L. A. Frank, Radiation Measurements to 658, 300 Kilometers with Pioneer IV, State University of Iowa Report SUI-59-18 (August, 1959).

30. Pioneer IV Data Alters Van Allen Theory, Aviation Week (May 11, 1959), p. 31.

31. The Moon Probe - Pioneer IV, NASA, JPL Pamphlet.

32. S. F. Singer, Nuclear Explosions in Space, Missiles and Rockets, April 20, 1959, pp 26, 28-30.

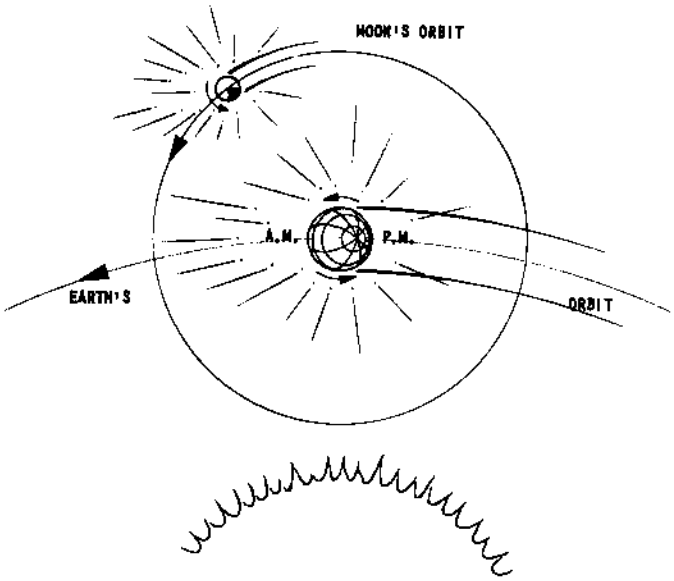

FIG. 9-1
MOON'S ORBIT

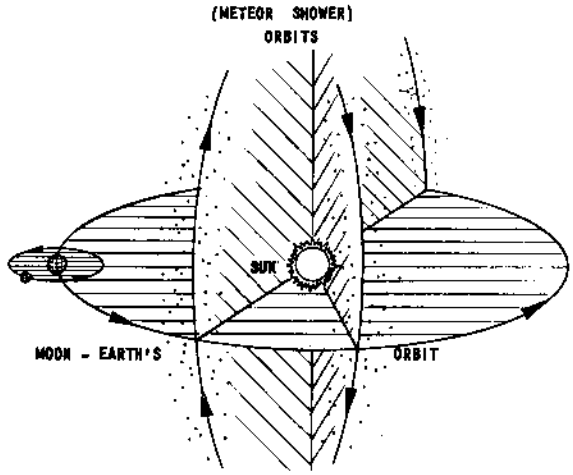

FIG. 9-2
INTERSECTION OF MOON-EARTH-METEOR ORBITS

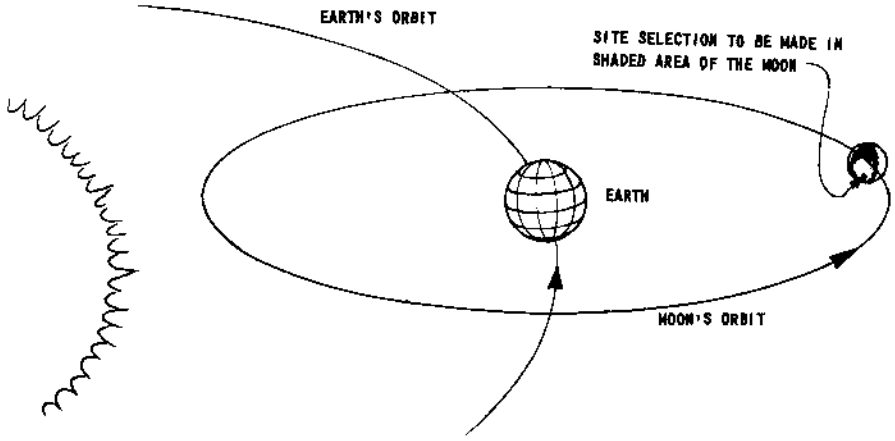

FIG. 9-3
SITE AREA

10-0 INSTRUMENTATION*

The instruments associated with the control system of this power plant have not been designed at this time.

A qualitative discussion of the instrumentation for the unique duty follows.

10-1 Ionization Chambers

The present state of the art has produced ionization chambers that have withstood 650° C for a little over 1000 hours at moderate radiation levels. It is not clear that the normal progress in the next few years will be able to increase the lifetime by a factor of 20.

The major factors still to be investigated are the effects of radiation damage on the resistance of the feedthrough seals, the combined effects of temperature and radiation damage on structural parts, and the adhesion or diffusion of the sensitive material (U^{235}) into the walls of the chamber.

It is known that the present-day ceramic seals show a decrease in resistance as a result of radiation damage or high temperature. It is not known if the 1000° temperature will have an annealing effect upon the radiation damage or whether these two effects are additive. However, the saving factor in this case is that the input impedance of the electronic circuits can be low enough so that a very high insulation resistance is not needed (1 megohm is sufficient).

Also, it is not known what long-term effect a high temperature will have upon the diffusion of the uranium into whatever materials is used to construct the ionization chamber. Probably titanium will be used if uranium will adhere to it. With the present flux of 2×10^{14} n/(cm^2)(sec) and the weighted cross section for U^{235} of 1.5 barns, the burnout over a two-year period is less than $\frac{1}{10}\%$. A coated area of about ten square centimeters would be sufficient to give us a current output at full power of about one milliampere.

One other factor that should be investigated is the effect of long-time high temperature upon welds. The problem is not particularly serious on earth, where the pressure is the same on both sides of the weld. However, on the moon's surface there will be a 15-pound differential existing across the weld, and under these conditions a slight leak would be serious over a two-year period.

---

* D. C. Thompson of the Electronic Division of the Argonne National Laboratory, 9700 South Cass Avenue, Argonne, Illinois.

10-2 Cables

The present day state of cable making has produced several cables that, at least the manufacturer claims, can be operated at 538° C. As far as is known, they have been tested only for a few hundred hours at these temperatures. The one cable that has been checked at Argonne for resistance at 538° C gave a reading of 500 megohms, which is more than adequate for ionization chamber use.

The same problems of radiation damage that are mentioned under ionization chambers also apply here. The common problem to both cables and ionization chambers, as far as resistance is concerned, is the time-temperature-power curve; that is, if one can bring the reactor up near the operating point flux-wise faster than the temperature rises, the installation problem will not be very severe. However, if one has to get the reactor up to temperature and then bring it up to full power, it may be difficult to maintain sufficiently high cable resistances.

10-3 Electronic Instruments

There are two major channels that will be required: one is the level indicator, and the other is the period indicator. The requirements for these two channels are that they must have a wide dynamic current input range, operate for two years without failure, be small and light weight, and require a small amount of power to operate.

The startup flux would give such a low current reading from the ionization chamber that magnetic amplifiers are out of the question at these fluxes, but they are certainly one of the answers at - or near - the operating power level. It appears that the answer to this would be two sets of instruments: one for startup and the intermediate range, and one set for the two-year operation at the fixed power level. The first set of instruments could be of a variety which have low reliability and whose detectors will be deliberately sacrificed. The present-day state of the art is sufficient to produce both sets of instruments if the two-year set is operated remotely. Excluding power supplied, each instrument can be built in a 7.6-cm cube with our present knowhow. That size can be reduced if necessary by special miniaturization techniques.

10-4 Detector Locations

The choice of the detector location is dictated by several factors. Among these is the value of the flux, temperature, absence of shadowing due to the motion of control rods, and the absence of any nearby material which could change the energy spectrum of the flux. With these considerations in mind, it appears that the best choice is underneath the alternator by the gas compressor. The advantage of this location is that the detectors are not shadowed by the motion of the control rods, and the minimum flux

they see is somewhat less than it would be at the interface between the core and the control rod, and the temperature is lower. Hopefully, the gas used to cool the compressor will not have a gamma-neutron reaction.

10-5 Dynamic Range

In considering the operating set of instruments, the practical limit of the dynamic range for both the linear level and period channels is about eight decades. This is based on the chamber current of 1 ma at full-power operation. The time constant of the linear level channel, assuming 0.8 km of cable, will be in the order of less than 1 msec at full power. This will also hold true for the period meter. However, real problems occur in the period meter when one is operating at a smaller current, in that the time constant will increase inversely proportional to the current. This means that at 10^{-10} amp the time constant of the period meter with 0.8 km of cable will be in the order of 10^{-100} sec. For use in controlling a fast reactor, this time constant seems out of the question. There are two possibilities of overcoming this problem. One may come about in the next few years in the development and use of radiation-resistant components which can be built into a pre-amp package located closer to the reactor which reduces the cable capacity. The second way is to provide two sets of instruments. The initial startup instrumentation will reduce the required dynamic range of the operational channels. If the reactor has a one-watt source or has a shutdown power of one watt, the reactor itself will cover only seven decades, so that a compromise certainly can be made in overlapping ranges.

The startup instruments will use larger detectors, so that one has a larger signal and a smaller time constant to contend with during the startup and intermediate range operation. At some predetermined current output of these instruments, the master programmer can be made to switch over to the operating set of instruments. The detectors for the startup channels can be located essentially on the ground level outside of the reactor. The startup instruments will probably have to be solar-battery powered. The radiation damage on this set will certainly be great enough so that they will be inoperative after a very short period of operation at full power. This in effect will prevent a second startup of the reactor.

10-6 The Master Programmer

Being located roughly 0.8 km away from the reactor and hopefully with some shielding due to the irregular surface of the moon, the present-day techniques of construction foresees no difficulties in building this particular unit, but there may be problems with some of the pressure and temperature and other transducers as far as radiation damage is concerned. However, with a little thought both pressure and temperature can be suitably transduced

by several means, such that the radiation damage will not be a problem. It is believed that ceramic-coated wire will give sufficient insulation to permit the operation of these transducers.

Both period and level information have been already used to provide, not only a very stable reactor power level, but a semiprogrammed startup.

Price $2.50 . *Available from the Office of Technical Services, Department of Commerce, Washington 25, D.C.*